TALLINN UNIVERSITY OF TECHNOLOGY
DOCTORAL THESIS
43/2020

Runup of Nonlinear Waves of Different Shapes on a Plane Beach Including Effects of Dispersion and Wave Breaking

AHMED ABDALAZEEZ

TAL TECH PRESS

TALLINN UNIVERSITY OF TECHNOLOGY
School of Science
Department of Marine Systems
This dissertation was accepted for the defence of the degree 22/10/2020

Supervisor: Dr. Ira Didenkulova
Department of Marine Systems
Tallinn University of Technology
Tallinn, Estonia

Co-supervisor: Dr. Denys Dutykh
Univ. Grenoble Alpes, Univ. Savoie Mont Blanc
CNRS, LAMA
Chambéry, France

Opponents: Dr. Finn Løvholt
Norwegian Geotechnical Institute
Department of Offshore Energy
Oslo, Norway

Prof. Maria Ana Viana Baptista
Instituto Superior Engenharia de Lisboa
Lisbon, Portugal

Defence of the thesis: 26/11/2020, Tallinn

Declaration:
Hereby I declare that this doctoral thesis, my original investigation and achievement, submitted for the doctoral degree at Tallinn University of Technology has not been submitted for doctoral or equivalent academic degree.

Ahmed Abdalazeez

---
signature

European Union
European Regional
Development Fund

Investing
in your future

ISSN 2585-6898 (publication)
ISBN 978-9949-83-619-2 (publication)
ISSN 2585-6901 (PDF)
ISBN 978-9949-83-620-8 (PDF)
Printed by Koopia Niini & Rauam

TALLINNA TEHNIKAÜLIKOOL
DOKTORITÖÖ
43/2020

Laine dispersiooni ja murdumise mõju mittelineaarsete lainete uhtekõrgusele erineva kujuga laugetel randadel

AHMED ABDALAZEEZ

TAL TECH
KIRJASTUS

Contents

List of Publications

The list of publications, on the basis of which the thesis has been prepared:

I. Abdalazeez, A., Didenkulova, I., Dutykh, D. 2019. Nonlinear deformation and runup of single tsunami waves of positive polarity: numerical simulations and analytical predictions. Natural Hazards and Earth System Sciences, 19, 2905−2913.10.5194/nhess- 19-2905-2019.

II. Torsvik, T., Abdalazeez, A., Dutykh, D., Denissenko, P., Didenkulova, I. 2019. Dispersive and non-dispersive nonlinear long wave transformations: Numerical and experimental results. In: A. Berezovski, T. Soomere (Ed.). Applied Wave Mathematics II. Selected Topics in Solids, Fluids, and Mathematical Methods and Complexity (41−60). Swizerland: Springer.10.1007/978-3-030-29951-4_3.

III. Abdalazeez, A., Didenkulova, I., Dutykh, D., Denissenko, P. 2020. Comparison of dispersive and nondispersive models for wave runup on a beach. IZvestiya. Atmospheric and Oceanic Physics, Vol. 56 (5), pp. 494–501.

IV. Abdalazeez, A., Didenkulova, I., Dutykh, D., Labart, C. 2020. Extreme Inundation Statistics on a Composite Beach. Water, 12 (6), 1573−1586. 10.3390/w12061573.

Author's Contribution to the Publications

Contribution to the papers in this thesis are:

*** complete contribution (100%)
** leading contribution (> 50%)
* supporting contribution (< 50%)

Publication	I	II	III	IV
Concept	**	*	**	**
Data processing	***	***	***	***
Manuscript preparation	***	*	***	***

1. INTRODUCTION

According to Rangel-Buitrago et al. (2020), there is an increase of people worldwide living in the coastal zone (about 10% of the world's population), which is linked to a risk of floods induced by storm surge, storm waves, tsunamis, and freak waves (Bevacqua et al., 2019, Marcos et al., 2019). Therefore, it is important to study the characteristics of inundation in coastal zones. In order to reduce the coastal risks and loss of lives arising from extreme waves, the development of the early warning systems is needed (LaBrecque et al., 2019, Thandlam and Rutgersson, 2019). Furthermore, studying irregular wind waves and its influence on beaches is also important for the assessment of coastal structures beachfront properties because these frequent motions deliver much of the energy responsible for dune and beach erosions (Stockdon et al., 2006, Suanez et al., 2011, Anthony, 2012).

Ocean waves of periods ranging from 5 min to 12 hr (tsunami, seiches, and storm surges, tides) are considered long waves (Stocker, 1957, Kinsman, 1965, Mei, 1983). Physically, long waves are characterized by $kh < 1$, where h is the water depth and k is the wave number (Sawaragi 1995, Holthuijsen, 2007). In the coastal area, the nearshore zone is divided into three zones; breaker zone, surf zone, and swash zone (Davis, 1985). The swash is generally defined as the time-varying location of the connection between the ocean and the beach ranging between the limit of rundown and the limit of runup. The wave runup is defined as a vertical elevation above the mean sea level. The process of wave runup on a beach is considered a very complex phenomenon because it depends on several physical factors, such as the incident wave conditions (e.g. wave periods, wave steepness, and wave heights) (Dean et al., 2005), and the nature of the beach (e.g. reflectivity, beach slope, and roughness) (Waal and Meer, 1993). The momentum flux drives the water wave climbing the beach until it reaches the ''maximum runup'', converting its kinetic energy into potential energy (Lin et al., 1999). This maximum point of wave runup represents one of the most important parameters needed to estimate the tsunami flooding. The breaking criterion of a wave climbing the beach can be classified into three types of wave breaking, spilling, plunging, and surging (Galvin, 1968, Battjes, 1975). These types can be classified based on Iribarren number, Ir, which is defined by $tan\alpha/\sqrt{H/L}$, where $tan\ \alpha$ is a beach slope, H is a wave height, and L is a wavelength in deep waters. The spilling occurs if $Ir < 0.5$, where the plunging occurs if $0.5 < Ir < 3.3$ and surging or collapsing if $Ir \geq 3.3$.

The tsunami waves may approach the beach having different shapes such as single waves of elevation or depression, *N*-waves, semi-periodic waves, and wave trains (Shuto, 1985). Usually, when a tsunami wave approaches the coast its exact shape is unknown (Didenkulova et al., 2008). In general, the most commonly used formulas in models or experiments to estimate the tsunami runup characteristics have a soliton wave shape. The solitary waves can be easily generated experimentally in laboratories, which makes them very popular for studies. Therefore, the tsunami runup height of incident solitary waves has been studied intensively during the last decades using different methods.

Carrier and Greenspan (1958) have found analytically a general solution for a long wave runup on a constant plane beach using nonlinear shallow water theory, NLSW, and a specialsolution for a regular wave runup. Later on, many other authors investigated the runup height of several other wave shapes with a special emphasis on solitary waves with respect to different inclined planes, initial incident wave conditions, and wave

breaking criteria using analytical, numerical, and experimental methods. For instance, Gjevik and Pedersen (1981), Pedersen and Gjevik (1983) studied the runup height of solitary waves with respect to different inclined planes. Synolakis (1987, 1988) studied the runup of breaking and non-breaking solitary waves on plane beaches using analytical solutions and experiments. Liu et al. (1990) summarized the twenty-six papers in the International Workshop on Long-Wave Runup. They mainly focused on tsunami runup and flooding, covered all the methodological studies to estimate runup phenomena. Grilli et al. (1994) investigated the shoaling of solitary waves using a fully nonlinear hydrodynamic model and the laboratory experiments for gentle and steep beach slopes, during the shoaling. The wave breaking during the shoaling reduced the wave reflection (Lin et al., 1994). Experimentally, the rapid decay of solitary waves has been observed after breaking and that is due to the transfer of the potential energy into the kinetic one (Grilli et al., 1997). In the last ten years, analytical and numerical methods have been developed with respect to the solitary wave breaking process in order to get more accurate predictions of wave runup, see for example (Yingli et al., 2002, Xiao et al., 2010, Young et al., 2010, Dutykh et al., 2011, Qu, 2019). However, several studies reported that the solitons are unsuitable to describe a real tsunami, suggested to use waves of longer duration than solitons, and downscaled records of real tsunami (Madsen and Fuhrman, 2008, Goseberg et al., 2013, Schimmels et al., 2016). The statistical data for tsunami waves in the Pacific Ocean showed that most of them (about 75%) are non-breaking waves (Mazova et al., 1983). However, large or long propagating tsunamis are breaking and often form a steep wave front when approaching the coast. During the large tsunami events, such as the 2004 Indian Ocean and 2011 Tohoku tsunamis, the nonlinear steepening of the tsunami wave front near the coast has been reported and observed by photos and videos. Analytically, Didenkulova et al. (2007) and Didenkulova (2009) studied the wave front steepness and its influences on wave runup height for regular waves. The wave front steepening of single waves during their propagations was also observed experimentally (Sriram et al., 2016). However, its influence on runup height on the beach has not been investigated. Therefore, in the **paper I,** we studied this influence of tsunami wave front steepness on runup height using numerical and analytical methods. In summary, the maximum tsunami runup height on a beach depends on the wave front steepness at the toe of the bottom slope. The corresponding new formula of the maximum runup height as a function of wave front steepness, wave period, and distance to the slope is suggested. Sometimes, in order to save time for tsunami forecast, especially for long distance wave propagation, the tsunami runup height is estimated by using analytical or empirical formulas (Glimsdal et al., 2019, Løvholt et al., 2012). Thus, we proposed using the formula suggested in the **paper I**. The face front steepness of the approaching tsunami wave can be estimated from the data of the simulated (computed) or real tide-gauge stations and then be used to estimate tsunami maximum runup height on a beach.

It has been observed that the tsunami waves generated by the earthquake of December 26, 2004 have a complicated temporal and spatial structure, where the waves had multiple amplitude and frequency components (Merrifield et al., 2005, Horrillo et al., 2006, Narayana et al., 2007, Rossetto et al., 2007). Horrillo et al. (2006) studied dispersive effects during 2004 Indian Ocean tsunami propagation by comparing the nonlinear shallow water model with the fully nonlinear Navier-Stokes equations (FNS) and dispersive model based on Boussinesq-type. They concluded that nonlinear shallow water models offered the more suitable framework for hazard assessments, bringing

together a very low computational cost. Although the NLSW model tended to overestimate the maximum wave runup, the over-prediction was considered to be within a reasonable range for a safety buffer. The nondispersive model usually described leading waves very well, whereas the trailing wave trains are more sensitive to wave dispersion (Løvholt et al., 2012). Therefore, in terms of tsunami early warning system, the nonlinear shallow water theory is generally considered more appropriate than the dispersive Boussinesq-type model (Glimsdal et al., 2013). However, the studies mentioned above were based on numerical results and were missing the mechanism of fidelity control. Therefore, in the **papers II** and **III** we take the advantages of available experimental data (collected from the Large Wave Flume, Hannover, Germany) of different wave types characterized by kh = 0.2 and compared their wave runup heights with the corresponding data from the dispersive model of Boussinesq type based on the modified Peregrine system (mPer) and nondispersive nonlinear shallow water model (NLSW). In the **paper II**, we studied the wave runup height on the almost frictionless bottom, provided that the bottom slope was covered by a smooth plastic. In the **paper III**, the bottom roughness corresponds to the rough asphalt pavement. Concluded that, in the given range of kh, for large-amplitude waves the dispersive effects are important, therefore, dispersive models should be applied, while for small-amplitude waves NLSW gives reasonable results and can still be used.

Individual waves in the irregular wave record are defined between two zero-downward crossings or zero-upward crossings (where, zero is the mean sea level). Irregular waves are characterized by the significant wave height, H_s, which is introduced as an averaged of the third of the highest waves (H_s), however, H_s is often defined as four times the standard deviation of the surface elevation. This issue has been discussed in detail in (Holthuijsen, 2007), showing that the second definition ($4\sqrt{\sigma}$, where σ is a standard deviation of the surface elevation) can be approximated to H_s. However, in our studies we used the first "classical" definition of significant wave height (H_s).

Theoretically, if the incident wave fields are distributed according to the narrowband Gaussian distribution, their heights are distributed by the Rayleigh distribution; see for example (Massel, 1996). Some authors confirmed this result in field measurements; see for example (Marshall, 1975, Forristall, 1978), on the other hand, many researchers pointed out that the experimental wave height distribution deviates from the Rayleigh distribution (Battjes, 1972, Goda, 1975, Rattanapitikon and Shibayama, 2007). During extreme wind conditions, the distribution of wave heights in shallow water significantly deviated from Rayleigh distribution, therefore, a composite Rayleigh-Weibull distribution can be used (Battjes and Groenendijk, 2000, Pullen et al., 2007, Mai et al., 2010). However, (You and Nielsen, 2013, Neelamani et al., 2007) reported that the wave height could be distributed according to a Weibull distribution. In the recent study, Teutsch et al. (2020) investigated random waves data collected from the southern North Sea covering the period 2011-2016 using radar measurements and wave buoy, found that the distribution of wave heights on average followed the Forristall distribution.

The most hazardous and risky waves born in the irregular wave field are the so-called freak waves. Their height is twice larger than the significant wave height ($H/H_S > 2$). They are extremely dangerous due to their height and sudden appearance; therefore, they are also called killer waves or monster waves, as they caused disappearing and damage of ships and human loss in deep and coastal waters. Many authors suggested explanations for the cause of the freak waves, e.g. Dean (1990), proposed the cause is due to the nonlinear superposition of waves. Kharif and Pelinovsky, (2006) in their

review paper listed several mechanisms of freak wave formation: the dispersion enhancement of transient wave packets, wave-bottom interaction, geometrical focusing, wave-current interaction, and modulational instability and soliton collisions. Didenkulova and Anderson (2010) analysed the data collected from the coastal zones of the Baltic Sea, 2.7 m depth, during June–July 2008, suggesting the dispersive focusing can be a mechanism of the generation of freak waves. Fedele et al. (2019) analysed different field measurements in various European locations, concluded that the rogue waves happen rarely on weakly nonlinear random seas. Didenkulova and Rodin (2012) studied freak waves in Tallinn Bay in the Baltic Sea based on the one-month wave measurements at 2.7 m water depth in the nearshore region and found that the Rayleigh distribution slightly overestimates the number of freak waves. Although the freak waves have been intensively studied in the last 25 years, still their phenomenon is not fully understood, especially what regards freak waves on a beach (freak runups). The collected databases are not enough for their statistical analysis.

Theoretically, there are many factors that affect the statistical distribution of wave runups, such as wave nonlinearity, the seafloor irregularity, and wave breaking (Stocker, 1957, Mei, 1983, Massel, 1996). The statistics of extreme runup events have been studied using different methods: experimental methods, numerical models, and field measurements. The statistical properties of long waves on a beach of constant slope have been investigated by (Didenkulova et al., 2011) using an analytical solution of NLSW for the infinite sloping beach. They found that the runup heights are distributed according to the Rayleigh distribution if the incident waves are represented by a normal distribution. Gurbatov and Pelinovsky (2019) studied the statistical runup of irregular narrow-band incident waves on a constant beach slope under the assumption of non-breaking waves, and found that for the runup distribution of even non-breaking waves, the Gaussian distribution is inappropriate. Denissenko et al. (2011) studied the runup of long irregular waves on a plane beach experimentally in order to reproduce the theoretical studies of (Didenkulova et al., 2011); however, their experimental record was not long enough for extreme wave analysis, and the initial wave field deviated from the Gaussian distribution. The higher statistical moments (skewness and kurtosis) of runup remained similar to those of incident waves. Later, Denissenko et al. (2013) conducted a series of experiments for wave fields with different bandwidth. Their results show that the bandwidths have a weak influence on runup height distribution, so still can be represented according to the Rayleigh distribution, which agrees with the theoretical results by Didenkulova et al. (2008). However, these experiments did not have long enough time-series to investigate the statistics of extreme runup heights especially in terms of freak runups. This gap could potentially be covered by field measurements on natural beaches. The statistical runup height of wide spectrum incident waves has been studied on sandy beaches in New South Wales (Nielsen and Hanslow, 1991); they found that runup heights are distributed according to the Rayleigh distribution. Unfortunately, the field measurements often have unknown initial wave conditions. Therefore, as it was mentioned above, the short time-series experiments and unknown initial wave conditions in the field measurements are considered as limiting factors to study the statistical distribution of extreme wave runup events. In the **paper IV,** we take an advantage of numerical computations by generating long-term numerical experiments using intensive numerical simulations with fixed initial wave fields in different bandwidths and nonlinearities.

The main objectives of the thesis

This thesis aims at understanding the effects of wave nonlinearity, dispersion, and wave breaking on the runup height on a plane beach. The particular objectives are summarized as follows.

- Studying nonlinear deformation and runup of single tsunami waves analytically and numerically.
- Investigating the dispersive effects of long periodic waves and their impact on runup height numerically and experimentally using the data of flume experiment.
- Studying extreme runup statistics of breaking irregular waves of different heights and bandwidths on a plane beach.

The methodology has been described in section 2. Several different methods have been used in the thesis. The semi-analytical approach (section 2.1) is based on the asymptotic solution of the nonlinear shallow water theory (NLSW), which has been used in the **paper I** to investigate the steepening wave front of a single tsunami wave and its influence on runup height. The nondispersive NLSW numerical model (section 2.2.1) has been used in all the papers**.** The dispersive numerical model mPer, based on the modified Peregrine equations (section 2.2.2) has been used in the **papers II** and **III**. In the **papers I, II,** and **III** the data of flume experiments obtained from the Hannover Large Wave Flume (GWK) (sections 2.3) are used.

Abbreviations

NLSW	Non-Linear Shallow Water System
mPer	Modified Peregrine System
GWK	The Large Wave Flume (Großer WellenKanal)

2. METHODOLOGY

2.1 Analytical methods

A general solution of nonlinear shallow water equations on a plane beach has been found by Carrier and Greenspan (1958), using the hodograph transformation. Subsequently, many authors using this solution studied different types of waves, see for example (Pedersen and Gjevik, 1983, Synolakis, 1987, Synolakis et al., 1988, Mazova et al., 1991, Pelinovsky and Mazova, 1992, Tadepalli and Synolakis, 1994, Brocchini and Gentile, 2001, Carrier et al., 2003, Kânoğlu, 2004, Tinti and Tonini, 2005, Kânoğlu and Synolakis 2006, Madsen and Fuhrman, 2008, Didenkulova et al., 2007, Didenkulova, 2009, Madsen and Schäffer, 2010). In the **paper I,** the analytical solution of nonlinear shallow water equations has been used in order to study the steepening of wave front of single tsunami waves of positive polarity and its influences on runup height. The one-dimensional equations of NLSW can be written as:

$$\frac{\partial u}{\partial t} + u\frac{\partial u}{\partial x} + g\frac{\partial \eta}{\partial x} = 0, \tag{1}$$

$$\frac{\partial \eta}{\partial t} + \frac{\partial}{\partial x}\left[(h(x)+\eta)u\right] = 0. \tag{2}$$

where $\eta(x, t)$ is the vertical displacement of the water surface with respect to the still water level, $u(x, t)$ –fluid particles horizontal velocity, $h(x)$ – unperturbed water depth, g is the gravitational acceleration, x is the coordinate directed onshore, and t is time. Eqs. (1) and (2) have been solved independently for the two bathymetries: a bathymetry of constant depth, $h(x) = h_0$ with length X_0 and a constant beach slope, where the water depth $h(x) = - x \tan\alpha$, (Fig. 1). The exact solutions of Eqs. (1) and (2) can be found for a few specific cases, e.g. (i) a basin of constrant depth and (ii) a plane beach.

During its propagation in the basin of constant depth, h_0, the wave transforms as a Riemann wave (Zahibo et al., 2008):

$$\eta(x,t) = \eta_0\left[t - \frac{x + X_0 + L}{V(x,t)}\right], \tag{3}$$

$$V(x,t) = 3\sqrt{g\left[h_0 + \eta(x,t)\right]} - 2\sqrt{gh_0}, \tag{4}$$

where $\eta_0(x = - L - X_0, t)$ is the water displacement at the left boundary. After the propagation over the section of constant depth, h_0, the incident wave has the following shape:

$$\eta_{X0}(t) = \eta_0\left[t - \frac{X_0}{V(x,t)}\right],\ V_{X0}(t) = 3\sqrt{g\left[h_0 + \eta_{X0}(t)\right]} - 2\sqrt{gh_0}, \tag{5}$$

Following the method developed in (Didenkulova et al., 2008), we let this nonlinearly deformed wave described by Eq. (5) run up on a plane beach, characterized by the water depth $h(x) = – x \tan\alpha$. This approach does not take into account the merging point of the two bathymetries and, therefore, does not account for reflection from the toe of the slope and wave interaction with the reflected wave. The long single pulses of positive polarity have been considered in this study:

$$\eta_0(t) = A\,\mathrm{sech}^2\left(\frac{t}{T}\right) \tag{6}$$

The maximum runup height, R_{max} of such wave Eq. (6) can be found from (Didenkulova et al., 2008, Sriram et al., 2016):

$$\frac{R_{max}}{A} = 2.8312\sqrt{\cot\alpha}\left(\frac{1}{gh_0}\left(\frac{2h_0}{\sqrt{3T}}\right)^2\right)^{1/4}. \tag{7}$$

If the initial wave is a soliton, then Eq. (7) coincides with the famous Synolakis's formula (Synolakis, 1987).

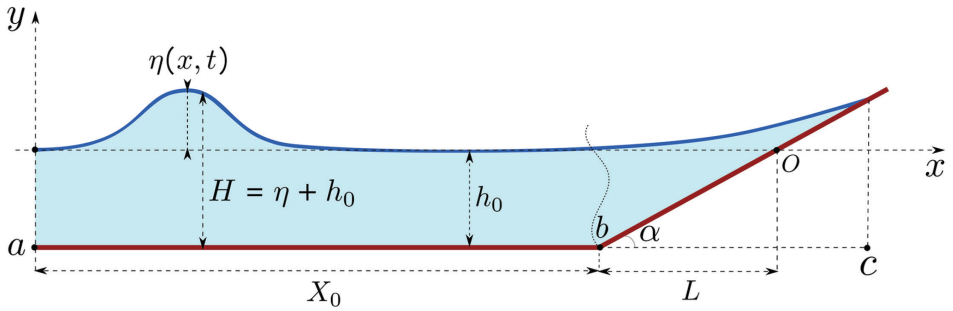

***Figure 1**: Sketch of the physical and computational domains*

2.2 Numerical models

The analytical solutions (Section 2.1) described above are not practical when the general wave types and variable depth conditions are considered. Developing numerical models that suitable to describe the tsunami propagation and its runup on a plane beach is an important task for coastal engineers and scientists. The most commonly used is NLSW model, which is preferred for the long wave runup calculation compared to dispersive models based on Boussinesq-type approximations. The instabilities of numerical schemes in the dispersive models make the computations more sensitive to numerical parameters (Bellotti and Brocchini, 2001). Moreover, the dispersive term in the Boussinesq system tend to zero at the shoreline, and therefore there the dispersive equations simplify to NLSW (Madsen et al., 1997). Nevertheless, the dispersive model is needed for calculating long wave runup if the shape of incident tsunami waves represents trailing waves, where the dispersive effects become more important, considering that the maximum wave is often not the first one (Candella et al., 2008, Rabinovich and Thomson, 2007). The numerical models have been validated against experimental data of wave propagation and runup in the Large Wave Flume (GWK) in Hanover, Germany. Finite volume method has been used, which is useful for problems where quantities should be preserved, e.g. mass or momentum. We applied the non-oscillatory UNO2 scheme, which is intended to constrain the number of local extrema in the numerical solution at each time step (Harten and Osher, 1987). The integration of the solution forward in time has been carried out by the Bogacki-Shampine time stepping method (Bogacki and Shampine, 1989). The nested Runge–Kutta methods of order 3 and 2, (Dutykh et al., 2011), is implemented in the MATLAB environment using the ode23 command, (Shampine and Mark Reichelt, 1997).

The time step is chosen to satisfy the Courant–Friedrichs–Lewy (CFL) condition for all considered significant wave heights. In the **papers I** and **IV**, an embedded second order method is used to estimate the local error and if necessary adapt the local time-step size, whereas in the **papers II** and **III** the characteristic time steps in the performed calculations are presented in Table 1. The Rankine–Hugoniot jump conditions have been used to approximate the wave breaking, see (Dutykh et al., 2011).

Boundary conditions

On the left extremity ($x = a$) of the computational domain, the Dirichlet boundary condition on the total water depth component $H(a, t) = h_0 + \eta_0(t)$ of the solution (H, Hu) is imposed. The boundary conditions are implemented in the finite volume scheme according to the method described in (Ghidaglia and Pascal, 2005), for more details on the application to the nonlinear shallow water equations, see (Dutykh, et al., 2011). In the **papers I** (for model validation), **II** and **III** on the left boundary ($x = a$) we used the most "clean" experimental recording of the wave gauge at the point closest to the wave maker, which was at a distance a = 50 m from the wave maker. In the **paper IV**, the function of free surface elevation, η_0, is drawn from a narrow- or wideband Gaussian signal (Eq. 8) depending on the experiment. The obtained data turn out to be enough to find a well-posed initial boundary-value problem provided that the flow is subcritical at the point $x = a$, *i.e.*, $u(a, t) < pgH(a, t)$, which is always the case for Riemann waves, see (Petcu and Temam, 2013), for the rigorous mathematical justification of this fact in case of transparent boundary conditions. The considered boundary condition (wave field offshore) is described according to the Gaussian distribution:

$$f(\xi) = \frac{1}{\sigma\sqrt{2\pi}} e^{-\frac{1}{2}\left(\frac{\xi-\mu}{\sigma}\right)^2}, \tag{8}$$

where μ is a mean value of the distribution and σ is a standard deviation. The Kolmogorov-Smirnov test has been applied to ensure all the individual time-series distributed according to the Gaussian distribution (Dodge, 2008). The spectrum of the generated waves is:

$$S(f) = \frac{S_0}{\sqrt{2\pi\,\Delta f / f_0}} e^{-\frac{(f/f_0-1)^2}{2\Delta f/f_0}}, \tag{9}$$

where Δf is the frequency band, f is the wave frequency, f_0 = 0.1 *Hz* is the central frequency, and S_0 is the constant, which is calculated in order to achieve the desired H_s. In this work, the case with $\Delta f/f_0$ = 0.1 is referred to as the narrow-band spectrum, while the case with $\Delta f/f_0$ = 0.4 is referred to as the wide-band spectrum.

Bathymetry description of the numerical experiments

The bathymetry described below has been used in all our papers. The corresponding bathymetry (Fig. 2) set-up as the flat part of the flume matches the beach of constant slope:

$$h(x) = \begin{cases} h_0, & x \in [a,b] \\ h_0 - (x-b)\tan\alpha & x \in [a,b] \end{cases}, \tag{10}$$

where, h_0 is the constant water depth, kept at 3.5 m for all simulations, the left and right boundaries of the numerical flume are [a, c], the point where the slope starts is [b], and $\tan\alpha$ = 1:6 is the tangent of the bottom slope. The length of the section of constant

depth is *b* = 251.5 *m*, and the right limit of the numerical flume is taken as *c* = 291.5 *m*. However, in the **paper I,** the length of the section of constant depth has not been fixed, where we used different lengths (between 600 *m* and 0 *m*) in order to investigate the wave steepening .

The roughness of the beach is important for investigating the maximum runup height. In the **papers II** and **III,** the Manning friction law, S_f is used, where $S_f = gc_f^2 u|u|/H^{(4/3)}$, S_f is the friction term, c_f^2 is the roughness coefficient (Dutykh et al., 2011). In the **paper III,** the corresponding roughness coefficient was taken equal to 0.016, which corresponds to the rough asphalt pavement, while in the **paper II** we used roughness coefficient equal to 0.009, which corresponds to the smooth plastic (https://www.engineeringtoolbox.com/mannings-rough- ness-d_799.html). The effect of friction during long wave runup on the coast was considered in (Apotsos et al, 2011).

Table 1*. A characteristic of numerical time step in the performed calculations*.

Wave type	mPer, *Δt*	NLSW, *Δt*
solitary wave	0.015	0.016
sine wave	0.012	0.013
bi-harmonic	0.012	0.013
ship wake	0.009	0.012

The number of points of the spatial grid in the **papers I, II and III** is constant and equal to 4000 for all experiments, so the spatial resolution was 6.3 *cm*. In the **paper IV**, the number of spatial grid points along the distance between [*a*] and [*c*] is fixed and equal to 1000 for all experiments. Each spatial grid step has a length equal to 25 cm, which corresponds to 4 cm vertical resolution for runup height. However, this also suggests that we have a low resolution and not so reliable statistics, especially for small amplitude waves H_s = 0.1 m. In a similar manner to the significant wave height, H_s, the significant runup height, R_s, is introduced as an average of one third of the largest runup heights in the time-series. The smallest significant runup height is R_s = 0.23 m, therefore, even in this case the resolution is considerable.

2.2.1 Nonlinear shallow water system

We solve the nonlinear shallow water equations Eqs. (11) and (12), written in a conservative form for total water depth:

$$H_t + (Hu)_x = 0, \tag{11}$$

$$(Hu)_t + \left(Hu^2 + \frac{g}{2}H^2\right)_x = gHh_x. \tag{12}$$

where $H = h + \eta$ is the total water depth, $\eta(x, t)$ is the water elevation with respect to the still water level, *u(x,t)* is the depth-averaged flow velocity, $h(x)$ is an unperturbed water depth described by Eq. (10), g is the gravitational acceleration, x is the coordinate directed onshore, and t is time. The numerical scheme dissipations are included, which are necessary for the stability of the scheme and should not influence much the runup characteristics. Namely, we employ the natural numerical method, which was developed especially for conservation laws–the finite-volume schemes.

2.2.2 Dispersive modified Peregrine system

The Boussinesq equations for long dispersive wave propagation, derived by Peregrine (1967), are:

$$\eta_t + \big((h+\eta)u\big)_x = 0, \tag{13}$$

$$u_t + uu_x + g\eta_x - \frac{h}{2}\big(hu\big)_{xxt} + \frac{h^2}{6}\big(u_{xxt}\big) = 0. \tag{14}$$

which can be applied under gently varying depth conditions. Durán et al. (2018) modified the classical Peregrine system in order to recover the conservative form of the equations. Thus, Eq. (13) of the mass conservation in new variables becomes:

$$H_t + Q_x = 0, \tag{15}$$

where $Q = Hu$ is the horizontal momentum. From Eq. (15), the momentum conservation equation becomes:

$$\left(1+\frac{1}{3}H_x^2 - \frac{1}{6}HH_{xx}\right)Q_t - \frac{1}{3}H^2Q_{xxt} - \frac{1}{3}HH_xQ_{xt} + \left(\frac{Q^2}{H} + \frac{g}{2}H^2\right)_x = gHh_x. \tag{16}$$

Eqs. (15) and (16) are called the modified Peregrine equations and are studied in detail in Durán et al. (2018).

2.3. GWK experiment

The Large Wave Flume (Großer Wellen Kanal, GWK) at Forschungszentrum Küste (FZK) in Hannover, Germany, was actually built for different purposes and has always been used for large-scale experiments on the wind wave (comparably short period) impact on coastal and offshore structures and wave interaction with sediments (Schimmels et al., 2016).

The experiments were carried out in 2012-2013 using a piston type wave maker for wave generation. The wave maker was equipped with a mechanism of active absorption of the reflected wave (Schmidt-Koppenhagen et al., 1997), which used signals from two wave gauges as input parameters: one in the immediate vicinity and the other 3.6 meters from the wave maker. The experimental set-up consisted of a 251 m long section of constant depth of 3.5 m and a plane beach with a slope angle 1:6. Experiments performed in 2012 and used in the **paper III** had GWK natural asphalt bed and slope, while experiments performed in 2013 used in the **paper II**, had the slope covered by a smooth plastic to minimize bottom friction. The bottom friction on the asphalt beach strongly affected the measurement of wave rundown. When the water run down from the edge, a layer of water remained on the slope, which touched the capacitive sensor wire and prevented the correct recording of the wave rundown. There were from 16 (experiments in 2013) to 18 (experiments in 2012) wave gauges recording wave propagation along the flume. The 16 wave gauges used in 2013 were mounted along the flume to measure the incident wave field at different distances from the wave maker. The positions of the wave gauges along the flume are 50 m, 51.9 m, 55.2 m, 60 m, 120 m, 140 m, 160 m, 180 m, 190 m, 200 m, 210 m, 220 m, 225 m, 230 m, 235 m, and 245.33 m, see Fig. 1. The positions of the 18 wave gauges are 50 m, 51.9 m, 55.2 m, 60 m, 140 m, 150 m, 160 m, 161.9 m, 165.2 m, 170 m, 180 m, 190 m, 200 m, 210 m, 220 m, 230 m, 240 m, and 250 m. The signal from wave gauges was recorded with

a sampling frequency of 200 Hz. The wave runup was measured by a capacitance probe, which was supplemented by two regular video cameras. The error in measuring the runup by a capacitive sensor is determined by the variation of the water edge across the slope. According to visual observations, the variation is about ± 3% at the level of the runup magnitude. The capacitance probe consisted of the two isolated copper wires suspended at a distance 10 cm from each other and 1 cm above the slope. A 100 kHz sinusoidal signal was applied to one of the wires. The signal from another wire was fed to the lock-in amplifier and the signal amplitude was recorded with the sampling frequency of 200 Hz (Denissenko et al., 2011). For more details about the experiments, see Denissenko et al. (2013). In the **papers II** and **III**, we used different types of wave shapes, its properties in the experimental set-up are shown in Table 2. In order to exclude the influence of even a small part of the wave reflected from the wave maker, only the first four waveswere used for calculations (before the wave reflected from the wave maker would approach the coast). The complete list of the studied waves included solitary-like waves, sine and bi-harmonic waves, as well as ship wakes modulated in frequency and amplitude, resembling characteristic wave records from high-speed vessels, (Torsvik et al., 2009, Torsvik et al., 2015). In such generated ship wakes, the wave period linearly decreased from 20 to 10 s.

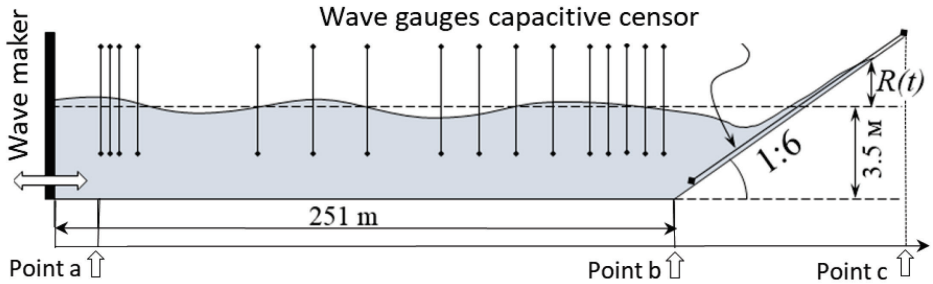

***Figure 2**: Scheme of a laboratory experiment in the GWK.*

***Table 2:** Wave types properties*

Run number	Wave type	W. height, m	W. period	Roughness bottom
1002	sine wave	0.2	20	Asphalt
1003	sine wave	0.3	20	Asphalt
1004	sine wave	0.25	20	Asphalt
1006	sine wave	0.15	20	Asphalt
1007	sine wave	0.4	20	Asphalt
1008	sine wave	0.6	20	Asphalt
1069	sine wave	0.45	20	Asphalt
1014	bi-harmonic	0.27	20, 10	Asphalt
1015	bi-harmonic	0.27	20, 10	Asphalt
1017	bi-harmonic	0.27	20, 10	Asphalt
1018	bi-harmonic	0.27	20, 10	Asphalt
1019	bi-harmonic	0.4	20, 10	Asphalt
1020	bi-harmonic	0.42	20, 10	Asphalt
1021	bi-harmonic	0.4	20, 10	Asphalt
1024	bi-harmonic	0.62	20, 10	Asphalt

1025	bi-harmonic	0.5	20, 10	Asphalt
1027	bi-harmonic	0.4	20, 10	Asphalt
1047	ship wake	0.1	20→10	Asphalt
1051	ship wake	0.2	20→10	Asphalt
1052	ship wake	0.3	20→10	Asphalt
1053	ship wake	0.4	20→10	Asphalt
2012	sine wave	0.1	20	Plastic
2013	sine wave	0.15	20	Plastic
2014	sine wave	0.2	20	Plastic
2015	sine wave	0.25	20	Plastic
2016	sine wave	0.3	20	Plastic
2017	sine wave	0.35	20	Plastic
2018	sine wave	0.4	20	Plastic
2019	sine wave	0.45	20	Plastic
2020	sine wave	0.5	20	Plastic
2021	sine wave	0.55	20	Plastic
2022	sine wave	0.6	20	Plastic
2074	solitary	0.24	20	Plastic
2075	solitary	0.2	20	Plastic
2076	solitary	0.15	20	Plastic
2077	solitary	0.1	20	Plastic

3. RESULTS AND DISCUSSION

3.1 Nonlinear deformation and runup of single tsunami waves

In this section, we investigated the effect of wave front steepening on the maximum runup height of single tsunami waves of positive polarity analytically and numerically (NLSW). We used the bathymetry described in Fig. 1. The results below correspond to **paper I.**

The nonlinear steepening of the periodic sine waves and its influences on runup height has been studied in (Didenkulova et al., 2007, Didenkulova et al., 2009). Found that the extreme runup height is increased proportional to the square root of the wave front steepness. In this section, we study the effects of the single wave front steepness on its runup height on a beach using analytical and numerical methods given in Section 2. The corresponding bathymetry used in analytical and numerical calculations is normalized on the water depth in the section of constant depth h_0 and is shown in Fig. 1. The input wave parameters such as effective wavelength, λ/X_0, where $\lambda = T\sqrt{gh_0}$, and wave amplitude, A/h_0 are changed. The beach slope is taken as $tan\,\alpha = 1{:}20$ for all simulations. In analytical solutions, we underline that the criterion of no wave breaking should be satisfied. Therefore, all the calculations in analytical and numerical solutions below are chosen for non-breaking waves. The numerical and analytical solutions have been validated against GWK experimental data, where the comparison of the runup height on a beach slope of the long single wave with an initial amplitude, A = 0.1 m and wave period, T = 20 s is shown in Fig. 3. It can be seen that the runup height in experiment is slightly smaller, which may be caused by the bottom friction. Both numerical and analytical models have a good agreement with the experiment. However, the numerical prediction of the runup height is slightly higher than the analytical one, which can be explained by the effects of wave interaction with the toe of the underwater beach slope, which is taken into account only in the numerical model.

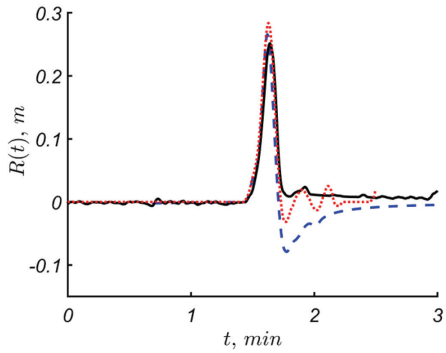

***Figure 3**. Runup height on a beach of the long solitary-like wave with an initial amplitude, A = 0.1 m and wave period, T = 20 s. The experimental record is shown by the black solid line, analytical solution is shown by the blue dashed line, and numerical solution is shown by the red dotted line.*

Fig. 4 shows the maximum runup height, R_{max}/A, as a function of distance to the slope, X_0/λ, for different amplitudes of the initial wave, A/h_0. The distance of the wave propagation X_0/λ changes from 0.8 to 9.4, kh_0 = 0.38. The numerical solution is shown with symbols (triangles, squares, and circles), while the analytical solution is shown with

lines. For smaller values of $X_0/\lambda < 6$, the analytical predictions provide relatively smaller runup values compared with numerical predictions, while for higher values of $X_0/\lambda > 6$, the differences are significantly reduced, whereas the analytical solution gives higher predictions of maximum runup height. As stated above, we consider that this can be a result of the interplay of two effects: the analytical prediction did not take into account the interaction with the underwater bottom slope, and the numerical scheme dissipation ("numerical error"), which affects the numerical results. Fig. 5 demonstrates the dependence of maximum runup height, R_{max}/A, on kh_0, taking the initial wave amplitude $A/h_0 = 0.03$. It can be seen that the discrepancy between numerical and analytical predictions decreases with an increase in kh_0. This effect can be explained by the wave interaction with the slope, which is not accounted in our analytical approach. As one can see in Fig. 6, this difference for a gentler beach slope $tan\ \alpha = 1{:}50$ is reduced, therefore, this result supports the conclusions drawn above.

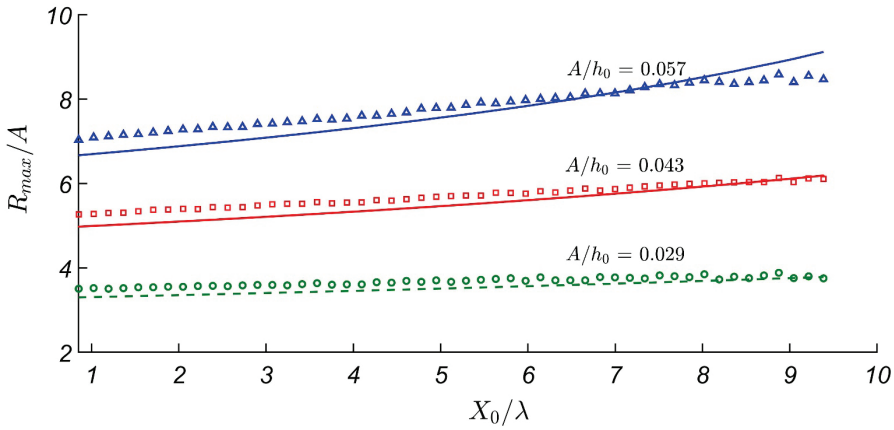

***Figure 4**: Maximum runup height, R_{max}/A, as a function of distance to the slope, X_0/λ for different amplitudes of the initial wave, A/h_0. Analytical solution is shown with lines and the numerical solution is shown with symbols (triangles, squares and circles) with matching colours, $kh_0 = 0.38$.*

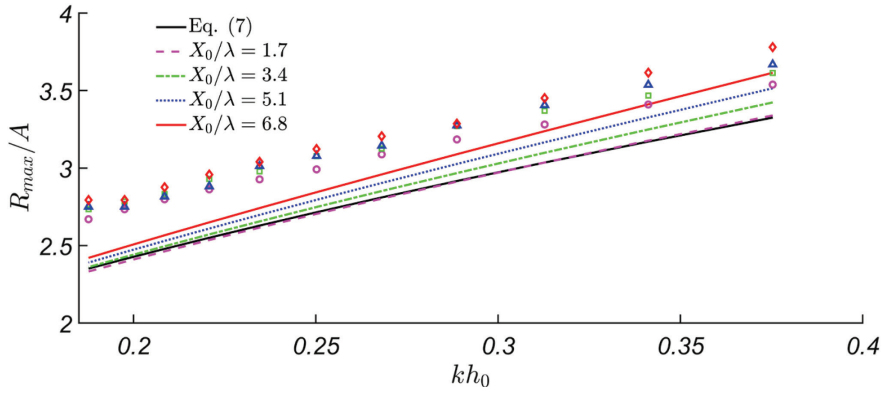

***Figure 5**: Maximum runup height, R_{max}/A, vs the initial wave amplitude, A/h_0, for different distances to the slope, X_0/λ. The numerical solution (NLSW) is shown with symbols (diamonds, triangles, squares and circles), the analytical solution is shown with lines with matching colours. The thick black line corresponds to Eq. (7), $kh_0 = 0.38$.*

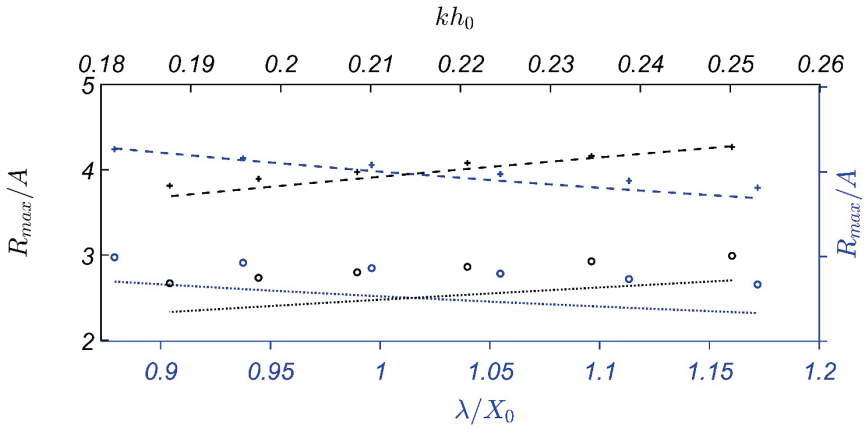

***Figure 6**: Maximum runup height, R_{max}/A vs λ/X_0 (blue axes), and kh_0 (black axes). Numerical solutions for tan α = 1:20 and tan α = 1:50 are shown with circles and crosses respectively, while analytical solutions for tan α = 1:20 and tan α = 1:50 are shown with dotted and dashed lines respectively, $A/h_0 = 0.03$.*

Fig. 7 enhances the conclusions mentioned above. Moreover, the dissimilarity between analytical and numerical results increases with an increase in the wave period. With respect to small wave periods, the numerical solution may coincide with the analytical one or even become smaller as in $kh_0 = 0.38$ for $X_0/\lambda > 8$. Noticeable, both analytical and numerical results in Figs. 5 and 8 demonstrate an increase in maximum runup height with an increase in the distance X_0/λ. This result confirmes the conclusions of Didenkulova et al. (2007) and Didenkulova (2009) for sinusoidal waves. The definition of the maximum wave front steepness s is the maximum of the time derivative of water displacement, $d(\eta/A)/d(t/T)$, and is calculated in relation with an initial wave front steepness, s_0, where

$$s(x) = \frac{\max\left(d\eta(x,t)/dt\right)}{A/T}, \quad s_0 = \frac{\max\left(d\eta(x=a,t)/dt\right)}{A/T}. \tag{17}$$

We should separate the incident wave and the wave reflected from the bottom slope, in order to calculate the incident wave front steepness at the beginning of the bottom slope from the results of numerical simulations. At the same time, the wave steepening along the basin of constant depth is described analytically, as demonstrated in Fig. 8.

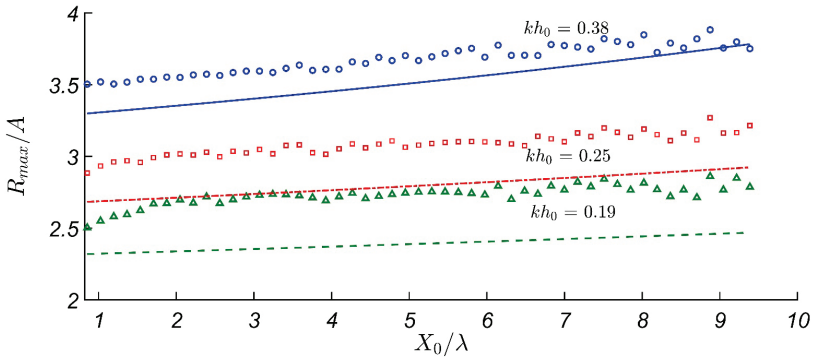

***Figure 7**. Maximum runup height, R_{max}/A as a function of the distance to the slope, X_0/λ for different kh_0. Analytical solution is shown with lines and the numerical solution is shown with symbols (triangles, squares and circles) with matching colors; $A/h_0 = 0.03$.*

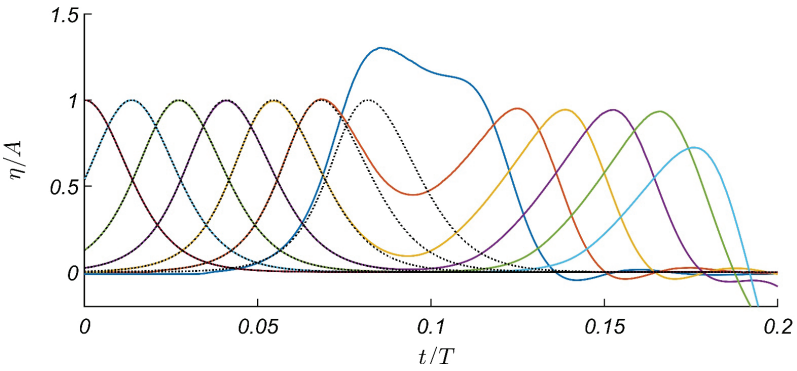

***Figure 8**: Wave evolution at different locations x/λ = 0, 0.85, 1.71, 2.56, 3.41, 4.27 and 5.12 along the section of constant depth for a basin with $X_0/\lambda = 5.12$ and tan α = 1:20. Numerical results are shown with solid lines, while the analytical predictions are given by the black dotted lines. The parameters of the wave: $A/h_0 = 0.03$, $kh_0 = 0.19$.*

It can be seen in Fig. 8 that the wave transformation is well described by the analytical solution, which has a good agreement with numerical simulations. Therefore, below we refer to the wave front steepness defined analytically; keeping in mind that it coincides well with the numerical predictions. In Fig. 9, we approach the main result of this section. The red solid line gives the analytical prediction. It is universal for single waves of positive polarity for different amplitudes A/h_0 and kh_0 and can be approximated well by the power fit (coefficient of determination $R^2 = 0.99$):

$$R_{\max}/R_0 = \left(s/s_0\right)^{0.42} \tag{18}$$

where R_{max}/A is the maximum runup height in the conjoined basin (with a section of constant depth); R_0/A is the corresponding maximum runup height on a plane beach (without a section of constant depth).

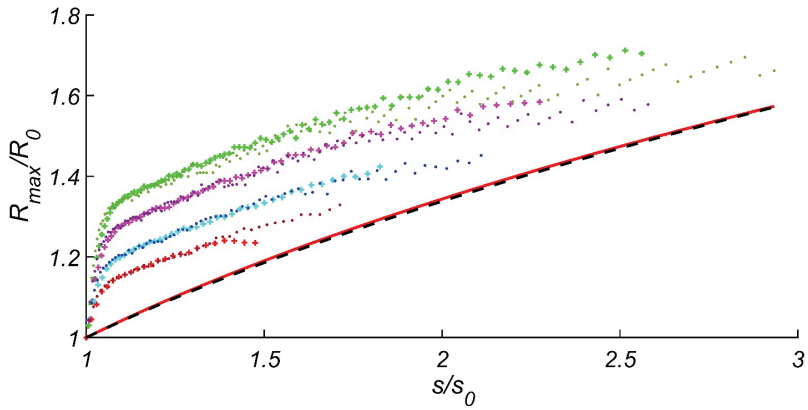

***Figure 9.** The maximum runup height in the conjoined basin, R_{max}/A normalized by the maximum runup height on a plane beach, R_0/A versus the wave front steepness, s/s_0 for $A/h_0 = 0.057$, $kh_0 = 0.38$ (brown points), $A/h_0 = 0.086$, $kh_0 = 0.38$ (red plus signs), $A/h_0 = 0.057$, $kh_0 = 0.29$ (blue points), $A/h_0 = 0.086$, $kh_0 = 0.29$ (turquoise plus signs), $A/h_0 = 0.057$, $kh_0 = 0.22$ (violet points), $A/h_0 = 0.086$, $kh_0 = 0.22$ (pink plus signs), $A/h_0 = 0.057$, $kh_0 = 0.19$ (dark green points), $A/h_0 = 0.086$, $kh_0 = 0.19$ (light green plus signs). The asymptotic analytical predictions are given by the red solid line, while all the markers correspond to the results of numerical simulations. The power fit of the analytical results Eq. (18) is shown by the dashed line.*

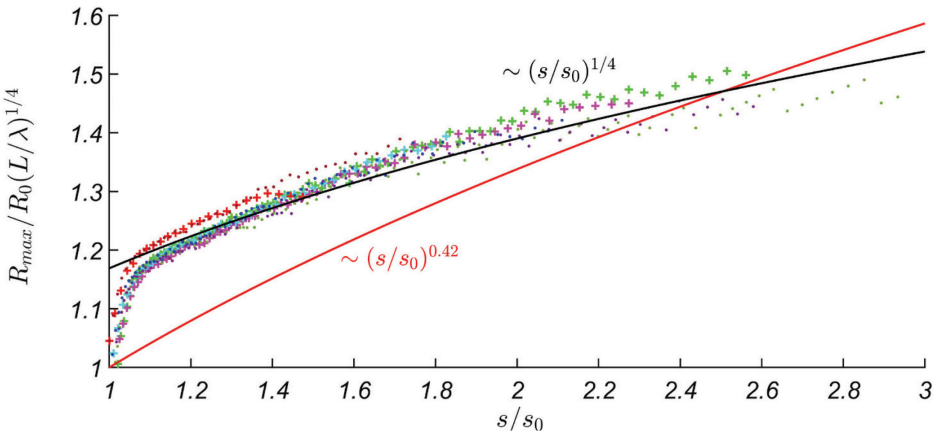

Figure 10: *The normalized maximum runup height $R_{max}/R_0(L/\lambda)^{1/4}$ calculated numerically versus the wave front steepness, s/s_0 for the same values of A/h_0 and kh_0 as in Figure 9. Red solid line corresponds to the "analytically estimated" Eq. (18), while black solid line corresponds to Eq. (19).*

The results of numerical simulations are shown in Fig. 9 with different markers corresponding to different incident wave conditions. It can be seen that numerical data for initial waves with the same period but different amplitudes follow the same curve. The runup is higher for waves with smaller kh_0. In our opinion, this dependence on kh_0 is a result of merging a plane beach with a flat bottom. This effect can be parameterized with the factor $(L/\lambda)^{1/4}$. The result of this parameterization is shown in Fig. 10. Here we can see that for smaller face front wave steepness, $s/s_0 < 1.5$, the runup height is parallel to the analytically estimated curve described by Eq. (19), while for larger face front wave steepness, $s/s_0 > 1.5$, the dependence on s/s_0 is weaker. This dependence for all numerical runup height data, presented in Fig. 10, can be approximated by the power fit (coefficient of determination R^2 =0.85):

$$R_{\max}/R_0 = 1.17\left(\lambda/L\right)^{1/4}\left(s/s_0\right)^{1/4} \tag{19}$$

3.2 Effects of dispersion on long wave runup

In this section, which is based on **papers II** and **III**, we study the applicability of the dispersive and nondispersive models to describe the propagation and runup of long periodic waves along a composite bottom topography: a flat bottom of constant depth is merged with a plane beach. Numerical calculations are carried out in the framework of NLSW and mPer models, and are compared with laboratory experiments for various types of waves: solitary-like waves, sine waves, bi-harmonic waves and "ship" wave packets, highly modulated in frequency and amplitude.

Typical estimates of the power spectral density for the three types of waves are presented in Fig. 11. The figure shows that for sine and bi-harmonic waves, the main period is the same and equal to 20 s, while for ship wakes the period of 20 s corresponds to the beginning of a wide peak. The length of such waves in the channel of h = 3.5 m depth is 117 m, and the parameter kh = 0.2, where k is the wave number. The numerical results of the runup height of periodic waves are compared with the available measurements. In particular, the calculated and measured maximum runup heights of the first four waves for each wave type are compared. The numbers 1, 2, 3 and 4 on the

graph represent the maximum runups of the first, second, third and fourth waves, respectively.

It can be seen that in the calculations made using the dispersive theory, mPer (right column in Fig. 12), the deviations from the experiment are smaller. It is also seen that with an increase in the wave amplitude, the difference between the calculations and the experiment decreases and, ultimately, leads to an underestimation of the runup height. This effect is associated with the wave breaking. With respect to the regular type of waves (sine waves), the rough asphalt reduces the values of the runup height to $\approx 20\%$ compare to the plastic (frictionless) bottom, see Table 2 and Table 3. Table 2 shows the wave characteristics while Table 3 shows the maximum runup heights of the first four waves for different wave shapes, (1) solitary, (2-a) sine wave on a plastic bottom, (2-b) sine wave on an asphalt bottom, (3) bi-harmonic waves, and (4) ship wakes. Fig. 13 shows the oscillations of the water surface for a sine wave with a height of 0.2 m. It can be seen that both NLSW and mPer describe the experimental data quite well. Fig. 14a shows a smooth runup of a sine wave with a small height of 0.2 m, while in Fig. 14b, we see the runup of a more nonlinear wave of 0.4 m high. It can be seen in Fig. 14a, that both models describe the runup of weakly nonlinear wave rather well. For runup of a more non-linear wave (Fig. 14b), mPer turns out to be a more adequate model. As noted before, when the wave run down the slope during experiments, a layer of water remained on the slope, so that the sensor poorly registered the descending sections of the signal. This is especially pronounced in recordings of large-amplitude waves, for which nonlinear effects are the most noticeable at the stage of wave rundown (Didenkulova et al, 2006, Didenkulova et al, 2014). Despite the fact that at a qualitative level, both models reproduce the experiment well, see Fig. 13 and Fig. 14, there are quantitative differences, which are especially noticeable for the large values of the maximum runup (Fig. 12). It is shown also in Fig. 12 that the dispersive theory is characterized by a smaller deviation from the experimental data and, in general, more reliably describes sine waves. It is also seen that both theories tend to underestimate the runup of large-amplitude waves, which is a consequence of the wave breaking (see Fig. 12).

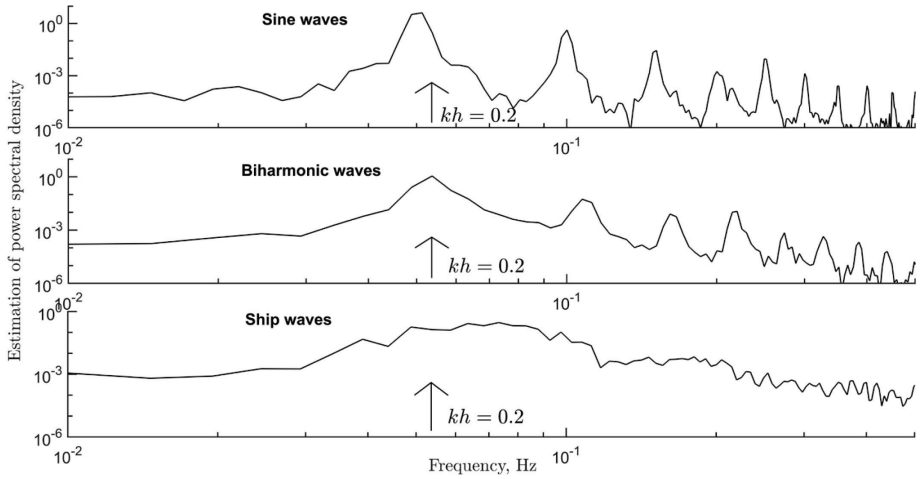

Figure 11. *Estimation of the power spectral density of the studied types of waves.*

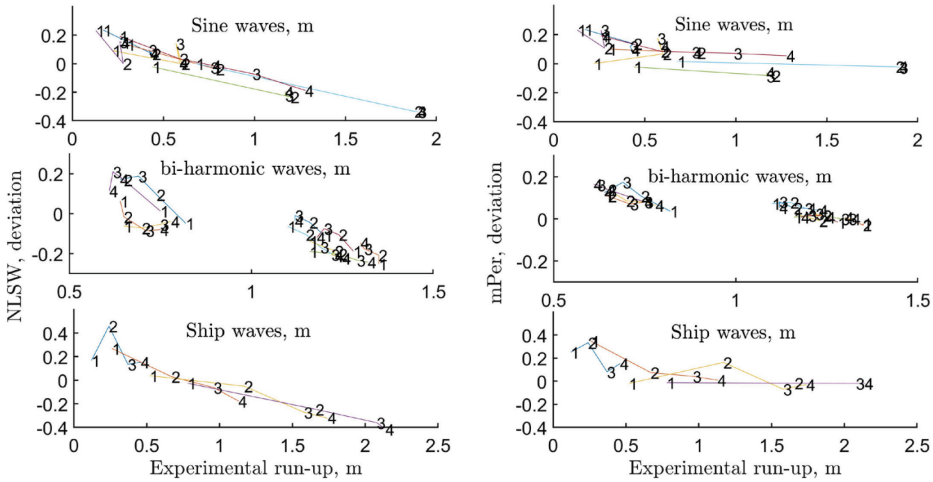

***Figure 12**. The deviations from the experiment of maximum runup heights calculated using NLSW (left column) and mPer (right column) for different types of waves. The numbers 1, 2, 3 and 4 correspond to the maximum runup height of the first, second, third and fourth waves.*

***Table 3.** Maximum runup heights of the first four waves of a solitary (1), sine (2), bi-harmonic (3) and ship wake (4)*

	Exp. NO.	Experiment				NLSW				mPer			
		1th	2th	3th	4th	1th	2th	3th	4th	1th	2th	3th	4th
	2074	0.8	0	0	0	0.98	0	0	0	0.84	0	0	0
	2075	0.61	0	0	0	0.71	0	0	0	0.65	0	0	0
	2076	0.44	0	0	0	0.5	0	0	0	0.48	0	0	0
	2077	0.29	0	0	0	0.3	0	0	0	0.29	0	0	0
	2012	0.17	0.23	0.23	0.23	0.22	0.29	0.27	0.28	0.18	0.24	0.22	0.24
	2013	0.26	0.37	0.38	0.37	0.32	0.46	0.47	0.44	0.25	0.36	0.38	0.36
	2014	0.37	0.56	0.56	0.56	0.44	0.65	0.64	0.59	0.34	0.51	0.49	0.51
	2015	0.48	0.75	0.77	0.77	0.57	0.81	0.81	0.77	0.45	0.65	0.66	0.67
(2-a)	2016	0.62	1	1.01	1.03	0.73	0.97	0.96	0.94	0.58	0.81	0.8	0.83
	2017	0.77	1.14	1.13	1.14	0.83	1.08	1.1	1.03	0.67	0.97	0.99	0.98
	2018	0.95	1.35	1.35	1.36	0.95	1.22	1.2	1.15	0.8	1.18	1.16	1.16
	2019	1.08	1.63	1.66	1.66	1.05	1.32	1.3	1.26	0.93	1.38	1.35	1.35
	2020	1.15	1.87	1.89	1.92	1.12	1.39	1.41	1.35	1.02	1.53	1.55	1.53
	2021	1.28	2.11	2.07	2.13	1.19	1.46	1.47	1.43	1.15	1.7	1.72	1.73
	2022	1.43	2.38	2.36	2.38	1.27	1.54	1.55	1.49	1.28	1.9	1.92	1.91
	1002	0.17	0.44	0.42	0.43	0.21	0.47	0.46	0.46	0.21	0.5	0.47	0.47
(2-b)	1003	0.3	0.79	0.76	0.77	0.34	0.76	0.74	0.76	0.33	0.85	0.82	0.83
	1004	0.22	0.6	0.57	0.59	0.24	0.6	0.65	0.59	0.22	0.64	0.67	0.66
	1006	0.13	0.28	0.26	0.27	0.16	0.28	0.3	0.31	0.16	0.31	0.32	0.32
	1007	0.44	1.2	1.17	1.17	0.43	0.92	0.91	0.94	0.43	1.1	1.07	1.1
	1008	0.68	1.88	1.9	1.9	0.68	1.25	1.26	1.26	0.69	1.84	1.85	1.86
	1069	0.26	0.59	0.99	1.28	0.31	0.61	0.92	1.04	0.31	0.64	1.06	1.35

	1014	0.82	0.74	0.69	0.64	0.78	0.81	0.82	0.75	0.85	0.82	0.81	0.72
	1015	0.64	0.65	0.71	0.75	0.68	0.64	0.65	0.69	0.71	0.72	0.76	0.81
	1017	0.65	0.7	0.75	0.78	0.61	0.65	0.71	0.75	0.74	0.76	0.81	0.83
	1018	0.75	0.65	0.62	0.61	0.76	0.76	0.75	0.68	0.81	0.74	0.72	0.71
	1019	1.16	1.24	1.29	1.32	0.94	0.99	0.99	1	1.17	1.26	1.29	1.32
(3)	1020	1.1	1.15	1.19	1.23	1.03	1.03	0.99	0.97	1.18	1.24	1.25	1.28
	1021	1.28	1.24	1.2	1.18	1.04	1.11	1.11	1.04	1.26	1.26	1.22	1.19
	1024	1.2	1.16	1.12	1.12	1.07	1.11	1.11	1.08	1.26	1.22	1.21	1.18
	1025	1.35	1.35	1.31	1.3	1.01	1.07	1.08	1.11	1.32	1.31	1.31	1.31
	1027	1.16	1.23	1.22	1.25	1	1	0.97	0.97	1.19	1.22	1.25	1.26
	1047	0.12	0.24	0.37	0.46	0.14	0.35	0.42	0.53	0.15	0.32	0.4	0.53
	1051	0.26	0.67	0.96	1.13	0.33	0.69	0.9	0.93	0.35	0.72	1	1.14
	1052	0.52	1.17	1.58	1.74	0.54	1.11	1.15	1.18	0.51	1.36	1.47	1.69
	1053	0.78	1.66	2.08	2.14	0.76	1.25	1.33	1.25	0.77	1.63	2.04	2.1

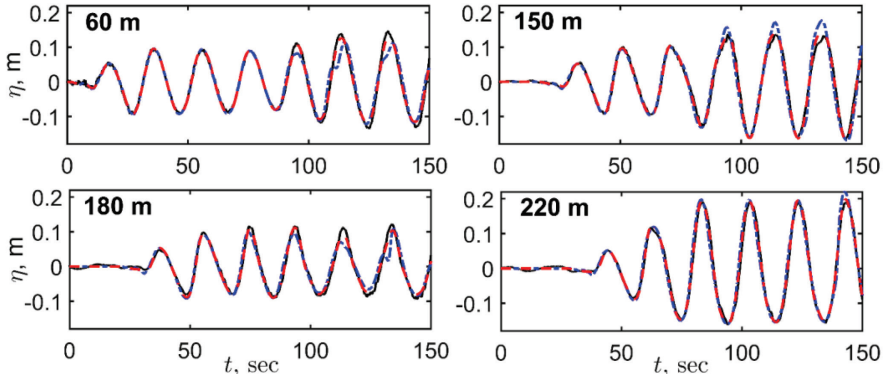

Figure 13. *Wave gauge records of the water surface for a sine wave with a height of 0.2 m. A solid line represents the experimental record, NLSW calculations are shown by a dash-dotted line, and mPer calculations are shown by a dashed line.*

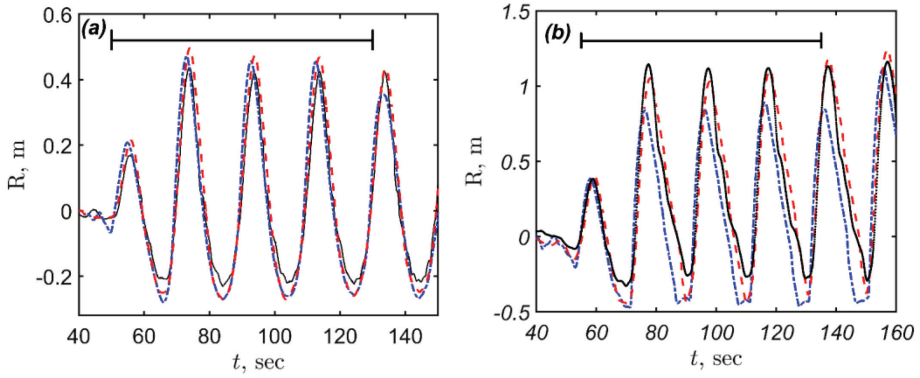

Figure 14. *Runup height time-series of the sine waves with a height of (a) 0.2 m and (b) 0.4 m. A solid black line represents the experimental record, NLSW calculations are shown by a blue dash-dotted line, and mPer calculations are shown by a red dashed line. The scale at the x-axis corresponds to the travel time from the coast to the wave maker and back.*

Fig. 15 shows that rundown of low-amplitude bi-harmonic waves is described even worse by the experiment than the case of sine waves. This is probably due to the presence of short wave components in the spectrum. For the considered range of wave heights, mPer seem to be more reliable model than NLSW (Fig. 15). At low wave amplitudes, it slightly overestimates the runup height (4–17%), while giving a smaller scatter than NLSW, which both overestimates (up to 20%) and underestimates (up to 10%) the runup height values. At higher amplitudes, it slightly underestimates (no more than 3%) the runup height, providing a minimum scatter in comparison with NLSW, which underestimates the values of runup heights up to 25%. Finally, let us consider the ''ship wakes'', the wave packets modulated in frequency and amplitude. The period of these waves decreases linearly from 20 to 10 s, see Fig. 11. The runup of these waves for experimental tests with heights 0.12 m and 0.42 m is shown in Fig. 16 and Table 3. It can be seen that both models well describe the waves of low amplitude (Fig. 16a). However, NLSW clearly fails describing high amplitude waves (Fig. 16b), underestimating the expected runup height by more than 40%. This is associated with the effects of wave breaking. The mPer model gives a smaller error in the description of ship wakes. Moreover, for mPer the underestimation of the runup height for the highest waves does not exceed 7%. As for the sine waves, the described tendency is observed for the majority of waves in the group (Fig. 12). If we compare directly between the predictions of two numerical models, it can be seen that, NLSW gives a larger error than mPer (Fig. 12). However, for ship wakes, the error of NLSW can be both positive (overestimation) and negative (underestimation).

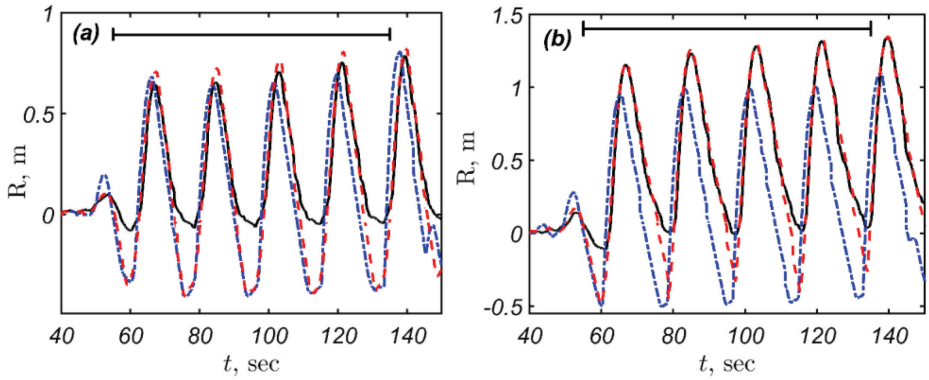

Figure 15. *Runup height time-series of the bi-harmonic waves with a height of (a) 0.27 m and (b) 0.4 m. A black solid line represents the experimental record, mPer calculations are shown by a red dashed line and NLSW calculations are shown by a blue dash-dotted line. The scale at the x-axis corresponds to the travel time from the coast to the wave maker and back.*

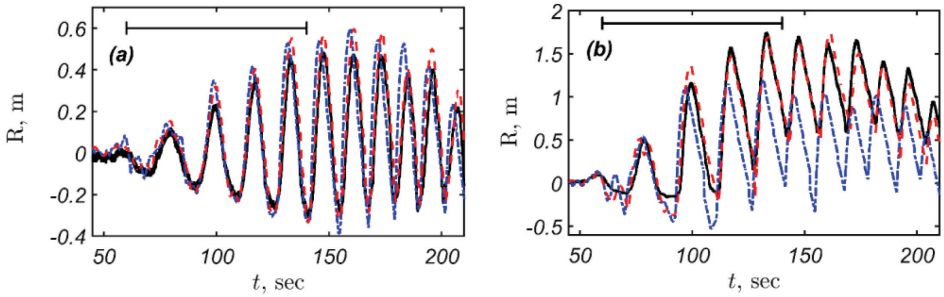

Figure 16. *Runup height time-series of ship wakes modulated in frequency and amplitude with a maximum height of a) 0.12 m and b) 0.42 m. A solid black line represents the experimental record, NLSW calculations are shown by a blue dash-dotted line, and mPer calculations are shown by a red dashed line. The scale at the x-axis corresponds to the travel time from the coast to the wave maker and back.*

3.3 Runup of irregular waves

The runup of initial Gaussian narrow-banded and wide-banded wave fields and its statistical characteristics are studied using direct numerical simulations, based on NLSW. We use the same bathymetry of the GWK experiment described in section (2.3), which consists of the section of a constant depth, which is matched with the beach of constant slope, see Fig. 2. The results below correspond to **paper IV**.

In order to study the influence of wave nonlinearity during irregular wave propagation and runup on the coast, time-series with five different significant wave heights are considered (H_s/h_0 = 0.03, 0.06, 0.09, 0.11, and 0.14) for both narrow-band ($\Delta f/f_0$ = 0.1) and wide-band ($\Delta f/f_0$ = 0.4) signals. The physical time for each H_s is 1000 hr(360,000 wave periods), 5000 hr for each bandwidth, and 10,000 hr in total. The computations of the numerical model were carried out in MATLAB, using a cluster containing 28 cores. The parameter kh_0 = 0.38 is at the border of validity of the shallow water theory, taking into account the horizontal extent of the wave tank. The wave parameters are selected to see the effects of wave breaking on the statistics of their runups. The types of wave breaking are classified based on the Iribarren number:

$$Ir = \frac{\alpha}{\sqrt{H/L}} \tag{20}$$

where L is the characteristic wavelength offshore, H is the wave height. It is spilling for $Ir \le 0.5$, plunging for $0.5 \le Ir \le 3.3$, and surging when $Ir \ge 3.3$. In our dataset, only the last two types of wave breaking, surging (including collapsing) and plunging, are observed. For the case of weak-nonlinearity (H_s/h_0 = 0.03), less than 1% of waves experience plunging breaking, while most of the waves are surging. With an increase in nonlinearity, the percentage of plunging waves increases, for H_s/h_0 = 0.06, 32–35% of the waves are plunging, for H_s/h_0 = 0.09, 61–65% of the waves are plunging, for H_s/h_0 = 0.11, 71–76% of the waves are plunging, and for the most nonlinear case, H_s/h_0 = 0.14, 85–88% of the waves are plunging.

The probability density functions (PDF) of narrow-band and wide-band incident wave fields for different nonlinearities, H_s/h_0 are shown in Fig. 17. The data of the narrow-band spectra, $\Delta f/f_0$ = 0.1 are shown by triangles (different colours correspond to different nonlinearities). The corresponding Gaussian distribution (μ = 0, σ = 0.25) is shown by the

black solid line. The data of the wide-band spectra, $\Delta f/f_0$ = 0.4 are shown by pluses, and the corresponding Gaussian distribution (μ = 0, σ = 0.27) is shown by the red solid line.

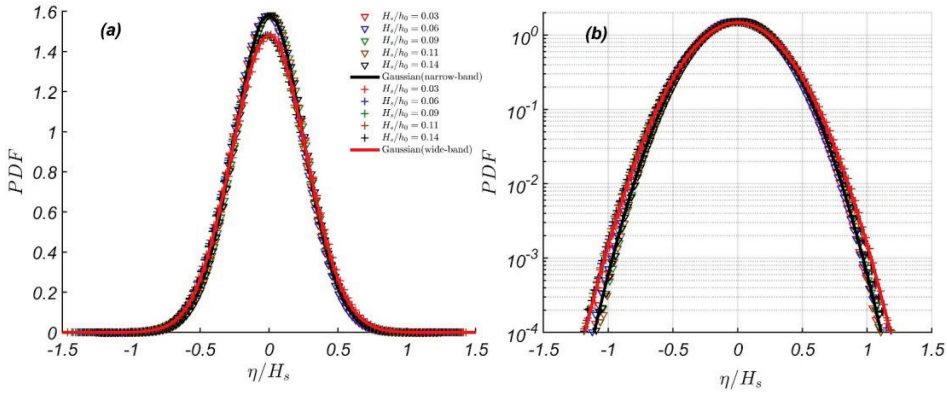

Figure 17. *Probability density functions of normalized narrow-band and wide-band wave fields offshore for different nonlinearities, H_s/h_0 in linear (a) and logarithmic (b) scales. Solid lines correspond to Gaussian distributions fitted to the corresponding datasets, shown with a black colour for wide-band data and with red colour for narrow band data.*

To describe the statistics of wave heights in Fig. 18, the Rayleigh distribution, which is well used for this type of problem (Massel, 1996), is applied:

$$f(\xi) = \begin{cases} \dfrac{\xi}{\lambda^2} e^{-\xi^2/(2\lambda^2)}, & \xi \geq 0 \\ 0, & \xi < 0 \end{cases} \tag{21}$$

where ξ is a data vector of wave heights, and λ is the scale parameter. However, a better fit for the wave heights has been found according to a Weibull distribution:

$$f(\xi) = \begin{cases} \dfrac{k}{\lambda}\left(\dfrac{\xi}{\lambda}\right)^{k-1} e^{-(\xi/\lambda)^k}, & \xi \geq 0 \\ 0, & \xi < 0 \end{cases}, \tag{22}$$

where λ is the scale parameter and k is the shape parameter. Fig. 18 demonstrates the wave height distributions of both narrow-band and wide-band wave fields. As expected, the narrow-band data are well described by a Rayleigh distribution (λ = 0.5), however, a Weibull distribution (λ = 0.74, k = 2.27) provides a slightly better fit than a Rayleigh distribution, which can be explained by the effects of wave breaking, which deviate the distribution from Rayleigh to Weibull. This result is confirmed by some field measurements (e.g. You and Nielsen, 2013, Neelamani et al., 2007). For the wide-band conditions, the wave heights have a tendency to be distributed according to a Weibull distribution (λ = 0.71, k = 2.06).

Also, it can be seen in Fig. 18, the probability of the freak wave ($H/H_s \geq 2$) occurrence in the initial wave field is higher for narrow-band signals than for wide-band ones.

The calculated significant runup heights (defined as a mean of one third of the largest runup heights), R_s for narrow-band and wide-band signals are shown in Fig. 19. It is interesting to see that R_s for wide-banded waves is always higher than for narrow-banded

waves and increases with an increase in H_s, which can be explained by the higher variability in wave periods for wide-banded waves as well as the more intense wave breaking in case of narrowband conditions, where the R_s/h_0 decreases with an increase in nonlinearity H_s/h_0.

Fig. 20 illustrates the probability distribution functions of runup oscillations, r/R_s for initial Gaussian narrow-banded and wide-banded wave signals. It can be seen from Fig. 20a that runup oscillations of narrow-banded waves are deviated from the normal distribution and are slightly shifted to the right towards larger positive values with an increase in nonlinearity. This effect was partially observed experimentally (Denissenko et al, 2011, Denissenko et al, 2013) and theoretically (Didenkulova, 2011, Gurbatov and Pelinovsky, 2019) for an infinite plane beach. However, the tails of these distributions show a relatively weak probability of extreme floods for narrow-banded waves, and are much thinner than of Gaussian distribution.

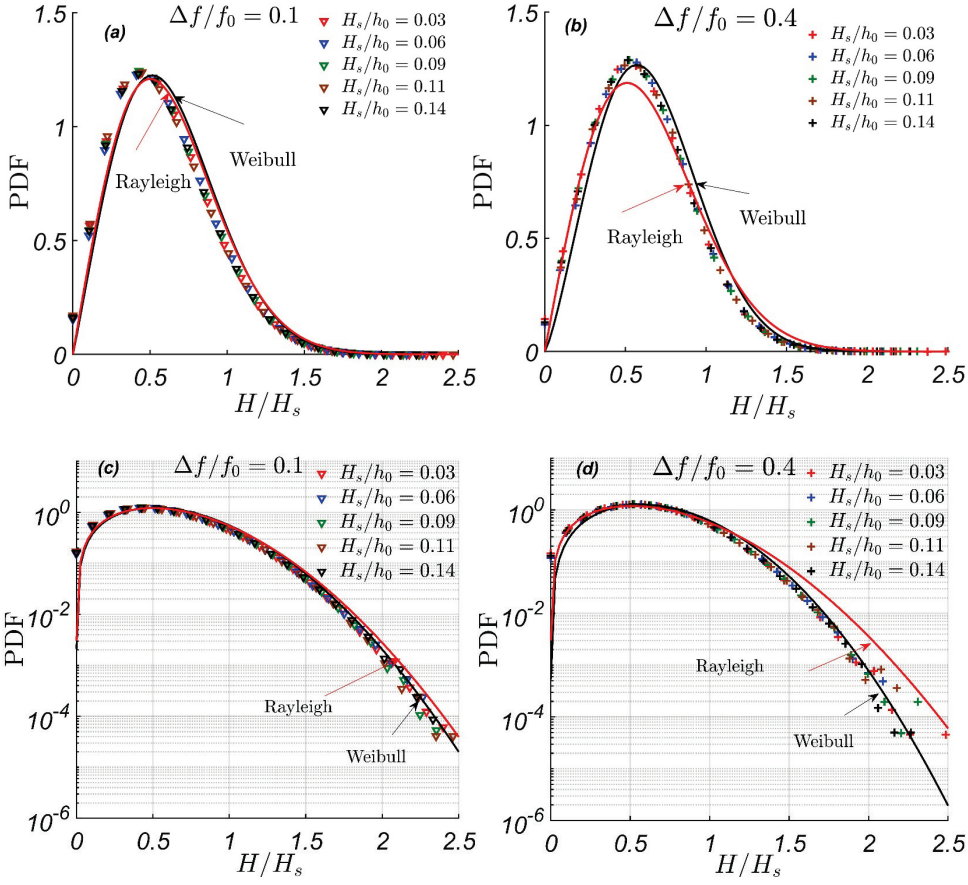

***Figure 18**. Probability density functions of normalized trough-to-crest wave heights of the initial narrow-band (a) and (c), and wide-band (b) and (d) wave fields for different nonlinearities, H_s/h_0 in linear (top) and logarithmic (bottom) scales. The red solid line corresponds to the Rayleigh distribution; the black solid line corresponds to the Weibull distribution fitted to the corresponding dataset.*

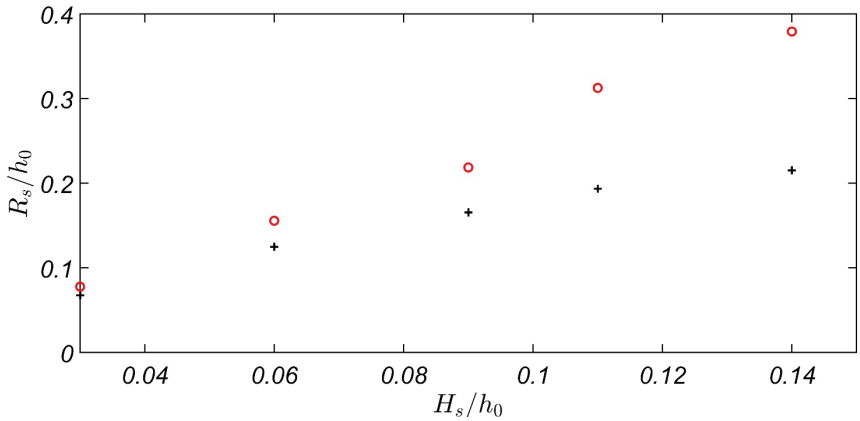

***Figure 19**. Significant runup heights, R_s for wide-band (red circles) and narrow-band (black crosses) signals for different nonlinearities.*

It can be seen that in the case of initial wide-band signal, the distributions of runup oscillations are also shifted to the right with an increase in nonlinearity, however, this shift is much larger compared to that of the narrow-band signal. Moreover, the tails of these distributions are much thicker than those of narrow-band ones. However, the distribution of runup oscillations is rather close to the normal distribution in case of the initial wide-band signal. It can also be seen that for both wide-banded and narrow-banded waves, the probability of large waves decreases with an increase in wave nonlinearity, which can be explained by wave breaking.

Fig. 21 depicts the statistical moments of narrow-banded and wide-banded waves offshore, normalized by H_s, and the corresponding runup oscillations on a beach, normalized by R_s. The statistical moments, mean,$< \xi >$, variance, σ, skewness, Sk, and (normalized) kurtosis, $Kurt$ are calculated as:

$$< \xi >= \frac{1}{n}\sum_{i=1}^{n}\xi_i \ , \ \sigma^2(\xi) = \frac{1}{n}\sum_{i=1}^{n}\left(\xi_i - < \xi >\right)^2 \tag{23}$$

$$Sk(\xi) = \sum_{i=1}^{n}\frac{1}{n\sigma^3(\xi)}\left(\xi_i - < \xi >\right)^3 \ , \ Kurt(\xi) = \sum_{i=1}^{n}\frac{1}{n\sigma^4(\xi)}\left(\xi_i - < \xi >\right)^4 - 3 \tag{24}$$

where ξ is a data vector, and n is its length.

Notably, the statistical moments (mean, skewness and kurtosis) of both narrow-banded and wide-banded initial wave fields are zero, providing the required Gaussian statistics. With respect to runup oscillations, it can be seen that for both narrow- and wide-banded waves, the mean of runup oscillations increases with the nonlinearity, which reflects the known effect of wave set-up on a beach. For relatively weak wave nonlinearities (H_s/h_0 = 0.03, 0.06, and 0.09), the set-up for narrow-banded waves is larger than for wide-banded ones, while for slightly strong wave nonlinearities (H_s/h_0 = 0.11, and 0.14), it is the opposite due to the wave breaking. For narrow-banded waves, the variance changes non-monotonically with an increase in nonlinearity, while for wide-banded waves the variance decreases. The higher moments (skewness and kurtosis) of runup oscillations for waves with a narrow-band spectrum are negative and decrease with an increase in wave nonlinearity, while for waves with a wide-band spectrum they are sign-variable.

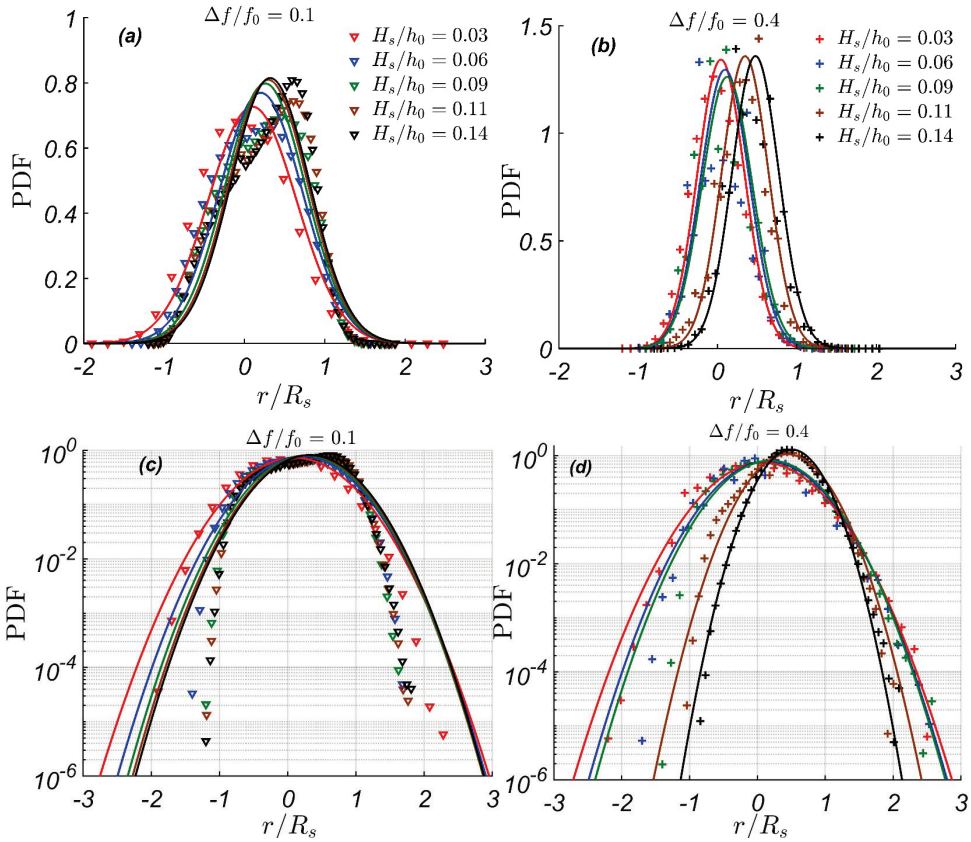

Figure 20. *Probability density functions of runup oscillations, normalized by a significant runup height, R_s, for different nonlinearities for narrow-banded (a) and (c), and wide-banded (b) and (d) waves in linear (top) and logarithmic (bottom) scales. Solid lines correspond to Gaussian distributions, fitted to the corresponding datasets, using the matching colours.*

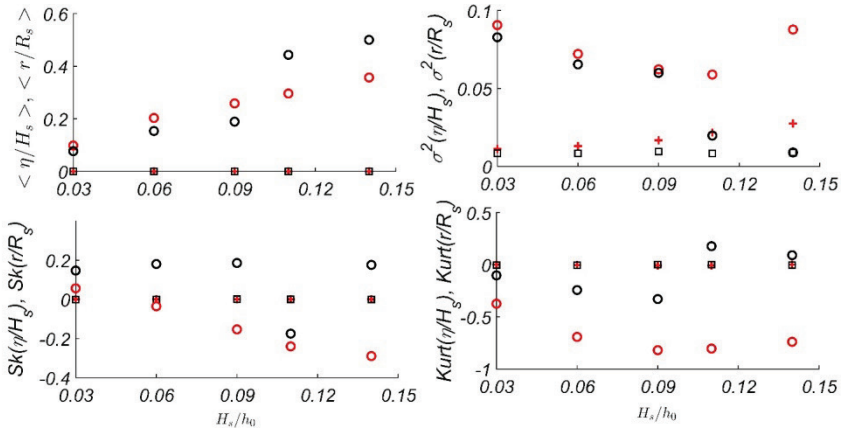

Figure 21. *Statistical moments of runup oscillations (normalized by R_s) of narrow-banded (red circles) and wide-banded (black circles) waves on a beach, r, versus nonlinearity, H_s/h_0. Statistical moments of narrow-band and wide-band wave fields offshore (normalized by H_s) are shown by red crosses and black squares, respectively.*

The distribution of extreme wave runup heights, $R_{extrm} = R/R_s \geq -th$, where th is some threshold value, in some way behaves similarly to a conditional Weibull law whose density is given by Eq. (25):

$$f(R_{extrm}) = \begin{cases} \frac{k}{\lambda}\left(\frac{R_{extrm}}{\lambda}\right)^{k-1} e^{-(R_{extrm}/\lambda)^k + (th/\lambda)^k}, & R_{extrm} \geq th \\ 0, & R_{extrm} < th \end{cases} \quad (25)$$

A conditional Weibull distribution (Eq. 25) is characterized by three parameters: the shape k, the scale λ and the threshold th. Given the data, $(R_{i\ extrm}) = 1...n$, th is fixed and k and λ are computed by maximum likelihood estimator. From Eq. (26), we obtaine the scale parameter, λ:

$$\lambda = \left(\frac{1}{n}\sum_{i=1}^{n}\left(R_{i\ extrm}^k - th^k\right)\right)^{\frac{1}{k}}. \quad (26)$$

where n is the number of extreme wave runups. In order to obtain the shape parameter, k, we should solve Eq. (27):

$$\frac{1}{k}(I_n - th^k) + (\ln th)th^k + M_n(I_n - th^k) - V_n = 0, \quad (27)$$

where $M_n = \frac{1}{n}\sum_{i=1}^{n}\ln R_{i\ extrm}$, $I_n = \frac{1}{n}\sum_{i=1}^{n}R_{i\ extrm}^k$, $V_n = \frac{1}{n}\sum_{i=1}^{n}(\ln R_{i\ extrm})R_{i\ extrm}^k$

On gentle beaches, such freak runups ($R/R_s \geq 2$) are manifested as unexpected floods and may result in human injuries and fatalities (Nikolkina and Didenkulova, 2012, García et al, 2017, Didenkulova, 2020). Fig. 22 shows the probability distribution functions of extreme runup heights ($R \geq 0.7\ R_s$), in different wave nonlinearities and bandwidths (narrow-band and wide-band).

It can be seen that the tails of distributions, corresponding to freak runup events ($R/R_s \geq 2$) for narrow-banded waves decay much faster than the ones offshore ($H/H_s \geq 2$). This means, the probability of occurrence of freak runups for narrow-banded waves is much less than the probability of freak wave occurrence in the sea coastal zone. Therefore, we believe that the gentle beach works as some kind of "filter" for narrow-banded freak events. This is also manifested in the numbers of actual freak events, given in Table 4. It can be seen that for narrow-banded non-breaking waves of the smallest significant wave height ($H_s/h_0 = 0.03$), the number of freak events on a beach was reduced twice compared to the original number of freak waves offshore, while for waves with the larger significant waves heights, which were affected by the wave breaking, there were no freak runups at all, see Table 4.

However, for wide-banded waves, the probability of freak events on a beach is more or less the same as in the sea coastal zone and may even be higher (Fig. 22 b). With an increase in nonlinearity (and consequently, wave breaking), the number of freak runups on a beach decreases. However, for waves of moderate nonlinearities, the number of freak runups is still larger than the number of freak waves offshore, which may be explained by a wide range of wave periods associated with the wide-banded waves. The runup height of regular waves is proportional to $1/T^2$, hence, as smaller period,

as larger the runup and this dependence is quadratic and more powerful than linear dependence on the initial wave amplitude. Therefore, it is possible, the freak runups in wide-banded wave fields are mostly governed by wave periods. However, the number of freak runups on a beach suddenly drops down (Table 4)for the waves strongly affected by the wave breaking ($H_s/h_0 = 0.11$ and 0.14). The probability of extreme runups decreases with an increase in wave nonlinearity for wide-banded waves and changes non-monotonically with nonlinearity for narrow-banded waves. It is interesting to see that the tails of distributions in Fig. 22 acan be separated in two groups for "relatively large H_s/h_0" and "relatively small H_s/h_0", where the small group is always higher than the large group, this separation into groups can be explained by the wave breaking. The extreme runup heights, ($R/R_s \geq 0.7$) are distributed according to a conditional Weibull distribution (Eq. (25)), which gives acceptable results especially for narrow-banded waves, therefore, can be used for the estimation of extreme inundations (freak runups) on a beach. Furthermore, in future applications, the statistical analysis provided hereby might also be advantageous for other applications, such as, wave impacts on structures placed in shallow water conditions (Fazeres-Ferradosa et al., 2018, Vanem et al., 2019).

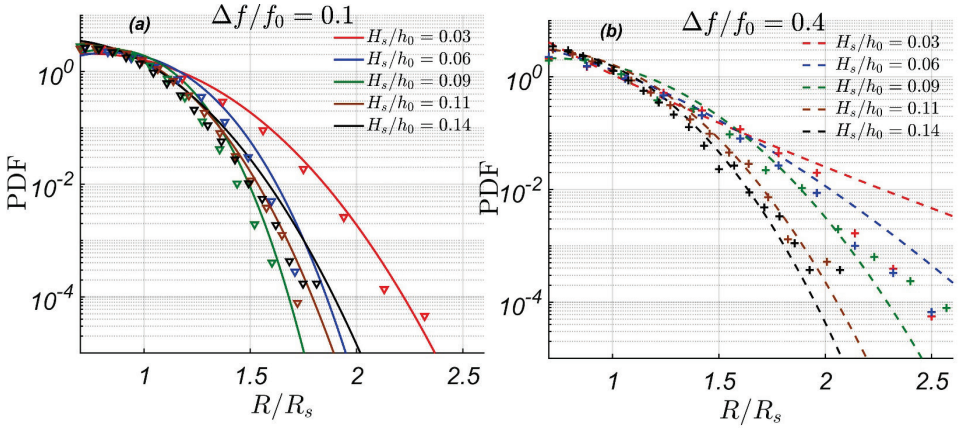

***Figure 22**. Probability density functions of large runup heights ($R \geq 0.7\ R_s$) for (a) narrow-banded (triangles) and (b) wide-banded (pluses) waves. Lines correspond to conditional Weibull distributions (Eq. 25), fitted to the narrow-band (solid lines) and wide-band (dashed lines) datasets, using the matching colours.*

***Table 4.** The number of freak events in the sea coastal zone and on a beach for different wave regimes.*

	$\Delta f/f_0 = 0.1$			$\Delta f/f_0 = 0.4$		
H_s/h_0	Number of Waves	Freak Waves Offshore	Freak Runups	Number of Waves	Freak Waves Offshore	Freak Runups
0.03	362255	125	61	389232	51	118
0.06	362380	117	0	389385	45	76
0.09	362096	89	0	389444	49	62
0.11	362319	88	0	389263	53	2
0.14	362302	102	0	389728	34	1

Table 5. *Parameters of a conditional Weibull distribution fitted to the corresponding datasets in Fig. 22.*

	$\Delta f/f_0 = 0.1$		$\Delta f/f_0 = 0.4$	
H_s/h_0	k	λ	k	λ
0.03	2.747	0.886	0.76	0.116
0.06	3.6	0.92	1.43	0.48
0.09	4.06	0.89	2.58	0.86
0.11	3.08	0.777	2.6	0.772
0.14	3.08	0.72	2.718	0.762

4. CONCLUSION

We studied the runup of nonlinear waves of different shapes (single tsunami waves, sinusoidal, bi-harmonic and ship wakes on a plane beach, taking into account wave nonlinearities, effects of dispersion and wave breaking. For all experiments, the bathymetry consisted of two sections: a flat bottom bathymetry with a constant depth merged with a constant beach slope. We used different methods: semi-analytical method, based on the solutions of the nonlinear shallow water theory, as well as nondispersive and dispersive numerical models, based on the nonlinear shallow water equations and modified Peregrine equations respectively. Both analytical and numerical results were compared with the experimental data obtained from Large Wave Flume (GWK), Hanover, Germany, between 2012 and 2013.

We studied the nonlinear deformation and runup of long single tsunami waves of positive polarity with kh changing from 0.18 to 0.38. Found that, the maximum tsunami runup height on a beach depends on the wave front steepness at the toe of the bottom slope. The corresponding formula, which could be used in tsunami early warning systems, is proposed.

The runup of periodic waves (regular, bi-harmonic and ship wakes) characterized by $kh = 0.2$ has been studied using dispersive and non-dispersive models and compared with experimental data from GWK. Concluded that, the dispersive effects in the given range of kh are principal for estimation of the runup height if the incident waves have large amplitudes, while for weakly nonlinear waves the nondispersive nonlinear shallow water theory is still good enough to estimate wave runup.

We studied the statistics of extreme wave runups using the numerical model based on the nonlinear shallow water theory with respect to different scenario of wave breaking, wave nonlinearity and bandwidth of the incident wave field. Found, that in the given range of $kh = 0.38$, wide-banded wave fields lead to a higher probability of freak runups on a beach compared to the probability of freak wave occurrence in the initial wave field. On the contrary, for narrow-banded wave signals, the slopping beach filters extreme runups, substantially reducing the probability of their occurrence. It is also suggested that the conditional Weibull distribution can be used for the description of extreme runup heights and for the assessment of extreme inundations.

Future work:

We aim to extend our investigations of the statistical analysis of freak wave's runup and the influences of dispersion effects on the extreme runup height on a plane beach using both dispersive and nondispersive models. We also would like to continue with the experiments on tsunami waves propagating over complex bathymetries (convex-plane beaches and plane-plane beaches). This work has already started and we foresee some interesting results there. We saw in GWK experiments with asphalt and plastic beach covers, that the beach roughness substantially reduces tsunami runup. Therefore, we would like to investigate the influence of beach roughness and bottom boundary layers on the runup height using available experimental data and to compare these results with dispersive and non-dispersive models. Numerically, we would like to examine different friction laws (Manning, Darcy, and Chézy laws).

References

Anthony, E. 2013. Storms, shoreface morphodynamics, sand supply, and the accretion and erosion of coastal dune barriers in the southern North Sea. Geomorphology, 199, pp. 8–21.

Battjes, J. 1972. Long-term wave height distributions at seven stations around the British Isles. Deutsche Hydrografische Zeitschrift, *25*(4), pp. 179–189.

Battjes, J. 1975. Surf similarity. In Coastal Engineering 1974 (pp. 466–480).

Battjes, J. and H.W. Groenendijk. 2000. Wave height distributions on shallow foreshores, Coastal Engineering, 40, 161–182.

Bellotti, G. and Brocchini, M. 2001. On the shoreline boundary conditions for Boussinesq-type models. International Journal for Numerical Methods in Fluids, 37(4), pp. 479–500.

Bevacqua, E., Maraun, D., Vousdoukas, M.I., Voukouvalas, E., Vrac, M., Mentaschi, L. and Widmann, M. 2019. Higher probability of compound flooding from precipitation and storm surge in Europe under anthropogenic climate change. Science advances, 5(9), p.eaaw5531.

Bogacki, P. and Shampine, L.F. 1989. A 3 (2) pair of Runge-Kutta formulas. Applied Mathematics Letters, 2(4), pp. 321–325.

Candella, R.N., Rabinovich, A.B. and Thomson, R. 2008. The 2004 Sumatra tsunami as recorded on the Atlantic coast of South America.

Carrier, G.F. and Greenspan, H. 1958. Water waves of finite amplitude on a sloping beach. Journal of Fluid Mechanics, 4(1), pp. 97–109.

Davis, R. 1985. Beach and nearshore zone. In *Coastal sedimentary environments* (pp. 379–444). Springer, New York, NY.

Dean, B., Collins, I., Divoky, D., Hatheway, D. and Scheffner, C.N. 2005. FEMA Coastal Flood Hazard Analysis and Mapping Guidelines Focused Study Report.

Dean, R. 1990. Freak waves: a possible explanation. In Water wave kinematics (pp. 609–612). Springer, Dordrecht.

Denissenko, P., Didenkulova, I., Rodin, A., Listak, M. and Pelinovsky, E. 2013. Experimental statistics of long wave runup on a plane beach. Journal of Coastal Research, (65), pp. 195–200.

De Waal, J.P. and Van der Meer, J.W. 1993. Wave runup and overtopping on coastal structures. In Coastal Engineering 1992 (pp. 1758–1771).

Didenkulova, I. 2009. Nonlinear long-wave deformation and runup in a basin of varying depth. Nonlinear Processes in Geophysics, 16(1), p. 23.

Didenkulova, I. and Anderson, C. 2010. Freak waves of different types in the coastal zone of the Baltic Sea. Natural Hazards and Earth System Sciences, 10(9), pp. 2021–2029.

Didenkulova, I. and Rodin, A. 2012. Statistics of shallow water rogue waves in Baltic Sea conditions: The case of Tallinn Bay. In 2012 IEEE/OES Baltic International Symposium (BALTIC).

Didenkulova, I.I., Kurkin, A.A. and Pelinovsky, E. 2007. Run-up of solitary waves on slopes with different profiles. Izvestiya, Atmospheric and Oceanic Physics, 43(3), pp. 384–390.

Didenkulova, I.I., Pelinovsky, E.N. and Didenkulova, O. 2014. Runup of long solitary waves of different polarities on a plane beach. Izvestiya, Atmospheric and Oceanic Physics, 50(5), pp. 532–538.

Didenkulova, I., Pelinovsky, E., Soomere, T. and Zahibo, N. 2007. Runup of nonlinear asymmetric waves on a plane beach. In Tsunami and nonlinear waves (pp. 175–190). Springer, Berlin, Heidelberg.

Didenkulova, I., Pelinovsky, E. and Soomere, T. 2008. Runup characteristics of symmetrical solitary tsunami waves of “unknown” shapes. In Tsunami Science Four Years after the 2004 Indian Ocean Tsunami (pp. 2249–2264). Birkhäuser Basel.

Di Luccio, D., Benassai, G., Budillon, G., Mucerino, L., Montella, R. and Pugliese Carratelli, E. 2018. Wave run-up prediction and observation in a micro-tidal beach. Natural Hazards & Earth System Sciences, 18(11).

Durán, A., Dutykh, D. and Mitsotakis, D. 2018. Peregrine’s system revisited. In Nonlinear Waves and Pattern Dynamics (pp. 3–43). Springer, Cham.

Dutykh, D., Katsaounis, T. and Mitsotakis, D. 2011. Finite volume schemes for dispersive wave propagation and runup. Journal of Computational Physics, 230(8), pp. 3035–3061.

Dutykh, D., Labart, C. and Mitsotakis, D. 2011. Long wave run-up on random beaches. Physical Review Letters, *107*(18), p. 184504.

Dutykh, D., Poncet, R. and Dias, F. 2011. The VOLNA code for the numerical modeling of tsunami waves: Generation, propagation and inundation. European Journal of Mechanics-B/Fluids, 30(6), pp. 598–615.

Earle, M. 1975. Extreme wave conditions during Hurricane Camille. Journal of Geophysical Research, 80(3), pp. 377–379.

Fazeres-Ferradosa, T., Taveira-Pinto, F., Vanem, E., Reis, M. T., & Neves, L. D. 2018. Asymmetric copula–based distribution models for met-ocean data in offshore wind engineering applications. Wind Engineering, 42(4), 304–334.

Fedele, F., Herterich, J., Tayfun, A. and Dias, F., 2019. Large nearshore storm waves off the Irish coast. Scientific reports, 9(1), pp. 1–19.

Forristall, G.Z. 1978. On the statistical distribution of wave heights in a storm. Journal of Geophysical Research: Oceans, 83(C5), pp. 2353–2358.

Galvin, C. 1968. Breaker type classification on three laboratory beaches. Journal of geophysical research, 73(12), pp. 3651–3659.

García-Medina, G., Özkan-Haller, H.T., Ruggiero, P., Holman, R.A. and Nicolini, T. 2018. Analysis and catalogue of sneaker waves in the US Pacific Northwest between 2005 and 2017. Natural Hazards, 94(2), pp. 583–603.

Gjevik, B. and Pedersen, G. 1981. Runup of long waves on an inclined plane. Preprint series. Mechanics and Applied Mathematics http://urn. nb. no/URN: NBN: no-23418.

Glimsdal, S., Pedersen, G.K., Atakan, K., Harbitz, C.B., Langtangen, H.P. and Lovholt, F. 2006. Propagation of the Dec. 26, 2004, Indian Ocean Tsunami: Effects of dispersion and source characteristics. International Journal of Fluid Mechanics Research, 33(1).

Glimsdal, S., Harbitz, C. B., & Løvholt, F. 2013. Dispersion of tsunamis: does it really matter?. Natural Hazards and Earth System Sciences, 13(6), 1507.Goseberg, N., Wurpts, A. and Schlurmann, T. 2013. Laboratory-scale generation of tsunami and long waves. Coastal Engineering, 79, pp. 57–74.

Glimsdal, S., Løvholt, F., Harbitz, C. B., Romano, F., Lorito, S., Orefice, S. and Babeyko, A. 2019. A new approximate method for quantifying tsunami maximum inundation height probability. Pure and Applied Geophysics, *176*(7), 3227–3246.

Goda, Y. 1975. Irregular wave deformation in the surf zone. Coastal Engineering in Japan, 18(1), pp. 13–26.

Grilli, S.T., Losada, M.A. and Martin, F. 1994. Characteristics of solitary wave breaking induced by breakwaters. Journal of Waterway, Port, Coastal, and Ocean Engineering, 120(1), pp. 74–92.

Grilli, S.T., Svendsen, I.A. and Subramanya, R. 1997. Breaking criterion and characteristics for solitary waves on slopes. Journal of waterway, port, coastal, and ocean engineering, 123(3), pp. 102–112.

Harten, A. and Osher, S. 1987. Uniformly high-order accurate nonoscillatory schemes. I. SIAM Journal on Numerical Analysis, 24(2), pp. 279–309.

Holthuijsen, H. 2010. Waves in oceanic and coastal waters. Cambridge university press.

Horrillo, J., Kowalik, Z. and Shigihara, Y. 2006. Wave dispersion study in the Indian Ocean-tsunami of December 26, 2004. Marine Geodesy, 29(3), pp. 149–166.

Kânoğlu, U. and Synolakis, C. 2006. Initial value problem solution of nonlinear shallow water-wave equations. Physical Review Letters, 97(14), p. 148501.

Kharif, C. and Pelinovsky, E. (2006). Freak waves phenomenon: physical mechanisms and modelling. In Waves in Geophysical Fluids (pp. 107–172). Springer, Vienna.

Kharif, C., Pelinovsky, E. and Slunyaev, A. 2008. Rogue waves in the ocean. Springer Science & Business Media.

Kinsman, B. (1965). Wind waves: their generation and propagation on the ocean surface. New York: Courier Corporation.

LaBrecque, J., Rundle, J.B., Bawden, G.W., Surface, E. and Area, I.F. 2019. Global navigation satellite system enhancement for tsunami early warning systems. Global Assessment Report on Disaster Risk Reduction, UN Off. for Disaster Risk Reduct., Geneva, Switzerland.

Larsen, B. E., and Fuhrman, D. 2019. Full-scale CFD simulation of tsunamis. Part 2: Boundary layers and bed shear stresses. Coastal engineering, 151, 42–57.

Lin, P., Chang, K.A. and Liu, P.F. 1999. Runup and rundown of solitary waves on sloping beaches. Journal of waterway, port, coastal, and ocean engineering, 125(5), pp. 247–255.

Liu, P.L.F., Synolakis, C.E. and Yeh, H. 1991. Report on the international workshop on long-wave run-up. Journal of Fluid Mechanics, 229, pp. 675–688.

Li, Y. and Raichlen, F. 2002. Non-breaking and breaking solitary wave runup. Journal of Fluid Mechanics, 456, p. 295.

Løvholt, F., Kaiser, G., Glimsdal, S., Scheele, L., Harbitz, C.B. and Pedersen, G.K. 2012. Modeling propagation and inundation of the 11 March 2011 Tohoku tsunami.

Nikolkina, I., Didenkulova, I., Pelinovsky, E. and Liu, P. 2011. Rogue waves in 2006-2010. Natural Hazards & Earth System Sciences, 11(11).

Madsen, P.A. and Fuhrman, D.R. 2008. Run-up of tsunamis and long waves in terms of surf-similarity. Coastal Engineering, 55(3), pp. 209–223.

Madsen, P.A. and Schaeffer, H.A. 2010. Analytical solutions for tsunami runup on a plane beach: single waves, N-waves and transient waves. Journal of Fluid Mechanics, 645, p. 27.

Madsen, P.A., Sørensen, O.R. and Schäffer, H.A. 1997. Surf zone dynamics simulated by a Boussinesq type model. Part I. Model description and cross-shore motion of regular waves. Coastal Engineering, 32(4), pp. 255–287.

Mai, S., Wilhelmi, J. and Barjenbruch, U. 2010. Wave height distributions in shallow waters. Coastal Engineering Proceedings, 1(32), waves.63. https://doi.org/10.9753/icce.v32.waves.

Manning, R. 1891. On the flow of water in open channels and pipes. Trans. Inst. Civil Engineers Ireland 20, 161–207.

Marcos, M., Rohmer, J., Vousdoukas, M.I., Mentaschi, L., Le Cozannet, G. and Amores, A. 2019. Increased extreme coastal water levels due to the combined action of storm surges and wind waves. Geophysical Research Letters, 46(8), pp. 4356–4364.

Massel, S.R. (1996). Ocean Surface Waves: Their Physics and Prediction. Advanced. (Vol. 11). World Scientific.

Massel S.R. (2007) Energy dissipation due to wave breaking. In: Ocean Waves Breaking and Marine Aerosol Fluxes. ATMOSPHERIC AND OCEANOGRAPHIC SCIENCES LIBRARY, vol 38. Springer, New York, NY.

Mazova, R.K., Pelinovsky, Y.N. and Solov'yev, S.L. 1983. Statistical Data on Runup of Tsunamis. Okeanologiya, 2J3, (6), pp. 932–937.

Mei, C. (1989). The Applied Dynamics of Ocean Surface Waves, World Scientific: Singapore.

Merrifield, M.A., Firing, Y.L., Aarup, T., Agricole, W., Brundrit, G., Chang-Seng, D., Farre, R., Kilonsky, B., Knight, W., Kong, L. and Magori, C. 2005. Tide gauge observations of the Indian Ocean tsunami, December 26, 2004. Geophysical Research Letters, 32(9).

Narayana, A.C., Tatavarti, R., Shinu, N. and Subeer, A. 2007. Tsunami of December 26, 2004 on the southwest coast of India: Post-tsunami geomorphic and sediment characteristics. Marine Geology, 242(1-3), pp. 155–168.

Neelamani, S., Al-Salem, K. and Rakha, K. 2007. Extreme waves for Kuwaiti territorial waters. Ocean Engineering, 34(10), pp. 1496–1504.

Qu, K., Sun, W.Y., Deng, B., Kraatz, S., Jiang, C.B., Chen, J. and Wu, Z.Y. 2019. Numerical investigation of breaking solitary wave runup on permeable sloped beach using a nonhydrostatic model. Ocean Engineering, 194, p. 106625.

Pedersen, G. and Gjevik, B. 1983. Runup of solitary waves. Journal of fluid mechanics, 135, pp. 283–299.

Pelinovsky, E. and Kharif, C. (2008). Extreme ocean waves. Berlin: Springer.

Pelinovsky, E.N. and Mazova, R.K. 1992. Exact analytical solutions of nonlinear problems of tsunami wave runup on slopes with different profiles. Natural Hazards, 6(3), pp. 227–249.

Petcu, M. and Temam, R. 2013. The one-dimensional shallow water equations with transparent boundary conditions. Mathematical Methods in the Applied Sciences, 36(15), pp. 1979–1994.

Pullen, T., N.W.H. Allsop, T. Bruce, A. Kortenhaus, H. Schüttrumpf, and J.W. van der Meer. 2007. EurOtop – Wave Overtopping of Sea Defences and Related Structures: Assessment Manual, Die Küste, 73, 193 pp.

Rabinovich, A.B. and Thomson, R.E. 2007. The 26 December 2004 Sumatra tsunami: Analysis of tide gauge data from the world ocean Part 1. Indian Ocean and South Africa. In Tsunami and Its Hazards in the Indian and Pacific Oceans (pp. 261–308). Birkhäuser Basel.

Rangel-Buitrago, N., Neal, W.J., Bonetti, J., Anfuso, G. and de Jonge, V.N. 2020. Vulnerability assessments as a tool for the coastal and marine hazards management: An overview. Ocean & Coastal Management, 189, p. 105134.

Rattanapitikon, W. and Shibayama, T. 2007. Estimation of shallow water representative wave heights. Coastal engineering journal, 49(03), pp. 291–310.

Rossetto, T., Peiris, N., Pomonis, A., Wilkinson, S.M., Del Re, D., Koo, R. and Gallocher, S. 2007. The Indian Ocean tsunami of December 26, 2004: observations in Sri Lanka and Thailand. Natural Hazards, 42(1), pp. 105–124.

Sawaragi, T. (1995). Coastal engineering-waves, beaches, wave-structure interactions. Elsevier.

Schmidt-Koppenhagen, R., Gerdes, M., Tautenhain, E. and Grüne, J. 1997. Online absorption control system for wave generation. In Proc. 3rd Intern. Symp. on Ocean Wave Measurements and Analysis (WAVES'97). ASCE, Virginia Beach, USA.

Schimmels, S., Sriram, V. and Didenkulova, I. 2016. Tsunami generation in a large scale experimental facility. Coastal Engineering, 110, pp. 32–41.

Schimmels, S., Sriram, V., Didenkulova, I. and Fernandez, H. 2014. On the generation of tsunami in a large scale wave flume. Coastal Engineering, pp. 1–10.

Shampine, L.F. and Reichelt, M.W. 1997. The matlab ode suite. SIAM journal on scientific computing, 18(1), pp. 1–22.

Shuto, N. 1985. The Nihonkai-Chubu earthquake tsunami on the North Akita coast. Coastal Engineering in Japan, 28(1), pp. 255–264.

Stockdon, H.F., Holman, R.A., Howd, P.A. and Sallenger Jr, A.H. 2006. Empirical parameterization of setup, swash, and runup. Coastal engineering, 53(7), pp. 573–588.

Stocker, J. (1957). Water Waves: The Mathematical Theory with Applications. New York: Interscience.

Suanez, S., Cariolet, J.M., Cancouët, R., Ardhuin, F. and Delacourt, C. 2012. Dune recovery after storm erosion on a high-energy beach: Vougot Beach, Brittany (France). Geomorphology, 139, pp. 16–33.

Sundar, V. 2017. Ocean wave mechanics: Applications in marine structures. John Wiley & Sons.

Synolakis, C.E. 1987. The runup of solitary waves. Journal of Fluid Mechanics, 185, pp. 523–545.

Synolakis C.E. and Skjelbreia, J.E. 1993. Evolution of maximum amplitude of solitary waves on plane beaches. Journal of waterway, port, coastal, and ocean engineering, 119(3), pp. 323–342.

Teutsch I., Weisse, R., Moeller J., Krueger O. 2020. A statistical analysis of rogue waves in the southern North Sea. Natural hazards and earth system sciences, 20, pp. 2665–2680.

Thandlam, V., Rutgersson, A., Rahaman, H. 2019. Are we in the right path in using early warning systems? Journal of Extreme Events, 6(02), p. 1950003.

Tinti, S. and Tonini, R. 2005. Analytical evolution of tsunamis induced by near-shore earthquakes on a constant-slope ocean. Journal of Fluid Mechanics, 535, p. 33.

Toffoli, A. and Bitner-Gregersen, E.M. 2017. Types of ocean surface waves, wave classification. Encyclopedia of Maritime and Offshore Engineering, pp. 1–8.

Torsvik, T., Didenkulova, I., Soomere, T. and Parnell, K.E. 2009. Variability in spatial patterns of long nonlinear waves from fast ferries in Tallinn Bay. Nonlinear Processes in Geophysics, 16, pp. 351–363.

Torsvik, T., Soomere, T., Didenkulova, I. and Sheremet, A. 2015. Identification of ship wake structures by a time-frequency method. Journal of Fluid Mechanics, 765, pp. 229–251.

Vanem, E., Fazeres-Ferradosa, T., Rosa-Santos, P. and Taveira-Pinto, F. 2019. Statistical description and modelling of extreme ocean wave conditions. In Proceedings of the Institution of Civil Engineers-Maritime Engineering (Vol. 172, No. 4, pp. 124–132). Thomas Telford Ltd.

Xiao, H., Young, Y.L. and Prévost, J.H. 2010. Hydro-and morpho-dynamic modeling of breaking solitary waves over a fine sand beach. Part II: Numerical simulation. Marine Geology, 269(3-4), pp. 119–131.

You, Z.J. and Nielsen, P. 2013. Extreme coastal waves, ocean surges and wave runup. In Coastal Hazards (pp. 677–733). Springer, Dordrecht.

Young, I.R., (1999). Wind generated ocean waves. Elsevier.

Young, Y.L., Xiao, H. and Maddux, T. 2010. Hydro-and morpho-dynamic modeling of breaking solitary waves over a fine sand beach. Part I: Experimental study. Marine Geology, 269(3-4), pp. 107–118.

Zahibo, N., Didenkulova, I., Kurkin A. and Pelinovsky, E. 2008. Steepness and spectrum of nonlinear deformed shallow water wave. Ocean Engineering, 35(1), pp. 47–52.

Acknowledgements

Praise be to Allah, who bestowed upon me the grace of finding and supplying. ''*Allah commandeth you that you restore deposits to their owners*'' Source: An-Nisa` 4:58. "*He has not thanked Allah who has not thanked people*." Source: Sunan Abu Dawud 4811. I can only extend my deepest thanks, gratitude to my advisor Dr. Ira Didenkulova, her directions and advice had the greatest impact to me. Without her guidance and persistent help, this thesis would not have been possible. Practically, I learned from her not only the science but also the humility, patience, and curiosity. My deepest thanks, gratitude also to my co-advisor Dr. Denys Dutykh, in his directions and advice and supporting me always during my PhD study, without his Knowledge and assistance this study would not have been successful.

Many thanks go to Tomas Torsvik, Céline Labart, and Petr Denisenko who contributed as co-authors of the publications of this thesis. I would like to thank also Victor Alari for his revising the thesis. I am also grateful to all Marine Systems Institute members, especially those who keep asking me about my study process. Special thanks also to Silvie Lainela, Sander Rikka, and Jüri Elken for translating the thesis abstract into the Estonian language.

I would like to thank all my family members and friends, who gave me their unequivocal support throughout, as always, for which my mere expression of thanks likewise does not suffice.

The computations were performed using the computer cluster of the Department of Marine Systems of Tallinn University of Technology. The work was supported by an ETAG grant (PUT1378). The PHC PARROT project (No. 37456YM) funded the visits to France and Estonia, thus facilitating this collaboration.

Abstract

Runup of nonlinear waves of different shapes on a plane beach including effects of dispersion and wave breaking

The runup of nonlinear waves of different shapes (single tsunami waves, regular, bi-harmonic and ship wakes) on a plane beach has been investigated in terms of dispersion, nonlinearity and wave breaking. We used a flat bottom bathymetry with a constant depth connected with a constant beach slope. We used different methods: (i) semi-analytical solution of the non-dispersive nonlinear shallow water theory, (ii) the corresponding numerical model, and (iii) dispersive numerical model based on the modified Peregrine equations. Both analytical and numerical results were compared with the experimental data obtained from Large Wave Flume (GWK), Hanover, Germany, in 2012-2013.

A single tsunami wave has been investigated for the nonlinear effects on the runup height analytically and numerically using the nonlinear shallow water theory. Found that, the maximum tsunami runup height on a beach depends on the wave front steepness at the toe of the bottom slope. The corresponding new formula of maximum runup height as a function of wave front steepening, wave period and distance to the slope is suggested.

The periodic waves characterized by kh = 0.2 have been studied using dispersive and nondispersive models and compared with experimental data. Concluded that, in the given range of kh, for large-amplitude waves the dispersive effects are important and dispersive models should be applied, while for small-amplitude waves the nondispersive nonlinear shallow water theory gives reasonable results and can still be used.

We studied the runup statistics of irregular waves with kh = 0.38 using the numerical model based on the nonlinear shallow water theory. The runup statistics is discussed with regard to different scenarios of wave breaking, wave nonlinearity and the bandwidth of the incident wave field. Found, that in the given range of kh = 0.38, wide-banded wave fields lead to a higher probability of freak runups on a beach compare to the probability of freak wave occurrence in the initial wave field. In contrary, for narrow-banded wave signals, the beach slope filters extreme runups, substantially reducing the probability of their occurrence. It is also suggested that the conditional Weibull distribution can be used for the description of extreme runup heights and the assessment of extreme inundations.

Lühikokkuvõte

Laine dispersiooni ja murdumise mõju mittelineaarsete lainete uhtekõrgusele erineva kujuga laugetel randadel

Uuriti erineva kujuga mittelineaarsete lainete (üksikud tsunami-, regulaarsed, bi-harmoonilised ja laevalained) uhtekõrgusi laugetel randadel erineva dispersiooni, mittelineaarsuse ja lainete murdumise korral. Kasutati kolme erinevat meetodit: (i) mittedispersiivse ja mittelineaarse madala vee teooria võrrandite poolanalüütiline lahendus, (ii) vastav numbriline mudel ja (iii) Peregrine'i võrranditega täiendatud dispersiivne numbriline mudel. Uhtekõrguse simulatsioonide jaoks kasutati lameda põhjaga ja ühtlase sügavusega batümeetriat, mis oli ühendatud konstantse kaldega rannanõlvaga. Töö analüütilisi ja numbrilisi tulemusi võrreldi katseandmetega, mis koguti Saksamaal Hannoveris asuvas lainebasseinis (Large Wave Flume (GWK)) aastatel 2012-2013.

Üksiku tsunamilaine mustri põhjal uuriti analüütiliselt ja numbriliselt mittelineaarseid efekte laine uhtekõrgusele. Leiti, et tsunaamilaine maksimaalne uhtekõrgus lauges rannas sõltub laine esiosa (frondi) järskusest. Antud töös esitatakse uus maksimaalse uhtekõrguse leidmise võrrand, mis sõltub laine järskusest, perioodist ja kaugusest rannanõlva alguseni.

Perioodilisi laineid režiimil kh = 0.2 uuriti dispersiivsete ja mittedisperssete mudelite abil ning saadud tulemusi võrreldi katseandmetega. Leiti, et teatud kh vahemikus on suure amplituudiga lainete korral dispersiivsed mõjud olulised ja tuleks rakendada dispersiivseid mudeleid. Samas väikese amplituudiga lainete korral annavad mittedispersiivsed mittelineaarsde madala vee võrrandid aktsepteeritavaid tulemusi. Uuriti ebaregulaarsete lainete uhtekõrguse statistikat režiimil kh = 0.38, kasutades mittelineaarse madala vee teoorial põhinevat numbrilist mudelit. Uhtekõrguse statistikat vaadeldi lainete murdumise, lainete mittelineaarsuse ja olemasoleva lainevälja erineva stsenaariumi osas. Laia spektriga laineväljadel ($\Delta f/f_0$ = 0.4) on suurem tõenäosus kaasa tuua suuri uhtekõrgusi rannal võrreldes avamere laineväljaga. Erinevalt laia spektriga laineväljadest, on rannanõlva profiili mõju kitsa spektriga lainetele ($\Delta f/f_0$ = 0.1) suur ja vähendab seeläbi hiidlainete esinemise tõenäosust. Lisaks leiti, et tingimuslik Weibulli sagedusjaotus on kasutatav ekstreemsete lainete uhtekõrguse ja rannalejooksu kauguse iseloomustamiseks.

Appendix

Publication I

Abdalazeez, A., Didenkulova, I., Dutykh, D. 2019. Nonlinear deformation and runup of single tsunami waves of positive polarity: numerical simulations and analytical predictions. Natural Hazards and Earth System Sciences, 19, 2905−2913.10.5194/nhess-19-2905-2019.

Nat. Hazards Earth Syst. Sci., 19, 2905–2913, 2019
https://doi.org/10.5194/nhess-19-2905-2019

Natural Hazards and Earth System Sciences
Open Access
EGU

Nonlinear deformation and run-up of single tsunami waves of positive polarity: numerical simulations and analytical predictions

Ahmed A. Abdalazeez[1], **Ira Didenkulova**[1,2], **and Denys Dutykh**[3]

[1]Department of Marine Systems, Tallinn University of Technology, Akadeemia tee 15A, Tallinn 12618, Estonia
[2]Nizhny Novgorod State Technical University n.a. R.E. Alekseev, Minin St. 24, Nizhny Novgorod 603950, Russia
[3]Univ. Grenoble Alpes, Univ. Savoie Mont Blanc, CNRS, LAMA, Chambéry, 73000, France

Correspondence: Ahmed A. Abdalazeez (ahabda@ttu.ee)

Received: 7 June 2019 – Discussion started: 20 June 2019
Revised: 15 October 2019 – Accepted: 8 November 2019 – Published: 20 December 2019

Abstract. The estimate of an individual wave run-up is especially important for tsunami warning and risk assessment, as it allows for evaluating the inundation area. Here, as a model of tsunamis, we use the long single wave of positive polarity. The period of such a wave is rather long, which makes it different from the famous Korteweg–de Vries soliton. This wave nonlinearly deforms during its propagation in the ocean, which results in a steep wave front formation. Situations in which waves approach the coast with a steep front are often observed during large tsunamis, e.g. the 2004 Indian Ocean and 2011 Tohoku tsunamis. Here we study the nonlinear deformation and run-up of long single waves of positive polarity in the conjoined water basin, which consists of the constant depth section and a plane beach. The work is performed numerically and analytically in the framework of the nonlinear shallow-water theory. Analytically, wave propagation along the constant depth section and its run up on a beach are considered independently without taking into account wave interaction with the toe of the bottom slope. The propagation along the bottom of constant depth is described by the Riemann wave, while the wave run-up on a plane beach is calculated using rigorous analytical solutions of the nonlinear shallow-water theory following the Carrier–Greenspan approach. Numerically, we use the finite-volume method with the second-order UNO2 reconstruction in space and the third-order Runge–Kutta scheme with locally adaptive time steps. During wave propagation along the constant depth section, the wave becomes asymmetric with a steep wave front. It is shown that the maximum run-up height depends on the front steepness of the incoming wave approaching the toe of the bottom slope. The corresponding formula for maximum run-up height, which takes into account the wave front steepness, is proposed.

1 Introduction

Evaluation of wave run-up characteristics is one of the most important tasks in coastal oceanography, especially when estimating tsunami hazard. This knowledge is required for planning coastal structures and protection works as well as for short-term tsunami forecasts and tsunami warning. Its importance is also confirmed by a number of scientific papers (see recent works, e.g. Tang et al., 2017; Touhami and Khellaf, 2017; Zainali et al., 2017; Raz et al., 2018; Yao et al., 2018).

The general solution of the nonlinear shallow-water equations on a plane beach was found by Carrier and Greenspan (1958) using the hodograph transformation. Later on, many other authors found specific solutions for different types of waves climbing the beach (see, for instance, Pedersen and Gjevik, 1983; Synolakis, 1987; Synolakis et al., 1988; Mazova et al., 1991; Pelinovsky and Mazova, 1992; Tadepalli and Synolakis, 1994; Brocchini and Gentile, 2001; Carrier et al., 2003; Kânoğlu, 2004; Tinti and Tonini, 2005; Kânoğlu and Synolakis 2006; Madsen and Fuhrman, 2008; Didenkulova et al., 2007; Didenkulova, 2009; Madsen and Schäffer, 2010).

Many of these analytical formulas have been validated experimentally in laboratory tanks (Synolakis, 1987; Li and Raichlen, 2002; Lin et al., 1999; Didenkulova et al., 2013). For most of them, the solitary waves have been used. The

soliton is rather easy to generate in the flume; therefore, laboratory studies of run-up of solitons are the most popular. However, (Madsen et al., 2008) pointed out that the solitons are inappropriate for describing the real tsunami and proposed to use waves of longer duration than solitons and downscaled records of real tsunami. Schimmels et al. (2016) and Sriram et al. (2016) generated such long waves in the Large Wave Flume of Hanover (GWK FZK) using the piston type of wave maker, while McGovern et al. (2018) did it using the pneumatic wave generator.

It should be mentioned that the shape of tsunami varies a lot depending on its origin and the propagation path. One of the best examples of tsunami wave shape variability is given in Shuto (1985) for the 1983 Sea of Japan tsunami, where the same tsunami event resulted in very different tsunami approaches in different locations along the Japanese coast. These wave shapes included the following: single positive pulses, undergoing both surging and spilling breaking scenarios; breaking bores; periodic wave trains, surging as well as breaking; and a sequence of two or three waves and undular bores. This is why there is no "typical tsunami wave shape", and therefore in the papers on wave run-up cited above, many different wave shapes, such as single pulses, N waves, and periodic symmetric and asymmetric wave trains, are considered. In this paper, we focus on the nonlinear deformation and run-up of long single pulses of positive polarity on a plane beach.

A similar study was performed for periodic sine waves (Didenkulova et al., 2007; Didenkulova, 2009). It was shown that the run-up height increases with an increase in the wave asymmetry (wave front steepness), which is a result of nonlinear wave deformation during its propagation in a basin of constant depth. It was found analytically that the run-up height of this nonlinearly deformed sine wave is proportional to the square root of the wave front steepness. Later on, this result was also confirmed experimentally (Didenkulova et al., 2013).

It should be noted that these analytical findings also match tsunami observations. Steep tsunami waves are often witnessed and reported during large tsunami events, such as 2004 Indian Ocean and 2011 Tohoku tsunamis. Sometimes the wave, which approaches the coast, represents a "wall of water" or a bore, which is demonstrated by numerous photos and videos of these events.

The nonlinear steepening of the long single waves of positive polarity has also been observed experimentally in Sriram et al. (2016), but its effect on wave run-up has not been studied yet. In this paper, we study this effect both analytically and numerically. Analytically, we apply the methodology developed in Didenkulova (2009) and Didenkulova et al. (2014), where we consider the processes of wave propagation in the basin of constant depth and the following wave run-up on a plane beach independently, not taking into account the point of merging of these two bathymetries. Numerically, we solve the nonlinear shallow-water equations.

The paper is organized as follows. In Sect. 2, we give the main formulas and briefly describe the analytical solution. The numerical model is described and validated in Sect. 3. The nonlinear deformation and run-up of the long single wave of positive polarity are described in Sect. 4. The main results are summarized in Sect. 5.

2 Analytical solution

We solve the nonlinear shallow-water equations for the bathymetry shown in Fig. 1:

$$\frac{\partial u}{\partial t} + u\frac{\partial u}{\partial x} + g\frac{\partial \eta}{\partial x} = 0, \tag{1}$$

$$\frac{\partial \eta}{\partial t} + \frac{\partial}{\partial x}\left[(h(x)+\eta)\,u\right] = 0. \tag{2}$$

Here $\eta(x,t)$ is the vertical displacement of the water surface with respect to the still water level, $u(x,t)$ is the depth-averaged water flow, $h(x)$ is the unperturbed water depth, g is the gravitational acceleration, x is the coordinate directed onshore and t is time. The system of Eqs. (1) and (2) is solved independently for the two bathymetries shown in Fig. 1: a basin of constant depth h_0 and length X_0 and a plane beach, where the water depth $h(x) = -x\tan\alpha$.

Equations (1) and (2) can be solved exactly for a few specific cases. In the case of constant depth, the solution is described by the Riemann wave (Stoker, 1957). Its adaptation for the boundary problem can be found in Zahibo et al. (2008). In the case of a plane beach, the corresponding solution was found by Carrier and Greenspan (1958). Both solutions are well-known and widely used, and we do not reproduce them here but just provide some key formulas.

As already mentioned, during its propagation along the basin of constant depth h_0, the wave transforms as a Riemann wave (Zahibo et al., 2008):

$$\eta(x,t) = \eta_0\left[t - \frac{x + X_0 + L}{V(x,t)}\right], \tag{3}$$

$$V(x,t) = 3\sqrt{g\left[h_0 + \eta(x,t)\right]} - 2\sqrt{gh_0}, \tag{4}$$

where $\eta_0(x = -L - X_0, t)$ is the water displacement at the left boundary. After the propagation over the section of constant depth h_0, the incident wave has the following shape:

$$\eta_{X0}(t) = \eta_0\left[t - \frac{X_0}{V(x,t)}\right], V_{X0}(t) = 3\sqrt{g\left[h_0 + \eta_{X0}(t)\right]} - 2\sqrt{gh_0}. \tag{5}$$

Following the methodology developed in Didenkulova (2008), we let this nonlinearly deformed wave described by Eq. (5) run up on a plane beach, characterized by the water depth $h(x) = -x\tan\alpha$. This approach does not take into account the merging point of the two bathymetries and, therefore, does not account for reflection from the toe of the slope and wave interaction with the reflected wave.

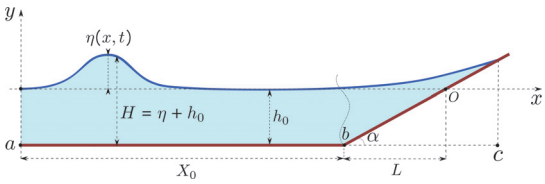

Figure 1. Bathymetry sketch. The wavy curve at the toe of the slope regards analytical solution, which does not take into account merging between the constant depth and sloping beach sections.

To do this, we represent the input wave η_{X0} as a Fourier integral:

$$\eta_{X0} = \int_{-\infty}^{+\infty} B(\omega) \exp(i\omega t)\, \mathrm{d}\omega. \tag{6}$$

Its complex spectrum $B(\omega)$ can be found in an explicit form in terms of the inverse Fourier transform:

$$B(\omega) = \frac{1}{2\pi} \int_{-\infty}^{+\infty} \eta_{X0}(t) \exp(-i\omega t)\, \mathrm{d}t. \tag{7}$$

Equation (7) can be rewritten in terms of the water displacement, produced by the wave maker at the left boundary (Zahibo et al., 2008):

$$B(\omega) = \frac{1}{2\pi i\omega} \int_{-\infty}^{+\infty} \frac{\mathrm{d}\eta_0}{\mathrm{d}z} \exp\left(-i\omega\left[z + \frac{x + X_0 + L}{V(\eta_0)}\right]\right),$$
$$\mathrm{d}z, z = t - \frac{x + X_0 + L}{V(\eta_0)}. \tag{8}$$

In this study we consider long single pulses of positive polarity:

$$\eta_0(t) = A\,\mathrm{sech}^2\left(\frac{t}{T}\right), \tag{9}$$

where A is the input wave height and T is the effective wave period at the location with the water depth h_0. The wave described by Eq. (9) has an arbitrary height and period and, therefore, does not satisfy properties of the soliton but just has a sech^2 shape. Substituting Eq. (9) into Eq. (8), we can calculate the complex spectrum $B(\omega)$.

Wave run-up oscillations at the coast $r(t)$ and the velocity of the moving shoreline $u(t)$ can be found from Didenkulova et al. (2008):

$$r(t) = R\left(t + \frac{u}{g\tan\alpha}\right) - \frac{u^2}{2g}, \tag{10}$$

$$u(t) = U\left(t + \frac{u(t)}{g\tan\alpha}\right), \tag{11}$$

$$R(t) = \sqrt{2\pi\tau(L)} \int_{-\infty}^{+\infty} \sqrt{|\omega|} H(\omega)$$
$$\exp\left\{i\left(\omega(t - \tau(L)) + \frac{\pi}{4}\mathrm{sign}(\omega)\right)\right\} \mathrm{d}\omega, \tag{12}$$

$$U(t) = \frac{1}{\tan\alpha}\frac{\mathrm{d}R}{\mathrm{d}t}, \tag{13}$$

where $\tau = 2L/\sqrt{gh_0}$ is the travel time to the coast.

We also compare this solution with the run-up of a single wave of positive polarity described by Eq. (9) (without nonlinear deformation). The maximum run-up height $R_{\max}$ of such a wave (Eq. 9) can be found from Didenkulova et al. (2008) and Sriram et al. (2016):

$$\frac{R_{\max}}{A} = 2.8312\sqrt{\cot\alpha}\left(\frac{1}{gh_0}\left(\frac{2h_0}{\sqrt{3T}}\right)^2\right)^{1/4}. \tag{14}$$

If the initial wave is a soliton, Eq. (14) coincides with the famous Synolakis formula (Synolakis, 1987).

3 Numerical model

Numerically, we solve the nonlinear shallow-water equations Eqs. (1) and (2), written in a conservative form for a total water depth. We include the effect of the varying bathymetry (in space) and neglect all friction effects. However, the resulting numerical model will be taken into account for some dissipation thanks to the numerical scheme dissipation, which is necessary for the stability of the scheme and should not influence many run-up characteristics. Namely, we employ the natural numerical method, which was developed especially for conservation laws – the finite-volume schemes.

The numerical scheme is based on the second order in space UNO2 reconstruction, which is briefly described in Dutykh et al. (2011b). In time we employ the third-order Runge–Kutta scheme with locally adaptive time steps in order to satisfy the Courant–Friedrichs–Lewy stability condition along with the local error estimator to bound the error term to the prescribed tolerance parameter. The numerical technique to simulate the wave run-up was described previously in Dutykh et al. (2011a). The bathymetry source term is discretized using the hydrostatic reconstruction technique, which implies the well-balanced property of the numerical scheme (Gosse, 2013).

The numerical scheme is validated against experimental data of wave propagation and run-up in the Large Wave Flume (GWK) in Hanover, Germany. The experiments were

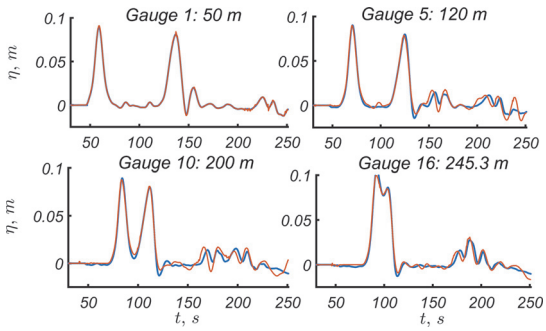

Figure 2. Water elevations along the 251 m long constant depth section of the Large Wave Flume (GWK), where $h_0 = 3.5$ m, $A = 0.1$ m, $T = 20$ s and $\tan\alpha = 1:6$. Results of numerical simulations are shown by the red line, and experimental data are shown by the blue line.

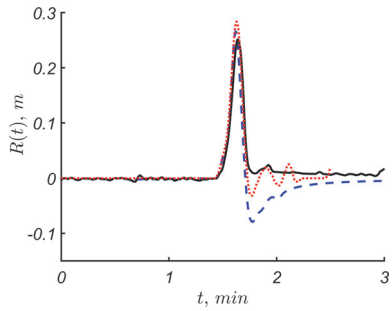

Figure 3. Run-up height of the long single wave with $A = 0.1$ m and $T = 20$ s on a beach slope, where $\tan\alpha = 1:6$. The numerical solution is shown by the red dotted line, the analytical solution is shown by the blue dashed line and the experimental record is shown by the black solid line.

set with a flat bottom, with a constant depth of $h_0 = 3.5$ m, length of $[a, b] = 251$ m and a plane beach with a slope of $\tan\alpha = 1:6$ (see Fig. 1). The flume had 16 wave gauges along the constant depth section and a run-up gauge on the slope. The incident wave had an amplitude of $A = 0.1$ m and period of $T = 20$ s. The detailed description of the experiments can be found in Didenkulova et al. (2013). The results of numerical simulations are in good agreement with the laboratory experiments along the constant depth section (see Fig. 2) as well as on the beach (Fig. 3). The comparison of the run-up height is calculated numerically and analytically using the approach described in Sect. 2 and with the experimental record shown in Fig. 3. It can be seen that the experimentally recorded wave is slightly smaller, which may be caused by the bottom friction, especially on the slope. Both numerical and analytical models describe the first wave of positive polarity rather well. The numerical prediction of run-up height is slightly higher than the analytical one. This additional increase in the run-up height in the numerical model may be explained by the nonlinear interaction with the reflected wave, which is not taken into account in the analytical model. The wave of negative polarity is much more sensitive to all the effects mentioned above than the wave of positive polarity and, therefore, looks different for all three lines in Fig. 3. By introducing additional dissipation in the numerical model, one can easily reach perfect agreement between the numerical simulations and experimental data. However, we do not do so, since below we focus on the analysis of analytical results and for clarity would like to avoid additional parameters in the numerical model. Also, we focus on the maximum run-up height and, therefore, expect small differences between the results of analytical and numerical models. The data used for all figures of this paper are available at https://doi.org/10.13140/rg.2.2.27658.41922 (Abdalazeez et al., 2019).

4 Results of numerical and analytical calculations

It is reported in Didenkulova et al. (2007) and Didenkulova (2009), for a periodic sine wave, that the extreme run-up height increases proportionally with the square root of the wave front steepness. In this section, we study the nonlinear deformation and steepening of waves described by Eq. (9) and their effect on the extreme wave run-up height. The corresponding bathymetry used in analytical and numerical calculations is normalized on the water depth in the section of constant depth h_0 and is shown in Fig. 1. The input wave parameters such as wave amplitude, A/h_0, and effective wave length, λ/X_0, where $\lambda = T\sqrt{gh_0}$, are changed. The beach slope is taken as $\tan\alpha = 1:20$ for all simulations.

We underline that in order to have analytical solution, the criterion of no wave breaking should be satisfied. Therefore, all analytical and numerical calculations below are chosen for non-breaking waves.

Figure 4 shows the dimensionless maximum run-up height, $R_{\max}/A$, as a function of the initial wave amplitude, A/h_0. The incident wave propagates over different distances to the bottom slope, $X_0/\lambda = 1.7$, 3.4, 5.1 and 6.8, where $kh_0 = 0.38$. The analytical solution described in Sect. 2 is shown with lines, and the numerical solution described in Sect. 3 is shown with symbols (diamonds, triangles, squares and circles). It can be seen that in most cases and especially for small values of $X_0/\lambda = 1.7$ and 3.4, numerical simulations give larger run-up heights than analytical predictions. These differences can be explained by the effects of wave interaction with the toe of the underwater beach slope, which are not taken into account in the analytical solution. For larger distances $X_0/\lambda = 6.8$, both analytical and numerical solutions give similar results, supported by the numerical scheme dissipation described in Sect. 3, which can be considered a "numerical error". It should be mentioned that we use a physical dissipation rate of zero for these simula-

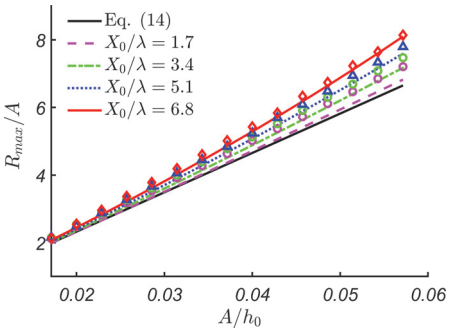

Figure 4. Maximum run-up height, $R_{\max}/A$, as a function of initial wave amplitude, A/h_0, for different distances to the slope, X_0/λ. Analytical solution described in Sect. 2 is shown by lines, and numerical solution described in Sect. 3 is shown by symbols (diamonds, triangles, squares and circles) with matching colours. The thick black line corresponds to Eq. (14) for wave run-up on a beach without constant depth section, where $kh_0 = 0.38$.

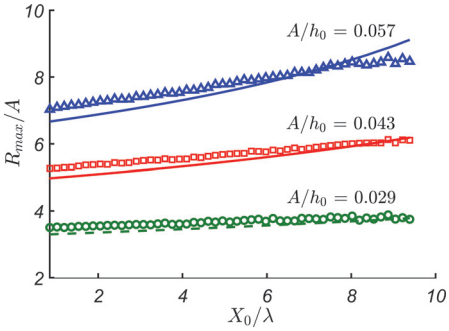

Figure 5. Maximum run-up height, $R_{\max}/A$, as a function of distance to the slope, X_0/λ, for different amplitudes of the initial wave, A/h_0. Analytical solution described in Sect. 2 is shown by lines, and numerical solution described in Sect. 3 is shown by symbols (triangles, squares and circles) with matching colours, where $kh_0 = 0.38$.

tions; however, a small dissipation for stability of the numerical scheme is still needed, and this may become noticeable at large distances. For the sech^2-shaped wave ($A/h_0 = 0.03$, $\lambda/X_0 = 0.12$) propagation, the reduction of initial wave amplitude constitutes $\sim 2\,\%$.

It is worth mentioning that for small initial wave amplitudes, all run-up heights are close to each other and are close to the thick black line, which corresponds to Eq. (14) for wave run-up on a beach without constant depth section. This means that the effects we are talking about are important only for nonlinear waves and irrelevant for weakly nonlinear or almost linear waves.

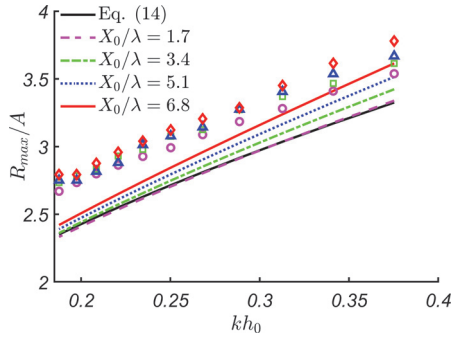

Figure 6. Maximum run-up height, $R_{\max}/A$, as a function of kh_0 for different distances to the slope, X_0/λ. Analytical solution described in Sect. 2 is shown by lines, and numerical solution described in Sect. 3 is shown by symbols (diamonds, triangles, squares and circles) with matching colours. The thick black line corresponds to Eq. (14) for wave run-up on a beach without constant depth section ($A/h_0 = 0.03$).

The same effects can be seen in Fig. 5, which shows the maximum run-up height, $R_{\max}/A$, as a function of distance to the slope, X_0/λ, for different amplitudes of the initial wave, A/h_0. The distance X_0/λ changes from 0.8 to 9.4, where $kh_0 = 0.38$. The analytical solution is shown with lines, while the numerical solution is shown with symbols (triangles, squares and circles). It can be seen in Fig. 5 that for smaller values of $X_0/\lambda < 6$, numerical predictions provide relatively larger run-up values compared with analytical predictions, while for higher values of $X_0/\lambda > 6$, the differences are significantly reduced. A relevant change of this behaviour is given for $A/h_0 = 0.06$. We can observe that numerical predictions for this amplitude become smaller than analytical predictions for $X_0/\lambda > 8$. As stated above, we believe that this can be a result of interplay of two effects: interaction with the underwater bottom slope, which is not taken into account in the analytical prediction, and the numerical scheme dissipation ("numerical error"), which affects the numerical results.

The dependence of maximum run-up height, $R_{\max}/A$, on kh_0 is shown in Fig. 6 for $A/h_0 = 0.03$. It can be seen that the difference between numerical and analytical results decreases with an increase in kh_0. We relate this effect with the wave interaction with the slope, which is not properly accounted in our analytical approach. As one can see in Fig. 7, this difference for a milder beach slope $\tan\alpha = 1:50$ is reduced.

The next figure, Fig. 8, supports all the conclusions drawn above. It also shows that the difference between analytical and numerical results increases with an increase in the wave period. As pointed out before for small wave periods, the numerical solution may coincide with the analytical one or even become smaller as in $kh_0 = 0.38$ for $X_0/\lambda > 8$.

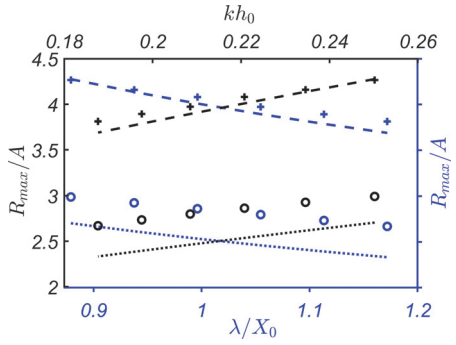

Figure 7. Maximum run-up height, $R_{\max}/A$, as a function of initial effective wave length, λ/X_0 (blue axes) and kh_0 (black axes). Analytical solutions for $\tan\alpha = 1:20$ and $\tan\alpha = 1:50$ are shown by dotted and dashed lines, respectively, while numerical simulations for $\tan\alpha = 1:20$ and $\tan\alpha = 1:50$ are shown by circles and crosses, respectively ($A/h_0 = 0.03$).

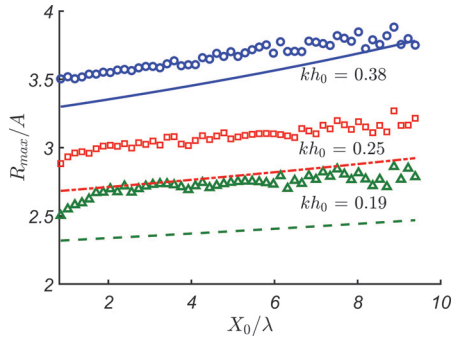

Figure 8. Maximum run-up height, $R_{\max}/A$, as a function of the distance to the slope, X_0/λ , for different values of kh_0. Analytical solution described in Sect. 2 is shown by lines, and numerical solution described in Sect. 3 is shown by symbols (triangles, squares and circles) with matching colours ($A/h_0 = 0.03$).

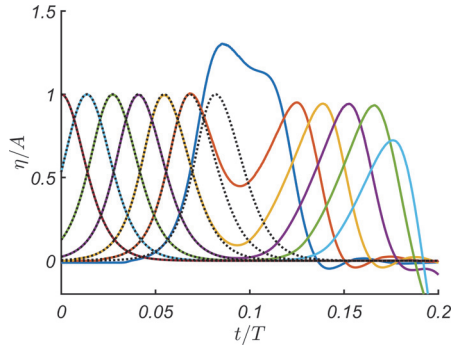

Figure 9. Wave evolution at different locations, $x/\lambda = 0, 0.85, 1.71, 2.56, 3.41, 4.27$ and 5.12, along the section of constant depth for a basin with $X_0/\lambda = 5.12$ and $\tan\alpha = 1:20$. Numerical results are shown by solid lines, while the analytical predictions are given by the black dotted lines. The parameters of the wave are $A/h_0 = 0.03$ and $kh_0 = 0.19$.

It is important that both analytical and numerical results in Figs. 5 and 8 demonstrate an increase in maximum run-up height with an increase in the distance X_0/λ. This result is in agreement with the conclusions of Didenkulova et al. (2007) and Didenkulova (2009) for sinusoidal waves. In order to be consistent with the results of Didenkulova et al. (2007) and Didenkulova (2009), we connect the distance X_0/λ with the incident wave front steepness in the beginning of the bottom slope. The wave front steepness s is defined as the maximum of the time derivative of water displacement, $\mathrm{d}(\eta/A)/\mathrm{d}(t/T)$, and is studied in relation with the initial wave front steepness, s_0, where

$$s(x) = \frac{\max\left(\mathrm{d}\eta(x,t)/\mathrm{d}t\right)}{A/T}, \quad s_0 = \frac{\max\left(\mathrm{d}\eta(x=a,t)/\mathrm{d}t\right)}{A/T}. \quad (15)$$

In order to calculate the incident wave front steepness in the beginning of the bottom slope from results of numerical simulations, we should separate the incident wave and the wave reflected from the bottom slope. At the same time, the wave steepening along the basin of constant depth is very well described analytically, as demonstrated in Fig. 9.

It can be seen that the wave transformation described by the analytical model is in a good agreement with numerical simulations. Therefore, below we make reference to the analytically defined wave front steepness, keeping in mind that it coincides well with the numerical one. Having said this, we approach the main result of this paper, which is shown in Fig. 10. The red solid line gives the analytical prediction. It is universal for single waves of positive polarity for different amplitudes A/h_0 and kh_0 and can be approximated well by the power fit (coefficient of determination $R^2 = 0.99$):

$$R_{\max}/R_0 = (s/s_0)^{0.42}, \quad (16)$$

where $R_{\max}/A$ is the maximum run-up height in the conjoined basin (with a section of constant depth); R_0/A is the corresponding maximum run-up height on a plane beach (without a section of constant depth).

The fit is shown in Fig. 10 by the black dashed line. For comparison, the dependence of the maximum run-up height on the wave front steepness obtained using the same method for a sine wave is stronger than for a single wave of positive polarity (Didenkulova et al., 2007) and is proportional to the square root of the wave front steepness. This is logical, as the sinusoidal wave has a sign-variable form and, therefore, excites a higher run-up. For possible mechanisms, see the discussion on N waves in Tadepalli and Synolakis (1994).

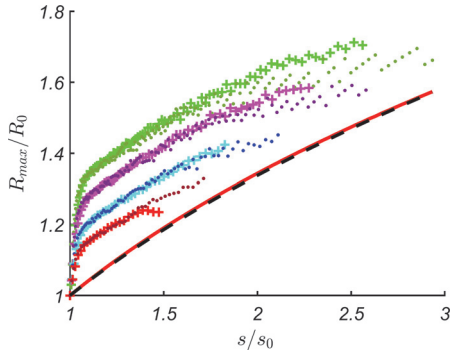

Figure 10. The ratio of maximum run-up height in the conjoined basin, $R_{\max}/A$, and the maximum run-up height on a plane beach, R_0/A, versus the wave front steepness, s/s_0, for $A/h_0 = 0.057$, $kh_0 = 0.38$ (brown points); $A/h_0 = 0.086$, $kh_0 = 0.38$ (red plus signs); $A/h_0 = 0.057$, $kh_0 = 0.29$ (blue points); $A/h_0 = 0.086$, $kh_0 = 0.29$ (turquoise plus signs); $A/h_0 = 0.057$, $kh_0 = 0.22$ (violet points); $A/h_0 = 0.086$, $kh_0 = 0.22$ (pink plus signs); $A/h_0 = 0.057$, $kh_0 = 0.19$ (dark-green points); and $A/h_0 = 0.086$, $kh_0 = 0.19$ (light-green plus signs). All markers correspond to the results of numerical simulations, while the asymptotic analytical predictions are given by the red solid line. Black dashed line corresponds to the power fit of the analytical results of Eq. (16).

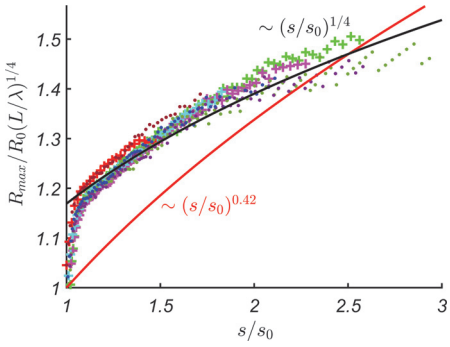

Figure 11. The normalized maximum run-up height, $R_{\max}/R_0 (L/\lambda)^{1/4}$, calculated numerically versus the wave front steepness, s/s_0, for the same values of A/h_0 and kh_0 as in Fig. 10. Red solid line is proportional to the "analytically estimated" Eq. (16), while black solid line corresponds to Eq. (17).

The results of numerical simulations are shown in Fig. 10 with different markers. It can be seen that numerical data for the same period but different amplitudes follow the same curve. The run-up is higher for waves with smaller kh_0. In our opinion, this dependence on kh_0 is a result of merging a plane beach with a flat bottom. This effect can be parameterized with the factor $(L/\lambda)^{1/4}$. The result of this parameterization is shown in Fig. 11. Here we can see that for smaller face front wave steepness, $s/s_0 < 1.5$, the run-up height is proportional to the analytically estimated curve shown by Eq. (16), while for larger face front wave steepness, $s/s_0 > 1.5$, the dependence on s/s_0 is weaker. This dependence for all numerical run-up height data, presented in Fig. 11, can be approximated by the power fit (coefficient of determination $R^2 = 0.85$):

$$R_{\max}/R_0 = 1.17(\lambda/L)^{1/4}(s/s_0)^{1/4}. \quad (17)$$

5 Conclusions and discussion

In this paper, we study the nonlinear deformation and run-up of tsunami waves, represented by single waves of positive polarity. We consider the conjoined water basin, which consists of a section of constant depth and a plane beach. While propagating in such basin, the wave shape changes forming a steep front. Tsunamis often approach the coast with a steep wave front, as was observed during large tsunami events, e.g. the 2004 Indian Ocean Tsunami and 2011 Tohoku tsunami.

The study is performed both analytically and numerically in the framework of the nonlinear shallow-water theory. The analytical solution considers nonlinear wave steepening in the constant depth section and wave run-up on a plane beach independently and, therefore, does not take into account wave interaction with the toe of the bottom slope. The propagation along the bottom of constant depth is described by a Riemann wave, while the wave run-up on a plane beach is calculated using rigorous analytical solutions of the nonlinear shallow-water theory following the Carrier–Greenspan approach. The numerical scheme does not have this limitation. It employs the finite-volume method and is based on the second-order UNO2 reconstruction in space and the third-order Runge–Kutta scheme with locally adaptive time steps. The model is validated against experimental data.

The main conclusions of the paper are the following.

- It is found analytically that the maximum tsunami run-up height on a beach depends on the wave front steepness at the toe of the bottom slope. This dependence is general for single waves of different amplitudes and periods and can be approximated by the power fit: $R_{\max}/R_0 = (s/s_0)^{0.42}$.
- This dependence is slightly weaker than the corresponding dependence for a sine wave, proportional to the square root of the wave front steepness (Didenkulova et al., 2007). The stronger dependence of a sine wave run-up on the wave front steepness is consistent with the philosophy of N waves (Tadepalli and Synolakis, 1994).
- Numerical simulations in general support this analytical finding. For smaller face front wave steepness

($s/s_0 < 1.5$), numerical curves of the maximum tsunami run-up height are parallel to the analytical ones, while for larger face front wave steepness ($s/s_0 > 1.5$), this dependence is milder. The latter may be a result of numerical dissipation (error), which is larger for a longer wave propagation and, consequently, larger wave steepness. The suggested formula, which gives the best fit with the data of numerical simulations in general, is $R_{\max}/R_0 = 1.17(\lambda/L)^{1/4}(s/s_0)^{1/4}$.

– These results can also be used in tsunami forecasts. Sometimes, in order to save time for tsunami forecasts, especially for long distance wave propagation, the tsunami run-up height is not simulated directly but estimated using analytical or empirical formulas (Glimsdal et al., 2019; Løvholt et al., 2012). In these cases we recommend using formulas which take into account the face front wave steepness. The face front steepness of the approaching tsunami wave can be estimated from the data of the virtual (computed) or real tide-gauge stations and then be used to estimate the tsunami maximum run-up height on a beach.

The nonlinear shallow-water equations, which are used in this study and commonly utilized for tsunami modelling, are also known to neglect dispersive effects. In this context, it is important to mention the recent work of Larsen and Fuhrman (2019). They used Reynolds-averaged Navier–Stokes (RANS) equations and k–ω model for turbulence closure to simulate the propagation and run-up of positive single waves, including full resolution of dispersive short waves (and their breaking) that can develop near a positive tsunami front. They similarly showed that this effect depends on the propagation distance prior to the slope if a simple toe with a slope type of bathymetry is utilized. This work shows that these short waves have little effect on the overall run-up and hence give additional credence to the use of shallow-water equations. These results largely confirm what was previously hypothesized by Madsen et al. (2008), namely that these short waves would have little effect on the overall run-up and inundation of tsunamis (though they found that they could significantly increase the maximum flow velocities).

Data availability. The data used for all figures of this paper are available at https://doi.org/10.13140/rg.2.2.27658.41922 (Abdalazeez et al., 2019). The source code (in MATLAB) used to generate these data may be shared upon request.

Author contributions. AAA ran all the calculations, prepared the data for sharing, discussed the results and wrote the first draft of the manuscript. ID initiated this study, provided the numerical code for analytical solution, discussed the results and contributed to the writing of the manuscript. DD developed and provided numerical solvers for nonlinear shallow-water equations, discussed the results and contributed to the writing of the manuscript. All authors reviewed the final version of the paper.

Competing interests. The author declares that there is no conflict of interest.

Acknowledgements. The authors are very grateful to Professor Efim Pelinovsky, who came up with the idea for this study a few years ago.

Financial support. Analytical calculations were performed with the support of Russian Science Foundation grant no. 16-17-00041. Numerical simulations and their comparison with the analytical findings were supported by ETAG grant no. PUT1378. The authors also thank the PHC PARROT project no. 37456YM, which funded the authors' visits to France and Estonia and allowed this collaboration.

Review statement. This paper was edited by Mauricio Gonzalez and reviewed by two anonymous referees.

References

Abdalazeez, A. A., Didenkulova, I., and Dutykh, D.: Data_Nonlinear deformation and run-up of single tsunami waves of positive polarity numerical simulations and analytical predictions.zip, https://doi.org/10.13140/rg.2.2.27658.41922, 2019.

Brocchini, M. and Gentile, R.: Modelling the run-up of significant wave groups, Cont. Shelf Res., 21, 1533–1550, https://doi.org/10.1016/S0278-4343(01)00015-2, 2001.

Carrier, G. F. and Greenspan, H. P.: Water waves of finite amplitude on a sloping beach, J. Fluid Mech., 4, 97–109, https://doi.org/10.1017/S0022112058000331, 1958.

Carrier, G. F., Wu, T. T., and Yeh, H.: Tsunami run-up and draw-down on a plane beach, J. Fluid Mech., 475, 79–99, https://doi.org/10.1017/S0022112002002653, 2003.

Didenkulova, I.: New trends in the analytical theory of long sea wave runup, in: Applied Wave Mathematics, edited by: Quak, E. and Soomere, T., Springer, Berlin, Heidelberg, Germany, 265–296, https://doi.org/10.1007/978-3-642-00585-5_14, 2009.

Didenkulova, I., Pelinovsky, E., Soomere, T., and Zahibo, N.: Runup of nonlinear asymmetric waves on a plane beach, in: Tsunami and nonlinear waves, edited by: Kundu, A., Springer, Berlin, Heidelberg, Germany, 175–190, https://doi.org/10.1007/978-3-540-71256-5_8, 2007.

Didenkulova, I., Pelinovsky, E., and Soomere, T.: Runup characteristics of symmetrical solitary tsunami waves of "unknown" shapes, Pure Appl. Geophys., 165, 2249–2264, https://doi.org/10.1007/978-3-0346-0057-6_13, 2008.

Didenkulova, I., Denissenko, P., Rodin, A., and Pelinovsky, E.: Effect of asymmetry of incident wave on

the maximum runup height, J. Coastal Res., 65, 207–212, https://doi.org/10.2112/SI65-036.1, 2013.

Didenkulova, I., Pelinovsky, E. N., and Didenkulova, O. I.: Run-up of long solitary waves of different polarities on a plane beach. Izvestiya, Atmos. Ocean. Phys., 50, 532–538, https://doi.org/10.1134/S000143381405003X, 2014.

Dutykh, D., Poncet, R., and Dias, F.: The VOLNA code for the numerical modeling of tsunami waves: Generation, propagation and inundation, Eur. J. Mech. B-Fluid., 30, 598–615, https://doi.org/10.1016/j.euromechflu.2011.05.005, 2011a.

Dutykh, D., Katsaounis, T., and Mitsotakis, D.: Finite volume schemes for dispersive wave propagation and runup, J. Comput. Phys., 230, 3035–3061, https://doi.org/10.1016/j.jcp.2011.01.003, 2011b.

Glimsdal, S., Løvholt, F., Harbitz, C. B., Romano, F., Lorito, S., Orefice, S., Brizuela, B., Selva, J., Hoechner, A., Volpe, M., Babeyko, A., Tonini, R., Wronna, M., and Omira, R.: A new approximate method for quantifying tsunami maximum inundation height probability, Pure Appl. Geophys., 176, 3227–3246, https://doi.org/10.1007/s00024-019-02091-w, 2019.

Gosse, L.: Computing qualitatively correct approximations of balance laws: exponential-fit, well-balanced and asymptotic-preserving, Springer Milan, Italy, 2013.

Kânoğlu, U.: Nonlinear evolution and runup–rundown of long waves over a sloping beach, J. Fluid Mech., 513, 363–372, https://doi.org/10.1017/S002211200400970X, 2004.

Kânoğlu, U. and Synolakis, C.: Initial value problem solution of nonlinear shallow water-wave equations, Phys. Rev. Lett., 97, 148501, https://doi.org/10.1103/PhysRevLett.97.148501, 2006.

Larsen, B. E. and Fuhrman, D. R.: Full-scale CFD simulation of tsunamis. Part 1: Model validation and run-up, Coast. Eng., 151, 22–41, https://doi.org/10.1016/j.coastaleng.2019.04.012, 2019.

Li, Y. and Raichlen, F.: Non-breaking and breaking solitary wave run-up, J. Fluid Mech., 456, 295–318, https://doi.org/10.1017/S0022112001007625, 2002.

Lin, P., Chang, K. A., and Liu, P. L. F.: Runup and rundown of solitary waves on sloping beaches, J. Waterw. Port C., 125, 247–255, https://doi.org/10.1061/(ASCE)0733-950X(1999)125:5(247), 1999.

Løvholt, F., Glimsdal, S., Harbitz, C. B., Zamora, N., Nadim, F., Peduzzi, P., Dao, H., and Smebye, H.: Tsunami hazard and exposure on the global scale, Earth-Sci. Rev., 110, 58–73, https://doi.org/10.1016/j.earscirev.2011.10.002, 2012.

Madsen, P. A. and Fuhrman, D. R.: Run-up of tsunamis and long waves in terms of surf-similarity, Coast. Eng., 55, 209–223, https://doi.org/10.1016/j.coastaleng.2007.09.007, 2008.

Madsen, P. A. and Schäffer, H. A.: Analytical solutions for tsunami run-up on a plane beach: single waves, N-waves and transient waves, J. Fluid Mech., 645, 27–57, https://doi.org/10.1017/S0022112009992485, 2010.

Madsen, P. A., Fuhrman, D. R., and Schäffer, H. A.: On the solitary wave paradigm for tsunamis, J. Geophys. Res.-Oceans, 113, 1–22, https://doi.org/10.1029/2008JC004932, 2008.

Mazova, R. K., Osipenko, N. N., and Pelinovsky, E. N.: Solitary wave climbing a beach without breaking, Rozprawy Hydrotechniczne, 54, 71–80, 1991.

McGovern, D. J., Robinson, T., Chandler, I. D., Allsop, W., and Rossetto, T.: Pneumatic long-wave generation of tsunami-length waveforms and their runup, Coast. Eng., 138, 80–97, https://doi.org/10.1016/j.coastaleng.2018.04.006, 2018.

Pedersen, G. and Gjevik, B.: Run-up of solitary waves, J. Fluid Mech., 135, 283–299, https://doi.org/10.1017/S002211208700329X, 1983.

Pelinovsky, E. N. and Mazova, R. K.: Exact analytical solutions of nonlinear problems of tsunami wave run-up on slopes with different profiles, Nat. Hazards, 6, 227–249, https://doi.org/10.1007/BF00129510, 1992.

Raz, A., Nicolsky, D., Rybkin, A., and Pelinovsky E.: Long wave runup in asymmetric bays and in fjords with two separate heads, J. Geophys. Res.-Oceans, 123, 2066–2080, https://doi.org/10.1002/2017JC013100, 2018.

Schimmels, S., Sriram, V., and Didenkulova, I.: Tsunami generation in a large scale experimental facility, Coast. Eng., 110, 32–41, https://doi.org/10.1016/j.coastaleng.2015.12.005, 2016.

Shuto, N.: The Nihonkai-chuubu earthquake tsunami on the north Akita coast, Coastal Engineering Japan, JSCE, 28, 255–264, https://doi.org/10.1080/05785634.1985.11924420, 1985.

Sriram, V., Didenkulova, I., Sergeeva, A., and Schimmels, S.: Tsunami evolution and run-up in a large scale experimental facility, Coast. Eng., 111, 1–12, https://doi.org/10.1016/j.coastaleng.2015.11.006, 2016.

Stoker, J. J.: Water waves, the mathematical theory with applications, Interscience Publishers Inc., New York, 1957.

Synolakis, C. E.: The run-up of solitary waves, J. Fluid Mech., 185, 523–545, https://doi.org/10.1017/S002211208700329X, 1987.

Synolakis, C. E., Deb, M. K., and Skjelbreia, J. E.: The anomalous behavior of the runup of cnoidal waves, Phys. Fluids, 31, 3–5, https://doi.org/10.1063/1.866575, 1988.

Tadepalli, S. and Synolakis, C. E.: The run-up of N-waves, P. Roy. Soc. Lond. A, 445, 99–112, https://doi.org/10.1098/rspa.1994.0050, 1994.

Tang, J., Shen, Y., Causon, D. M., Qian, L., and Mingham, C. G.: Numerical study of periodic long wave run-up on a rigid vegetation sloping beach, Coast. Eng., 121, 158–166, https://doi.org/10.1016/j.coastaleng.2016.12.004, 2017.

Tinti, S. and Tonini, R.: Analytical evolution of tsunamis induced by near-shore earthquakes on a constant-slope ocean, J. Fluid Mech., 535, 33–64, https://doi.org/10.1017/S0022112005004532, 2005.

Touhami, H. E. and Khellaf, M. C.: Laboratory study on effects of submerged obstacles on tsunami wave and run-up, Nat. Hazards, 87, 757–771, https://doi.org/10.1007/s11069-017-2791-9, 2017.

Yao, Y., He, F., Tang, Z., and Liu, Z.: A study of tsunami-like solitary wave transformation and run-up over fringing reefs, Ocean Eng., 149, 142–155, https://doi.org/10.1016/j.oceaneng.2017.12.020, 2018.

Zahibo, N., Didenkulova, I., Kurkin, A., and Pelinovsky E.: Steepness and spectrum of nonlinear deformed shallow water wave, Ocean Eng., 35 47–52, https://doi.org/10.1016/j.oceaneng.2007.07.001, 2008.

Zainali, A., Marivela, R., Weiss, R., Yang, Y., and Irish, J. L.: Numerical simulation of nonlinear long waves in the presence of discontinuous coastal vegetation, Mar. Geol., 396, 142–149, https://doi.org/10.1016/j.margeo.2017.08.001, 2017.

Publication II

Torsvik, T., Abdalazeez, A., Dutykh, D., Denissenko, P., Didenkulova, I. 2019. Dispersive and non-dispersive nonlinear long wave transformations: Numerical and experimental results. In: A. Berezovski, T. Soomere (Ed.). Applied Wave Mathematics II. Selected Topics in Solids, Fluids, and Mathematical Methods and Complexity (41−60). Swizerland: Springer.10.1007/978-3-030-29951-4_3.

Chapter 3
Dispersive and Nondispersive Nonlinear Long Wave Transformations: Numerical and Experimental Results

Tomas Torsvik, Ahmed Abdalazeez, Denys Dutykh, Petr Denissenko, and Ira Didenkulova

Abstract The description of gravity waves propagating on the water surface is considered from a historical point of view, with specific emphasis on the development of a theoretical framework and equations of motion for long waves in shallow water. This provides the foundation for a subsequent discussion about tsunami wave propagation and runup on a sloping beach, and in particular the role of wave dispersion for this problem. Wave tank experiments show that wave dispersion can play a significant role for the propagation and wave transformation of wave signals that include some higher frequency components. However, the maximum runup height is less sensitive to dispersive effects, suggesting that runup height can be adequately calculated by use of nondispersive model equations.

T. Torsvik (✉)
Norwegian Polar Institute, Fram Centre, Tromsø, Norway

Geophysical Institute, University of Bergen, Bergen, Norway
e-mail: Tomas.Torsvik@uib.no

A. Abdalazeez
Department of Marine Systems, School of Science, Tallinn University of Technology, Tallinn, Estonia
e-mail: ahmed.abdalazeez@taltech.ee

D. Dutykh
University Grenoble Alpes, University Savoie Mont Blanc, CNRS, LAMA, Chambéry, France
e-mail: Denys.Dutykh@univ-savoie.fr

P. Denissenko
School of Engineering, University of Warwick, Coventry, UK
e-mail: P.Denissenko@warwick.ac.uk

I. Didenkulova
Department of Marine Systems, School of Science, Tallinn University of Technology, Tallinn, Estonia

Nizhny Novgorod Technical University n.a. R.E. Alekseev, Nizhny Novgorod, Russia
e-mail: irina.didenkulova@taltech.ee

A. Berezovski, T. Soomere (eds.), *Applied Wave Mathematics II*, Mathematics of Planet Earth 6, https://doi.org/10.1007/978-3-030-29951-4_3

3.1 Introduction

Surface gravity waves propagating on the air–sea interface are categorised as *long waves* when their wave length λ is large compared with the average water depth h in a water basin. Waves of this type include very large scale phenomena such as tides and seiches, and local phenomena such as nonbreaking shoaling waves at the coast. In recent years much attention has been connected with the study of tsunamis, with respect to their propagation over vast distances in the open ocean, their transformation in coastal waters and their resulting inundation of coastal areas.

A range of different model equations have been discussed in connection with long wave propagation, including nonlinear shallow water (NLSW) equations and Boussinesq-type equations, which differ in their ability to represent nonlinear and dispersive effects. While elaborate model equations may provide more accurate representation of the wave propagation and transformation, they are generally more computationally demanding to integrate over time. In practical cases where a prediction of the wave behaviour is needed quickly, such as for a tsunami warning system, it has therefore been common practice to rely on simple NLSW equations rather than Boussinesq-type equations. Questions regarding the tradeoff between accuracy of prediction and efficiency of computation for shallow water model equations remain an active area of research to this day.

In this chapter we consider the problem of shallow water waves in a historical context, introducing some basic concepts of wave propagation. Thereafter we discuss the importance of these factors in the context of tsunami wave propagation and runup on a sloping beach. Finally we consider some examples of different wave types, and assess the suitability of NLSW equations and a Boussinesq-type equation for each of these.

3.2 Historical Background

The description of surface gravity wave propagation at the air–sea interface is one of the truly classical subjects in fluid mechanics, and developed in multiple stages with early contributions from some of the most prominent figures in science history such as Newton, Euler, Laplace, Lagrange, Poisson, Cauchy and Airy (see (Darrigol, 2003; Craik, 2004, 2005) for historical references).

For instance, in 1786 Lagrange demonstrated that small amplitude waves would propagate in shallow water with a velocity of $c = \sqrt{gh}$, where g represents the acceleration of gravity and h represents the water depth. Laplace (1776) was the first to pose the general initial value problem for water wave motion, i.e., *given a localised initial disturbance of the sea surface, what is the subsequent motion?* He was also the first to derive the full linear dispersion relation for water waves. A complete linear wave theory, which included wave dispersion, was later published by Airy (1845). Despite the long and extensive history of investigations into this problem, the study

of dispersive surface gravity waves continues to be an active field of research to this day.

3.2.1 Airy Wave Theory

In the following discussion we will restrict our attention to wave propagation in one horizontal dimension x on a surface that can be displaced in the vertical z direction (see Fig. 3.1). It is fairly simple to extend the theory to two horizontal dimensions, but we will not consider any examples where this is necessary, e.g. crossing wave patterns. A more thorough description of these equations can be found in standard fluid mechanics textbooks, e.g., (Kundu, 1990).

A simple model equation for the propagation of surface gravity waves can be derived under the assumption of irrotational fluid motion, ignoring viscous effects, in which case the flow velocity components can be expressed in terms of a *velocity potential* ϕ, defined by

$$u = \frac{\partial \phi}{\partial x} \quad \text{and} \quad w = \frac{\partial \phi}{\partial z}\,, \tag{3.1}$$

for horizontal and vertical velocity components u and w, respectively. We do not consider effects due to surface tension, which is an important effect for short and steep waves but do not contribute significantly to long crested waves. Lastly, we assume that the water depth does not change very abruptly, i.e., that the water depth is fairly constant over the wave length.

The basic equation of motion is derived from the continuity equation

$$\frac{\partial u}{\partial x} + \frac{\partial w}{\partial z} = 0\,, \tag{3.2}$$

which is transformed to the Laplace equation

$$\frac{\partial^2 \phi}{\partial x^2} + \frac{\partial^2 \phi}{\partial z^2} = 0\,, \tag{3.3}$$

with substitution of the velocity potential. The sea bed is traditionally considered to be rigid and nonpermeable, which implies that flow is only permitted along the bed profile. Under this assumption the boundary condition at the sea bed requires a zero

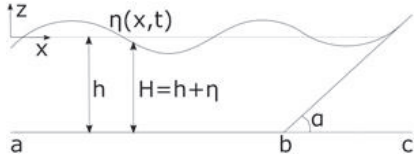

Fig. 3.1 Reference coordinate system for surface gravity waves.

normal velocity to the bed surface itself, which for a flat sea bed simplifies to

$$w = \left.\frac{\partial \phi}{\partial z}\right|_{z=\eta} = 0\,. \tag{3.4}$$

At the sea surface the fluid parcels are not restricted by any rigid boundary, and in fact the location of this free surface boundary is a variable, we wish to determine by solving the equations of motion. If the wave field is sufficiently smooth we can assume that this boundary is well represented by a material surface, i.e., that fluid parcels at the boundary never leave the surface. Under this assumption the kinematic boundary condition prescribed at $z = \eta$ becomes

$$\left.\frac{\partial \eta}{\partial t} + u\frac{\partial \eta}{\partial x}\right|_{z=\eta} = \left.\frac{\partial \phi}{\partial z}\right|_{z=\eta}\,. \tag{3.5}$$

Provided the nonlinear term in (3.5) is sufficiently small, this expression can be replaced by the linear equation

$$\frac{\partial \eta}{\partial t} = \left.\frac{\partial \phi}{\partial z}\right|_{z=\eta}\,. \tag{3.6}$$

Finally, the dynamic boundary condition prescribes that the pressure is continuous across the free surface boundary, which is expressed by the linear form of the Bernoulli equation

$$\frac{\partial \phi}{\partial t} + \frac{P}{\rho} + gz = 0\,, \tag{3.7}$$

where P is pressure and ρ is density. Assuming that the ambient pressure is zero at the free surface, i.e., $P = 0$ at $z = \eta$, this condition simplifies to

$$\frac{\partial \phi}{\partial t} + g\eta = 0 \quad \text{at} \quad z = \eta\,. \tag{3.8}$$

The complete boundary value problem is defined by (3.3), (3.4), (3.6), and (3.8).

In order to solve the equations we need to assume an initial wave form. By Fourier analysis it is possible to decompose any continuous disturbance into a sum of sinusoidal components, hence we will assume an initial condition specified by one such component with wave number k and angular frequency ω

$$\eta(x, t) = a\cos(kx - \omega t)\,. \tag{3.9}$$

The wave number and angular frequency represents the number of wave cycles (in radians) per unit length and unit time, respectively, and are defined in terms of the

wave length λ and wave period T as

$$k = \frac{2\pi}{\lambda} \quad \text{and} \quad \omega = \frac{2\pi}{T}.$$

Solving the Laplace equation (3.3) with kinematic boundary c ditions (3.4) and (3.6) with this initial condition results in a velocity potential

$$\phi = \frac{a\omega}{k} \frac{\cosh k(z+h)}{\sinh kh} \sin(kx - \omega t), \tag{3.10}$$

and the original velocity components become

$$u = a\omega \frac{\cosh k(z+h)}{\sinh kh} \cos(kx - \omega t), \tag{3.11}$$

$$w = a\omega \frac{\sinh k(z+h)}{\sinh kh} \sin(kx - \omega t). \tag{3.12}$$

By combining this solution with the dynamic boundary condition (3.8) we find the *dispersion relation* between k and ω as

$$\omega = \sqrt{gk \tanh kh}, \tag{3.13}$$

and the corresponding *phase velocity*

$$c_p \equiv \frac{\omega}{k} = \sqrt{\frac{g}{k} \tanh kh}. \tag{3.14}$$

The dispersion relation Eq. (3.13) links the wave number k with the angular frequency ω, and represents a necessary condition for consistency of linear wave solutions for the equations of motion. This implies that sinusoidal wave solutions Eq. (3.9) can exist if and only if the wave length and period are strictly linked with each other according to (3.13). Equation (3.14) demonstrates that the speed of propagation for linear waves depends on the wave number (equivalently, wave length), hence an initial disturbance that contains wave components with various wave numbers will tend to separate into clusters of individual components as the waves propagate away from the source.

For waves in a dispersive medium, the energy of wave components does not propagate with the phase velocity c_p (3.14), but with the *group velocity* $c_g = d\omega/dk$. With dispersion relation (3.13), the group velocity becomes

$$c_g \equiv \frac{d\omega}{dk} = \frac{c_p}{2} \left(1 + \frac{2kh}{\sinh 2kh}\right). \tag{3.15}$$

3.2.1.1 Deep and Shallow Water Approximations

As seen in (3.14), the phase velocity for wave components with different wave numbers depends on the hyperbolic tangent function. It is instructive to consider the behaviour of this equation in the deep and shallow water conditions, which is determined by the value of kh (i.e., water depth relative to wave length). A commonly used classification is to consider $kh \geq \pi$ as deep water, $kh \leq \pi/10$ as shallow water, and $\pi/10 < kh < \pi$ as intermediate water depth. This classification should be considered a "rule-of-thumb" rather than a strict rule, as the dispersion relation varies continuously over the range of kh.

For the deep water approximation, the hyperbolic functions in (3.14) and (3.15) can be approximated as

$$\lim_{kh\to\infty} \tanh kh = 1 \quad \text{and} \quad \lim_{kh\to\infty} \frac{2kh}{\sinh 2kh} = 0\,,$$

in which case the phase and group speed in deep water become

$$c_p = \sqrt{\frac{g}{k}} \quad \text{and} \quad c_g = \frac{c_p}{2}\,, \tag{3.16}$$

respectively. This implies that short waves in deep water propagate slower than longer waves, and the wave energy propagates slower than the wave phase. Note that (3.16) is derived under the assumption that gravity is the only relevant restoring force, which is not always correct. For instance, at very short wave lengths (cm scale at the air–water interface) surface tension becomes the dominant restoring force, which allows shorter wave components to propagate faster than longer wave components. The velocity components simplify to

$$u = a\omega e^{kz} \cos(kx - \omega t)\,, \tag{3.17}$$

$$w = a\omega e^{kz} \sin(kx - \omega t)\,, \tag{3.18}$$

which are circular orbits with a radius of a at the surface. It should be noted that the linear wave theory assumes that effects due to the finite wave amplitude are negligible. In reality waves have a finite amplitude, which induces a slow drift in the direction of wave propagation, and therefore the orbits of fluid parcels are not perfect circles but display a coil-like behaviour. This effect is called *Stokes drift*.

In shallow water the hyperbolic functions in (3.14) can be replaced by kh because

$$\tanh kh = kh + O\left[(kh)^2\right] \quad \text{as} \quad kh \to 0\,,$$

and the hyperbolic function in (3.15) can be approximated as

$$\lim_{kh\to 0} \frac{2kh}{\sinh 2kh} = 1\,,$$

hence the simplified expressions for the phase speed and group speed become

$$c_p = \sqrt{gh} \quad \text{and} \quad c_g = c_p\,, \tag{3.19}$$

respectively. In this case the phase velocity is not dependent on the wave number k, hence waves in the shallow water limit are nondispersive. This is also reflected in the group velocity, which becomes identical to the phase velocity in shallow water. In the special case of unidirectional flow, the shallow water wave field therefore becomes stationary in the coordinate system that follows the phase speed c_p. The velocity components for shallow water waves (of small but finite depth) are

$$u = \frac{a\omega}{kh}\cos(kx - \omega t)\,, \tag{3.20}$$

$$w = a\omega\left(1 + \frac{z}{h}\right)\sin(kx - \omega t)\,. \tag{3.21}$$

These are elliptic orbits where the vertical component is much smaller than the horizontal.

3.2.2 *Nonlinear Long Waves*

The wave theory developed by Airy is a linear system, requiring both the underlying equations of motion and boundary conditions to be linear, and therefore any wave solution to this system must conform to the superposition principle. This means that the net response to the system of two or more stimuli can be established by determining the response of each stimulus separately, and subsequently adding these together. Equivalently, any linear combination or scaling of valid solutions will produce a new valid solution to the problem.

In particular, this means that the wave amplitude, which can be altered by a scalar multiplication, must be an independent variable that cannot have any functional dependence on other wave properties. This property is specific for linear systems, whereas for nonlinear systems the wave amplitude will normally be linked with other wave properties. In fact, waves of this type had already been described at the time when Airy published his account.

A few years prior to the publication of Airy's wave theory, the naval engineer John Scott Russell had published accounts of observations and experiments devoted to surface gravity waves (Russell, 1844). Russell seem to have devoted most of his efforts to explain wave generation and propagation in channels, which was of practical importance for inland waterway transport at that time.

A particularly famous account describes his first observation of a *large, solitary, progressive wave*, which was generated by a boat in a channel and propagated upstream of the boat. Russell was able to follow this wave on horseback for more than a mile, and while it retained its original shape it then gradually subsided.

In a series of subsequent experiments he determined that the wave progressed upstream with a velocity $c = \sqrt{g(h+\eta)}$, and that the wave making resistance against the boat motion was at a maximum when the boat was traveling at this speed. He also proposed that tidal motion could be explained as solitary waves of very large extent, and suggested a mechanism whereby the tidal motion could generate tidal bores in rivers and channels.

Airy devoted some attention to Russell's experiments, but he dismissed Russell's treatment of solitary waves. According to Airy's wave theory, maintaining such a singular disturbance in the absence of any additional force would require the surface slope of the disturbance to be constant, but since the slope should vanish at infinity such a disturbance could not exist.

The existence and importance of solitary waves remained a contested issue for several decades after the initial treatments by Russell and Airy. For example, the prominent scientist Georges Gabriel Stokes first dismissed the possibility of such waves and their relevance to tidal motion in his 1846 hydrodynamic researches review (Stokes, 1846), but later became supportive of the idea after researching finite oscillatory waves.

In 1870 Adhémar Jean Claude Barré de Saint-Venant published an account of tidal bores in rivers (named *mascaret* in French), and the following year (de Saint-Venant, 1871) he presented a set of equations that described the phenomenon

$$\frac{\partial A}{\partial t} + \frac{\partial (Au)}{\partial x} = 0\,, \tag{3.22}$$

$$\frac{\partial u}{\partial t} + u\frac{\partial u}{\partial x} + g\frac{\partial \eta}{\partial x} = -\frac{P_w}{A}\frac{\tau}{\rho}\,, \tag{3.23}$$

where $A(x,t)$ is the channel cross section area, $u(x,t)$ is the depth averaged horizontal velocity component, $P_w(x,t)$ is the length of wetted channel perimeter at the cross section, $\tau(x,t)$ is the wall shear stress, and ρ is the water density.

The set of Eqs. (3.22) and (3.23) represent conservation of mass and balance of momentum, respectively, and is possibly the first version of NLSW equations to be presented in a publication. Due to the friction force induced by the shear stress at channel walls, the momentum of an initial disturbance will not be conserved in the model system. The shallow water equations (3.22, 3.23) can describe the propagation of a solitary wave, but the wave will transform over time, with a steepening of the wave front and a decrease in the slope behind the crest

While this behaviour nicely described the transformation of a regular tidal wave to a tidal bore in a channel, it did not provide an adequate framework for describing the solitary waves of constant shape observed by Russell. Although similar shallow water equations had been presented prior to Saint-Venant's treatment of mascarets

(Fenton, 2010), the one-dimensional (1D) version of the shallow water equations are often referred to as *Saint-Venant equations* in honour of his contribution to understand shallow water hydrodynamics.

The same year as Saint-Venant presented the NLSW equations for description of mascarets, one of his disciples, Joseph Boussinesq, presented the first approximate solution of a solitary wave propagating without deformation (Boussinesq, 1871), which finally provided a firm theoretical support for the existence of Russell's wave. The following year (Boussinesq, 1872) he presented a derivation of equations which permitted his wave solution

$$\frac{\partial \eta}{\partial t} + \frac{\partial (H u_b)}{\partial x} = \frac{h^3}{6} \frac{\partial^3 u_b}{\partial x^3}, \tag{3.24}$$

$$\frac{\partial u_b}{\partial t} + u_b \frac{\partial u_b}{\partial x} + g \frac{\partial \eta}{\partial x} = \frac{h^2}{2} \frac{\partial^3 u_b}{\partial t \partial x^2}, \tag{3.25}$$

where $H = h + \eta$ (Fig. 3.1) and u_b is the horizontal velocity at the sea bed $z = -h$. This is the original version of what is now called *Boussinesq equations*. In the absence of higher order derivatives (right-hand side of (3.24), (3.25)) the Boussinesq system becomes equivalent to the Saint-Venant equations (3.22), (3.23) without a friction term.

Boussinesq derived his equations from the Euler equations by eliminating the explicit dependence on the vertical coordinate z in these equations, while retaining nonlinear terms of highest order. This procedure, which is now commonly used when deriving shallow water equations, does not *a priori* stipulate the vertical reference level to be used for the horizontal velocity component or which higher order terms to retain in the derivation.

Numerous variations of Boussinesq-type systems can therefore be derived by selecting different reference variables and forms of nonlinear terms, resulting in equations with slightly different dispersive and nonlinear properties, as well as numerical stability properties. A particularly useful variation was derived by Peregrine (1967)

$$\frac{\partial \eta}{\partial t} + \frac{\partial (H u)}{\partial x} = 0, \tag{3.26}$$

$$\frac{\partial u}{\partial t} + u \frac{\partial u}{\partial x} + g \frac{\partial \eta}{\partial x} - \frac{h}{2} \frac{\partial^3 (h u)}{\partial^2 x \partial t} + \frac{h^2}{6} \frac{\partial^3 u}{\partial x^2 \partial t} = 0, \tag{3.27}$$

which can be applied under gently varying depth conditions.

While the achievement of Boussinesq is widely recognised, his results were not immediately seized upon by his contemporaries. Five years after Boussinesq presented his solitary wave solution, Lord Rayleigh independently derived a long wave equation for the solitary wave of constant shape (Rayleigh, 1876). When Korteweg and de Vries later derived their famous *Korteweg–de Vries (KdV) equation*,

they reference to Rayleigh's work but were apparently un ware of the e rlier contribution by Boussinesq (Korteweg and de Vries, 1895).

3.2.3 Model Equations for Long Wave Runup on a Beach

In the classical formulations of long wave equations it is usually assumed that the waves propagate in a water basin with small and gentle changes in water depth. However, we would like to apply these model equations to study wave runup on a beach, and this requires some modifications to the standard equation formulations. In the following we consider a depth profile

$$h(x) = \begin{cases} h_0\,, & \text{if } x \in [a,b] \\ h_0 - (x-b)\tan\alpha\,, & \text{if } x \in [b,c] \end{cases}, \tag{3.28}$$

with waves approaching the beach from the offshore point a (Fig. 3.1). The modified NLSW equations are defined as

$$\frac{\partial H}{\partial t} + \frac{\partial (Hu)}{\partial x} = 0\,, \tag{3.29}$$

$$\frac{\partial (Hu)}{\partial t} + \frac{\partial}{\partial x}\left(Hu^2 + \frac{g}{2}H^2\right) = gH\frac{\partial h}{\partial x}\,, \tag{3.30}$$

where $u(x,t)$ is the depth averaged flow velocity. For comparison, we use a Boussinesq-type equation based on Peregrine's formulation, which we call the modified Peregrine equations.

$$\frac{\partial H}{\partial t} + \frac{\partial Q}{\partial x} = 0\,, \tag{3.31}$$

$$\left(1 + \frac{1}{3}\frac{\partial H^2}{\partial x} - \frac{H}{6}\frac{\partial^2 H}{\partial x^2}\right)\frac{\partial Q}{\partial t} - \frac{H^2}{3}\frac{\partial^3 Q}{\partial x^2 \partial t} - \\ - \frac{H}{3}\frac{\partial H}{\partial x}\frac{\partial^2 Q}{\partial x \partial t} + \frac{\partial}{\partial x}\left(\frac{Q^2}{H} + \frac{g}{2}H^2\right) = gH\frac{\partial h}{\partial x}\,, \tag{3.32}$$

where $Q = Hu$ represents the horizontal momentum. The modified Peregrine equations have been studied in detail in (Durán et al., 2018).

3.2.4 Numerical Method

In the following discussion we will apply numerical methods for integration of the Boussinesq equations over time. For simple channel geometries it is possible to derive exact solitary wave and periodic wave solutions to the Boussinesq equations (Clarkson, 1990; Chen, 1998; Yan and Zhang, 1999). Furthermore, the runup properties of such general wave solutions can be investigated by analytical methods for some regular beach profiles (Pelinovsky and Mazova, 1992; Didenkulova et al., 2007; Didenkulova and Pelinovsky, 2011). However, such analytical methods are not practical when considering general wave types and variable depth conditions.

The numerical model we use is based on a finite volume method for both the modified NLSW and modified Peregrine equations (Dutykh et al., 2011; Durán et al., 2018). This involves discretisation of the governing equations, and obtaining solutions on a finite mesh covering the model domain. In the finite volume method, the divergence theorem is applied to convert divergence terms in the differential equations to surface integrals, which are evaluated as fluxes at the cell surfaces in the mesh. Finite volume methods are particularly useful for problems where quantities should be preserved, e.g., mass or momentum, since whatever quantity flows out of one grid cell surface will be identical to the inflow into the neighbouring grid cell.

The simplest approximation to a solution in the finite volume formulation is obtained by considering all variables as constant within each grid cell, whereby a piecewise constant solution can be obtained. However, using this approach, the spatial discretisation error will be determined by the grid size. In order to obtain more accurate results, a common method is to replace the piecewise constant data with a piecewise polynomial representation of the solution. In our simulations we have applied the nonoscillatory UNO2 scheme, which is designed to constrain the number of local extrema in the numerical solution at each time step (Harten and Osher, 1987).

Integration of the solution forward in time is achieved by the Bogacki–Shampine time stepping method (Bogacki and Shampine, 1989). This is a version of a Runge–Kutta method, and is a third order method with four stages. An embedded second order method is used to estimate the local error and if necessary adapt the timestep size.

3.3 Tsunami Propagation and Runup

Developing model equations that adequately describe the propagation and runup of tsunamis is a challenging task. Suggested model formulations range from simple nonlinear shallow water (NLSW) theory to the very elaborate fully nonlinear Navier–Stokes theory, with Boussinesq theory occupying an intermediate place in between. NLSW has often been favoured for long wave runup calculations over dispersive wave models represented by Boussinesq-type approximations. Wave runup calculated

using dispersive model formulations is prone to numerical instabilities, which make computations more sensitive to numerical parameters (Bellotti and Brocchini, 2001). Furthermore, the Boussinesq terms in the dispersive model tend to zero at the shoreline, so that dispersive equations simplify to NLSW in this region (Madsen et al., 1997).

High accuracy can be achieved by applying the fully nonlinear Navier–Stokes equations, but this approach requires large computational resources and a lengthy integration time, making it unsuitable for operational forecasting in oceanwide or even regional scale applications. Horrillo et al. (2006) studied dispersive effects during the 2004 Indian Ocean tsunami propagation by comparing NLSW with the fully nonlinear Navier–Stokes equations. They concluded that NLSW offered the more suitable framework for hazard assessments, providing an adequate assessment at a very low computational cost. Although the NLSW model tended to overpredict the maximum wave runup, the overprediction was considered to be within a reasonable range for a safety buffer, and hence did not degrade the overall assessment.

For tsunami warning purposes it is of critical importance to determine the time of arrival of the leading wave to different coastal sections. These leading waves are usually well described by NLSW, whereas the trailing wave train may contain shorter wave components that are more sensitive to wave dispersion (Løvholt et al., 2012). For this reason, the NLSW is often considered to be more appropriate than more elaborate Boussinesq-type methods for warning purposes (Glimsdal et al., 2013). Note that biggest wave is often not the first one, at least for tsunamis propagating over a long distance, see, for example, (Candella et al., 2008).

3.3.1 Wave Tank Experiment

Wave tank experiments were carried out at the Large Wave Flume (GWK) located in Hannover, Germany, which is the world's largest publicly available research facility of its kind. It has a length of about 310 m usable for experiments, a width of 5 m, and a maximum depth of 7 m. Access to this facility was granted by the Integrating Activity HYDRALAB IV program, and experiments were carried out over two periods; 10–16 Oct. 2012 and 29 July–9 August 2013. The basic experiment setup consisted of a wave generator at one end of the flume, a 251 m channel of constant depth, and a ramp of 1:6 slope at the opposite end of the flume representing the beach.

The water depth in the channel was kept at a constant $h_0 = 3.5$ m for all the experiments. Wave gauges were placed at 16–18 locations along the channel to measure the waves propagating in the channel and up the slope. The wave runup was measured by a capacitance probe and also recorded by two regular video cameras. A series of experiment runs were performed with different initial wave signals, and with varying roughness of the ramp slope surface. Details of the experiments are described in Didenkulova et al. (2013).

3.4 Measured and Modelled Wave Propagation and Runup

In order to illustrate the wave transformation and runup properties for different wave signals, we consider the four experimental test cases listed in Table 3.1. These consist of a regular sine wave, a biharmonic wave signal, a wave train that resembles a ship wake signal, and a single positive pulse. The wave maker produced waves of period $T = 20$ s, which remained constant for the sine and biharmonic signals, but gradually reduced to $T = 10$ s for the wake-like train. The initial wave amplitude was different for each experiment, with the largest initial wave amplitude $A = 0.20$ m for the sine wave (Fig. 3.2). However, the biharmonic wave signal contained two wave components with amplitude $A = 0.12$ m that could interfere constructively to produce instances of larger amplitude wave peaks than the sine wave (Fig. 3.3).

The wake-like train did not contain waves of equal amplitude. Instead, initially long, low amplitude waves were followed by progressively shorter and larger-amplitude waves (Fig. 3.4). The single positive pulses were generated with $A = 0.15$ m, but were not initiated as stable solitary wave shapes and hence reduced in amplitude to approximately $A = 0.10$ m at an early stage during the wave propagation (Fig. 3.5). Each figure shows a comparison between the experimental record and two model results; the dispersive modified Peregrine model (hereafter mPer) and the NLSW model solutions.

Figure 3.2 shows the sine wave propagation and runup. In this case mPer is fairly close to the measured waves throughout the propagation phase and for the runup, although there is a tendency for mPer to underestimate the runup height. It is noticeable that NLSW has a lower wave height near the wave maker than the measured wave, but increase in amplitude relative to the reference solution, and in the final stage produce significantly larger runup values than the measured values. It is clear that the dispersive properties of mPer in this case balance the nonlinear effect to produce a relatively stable wave train, while this feature is missing for NLSW and therefore results in excessive nonlinear steepening and amplification.

Note that the capacitance runup gauge does not record the wave form correctly in the receding phase. The reason is that the wires are submerged in the thin near surface layer of water when the bulk of the wave is gone. Therefore, only the rising front phase of the experimentally measured runup should be used for comparison with the simulations and the rundown values indicated by the gauge should be ignored.

Table 3.1 Parameters for four experiment runs of different wave types, and the measured runup for each case.

Type of waves	Wave period (s)	Initial wave amplitude (m)	Experimental runup (m)
Sine wave	20	0.20	0.571
Biharmonic wave	20	0.12	0.794
Wake-like train	$20 \rightarrow 10$	~ 0.10	0.517
Positive pulse	20	0.15	0.438

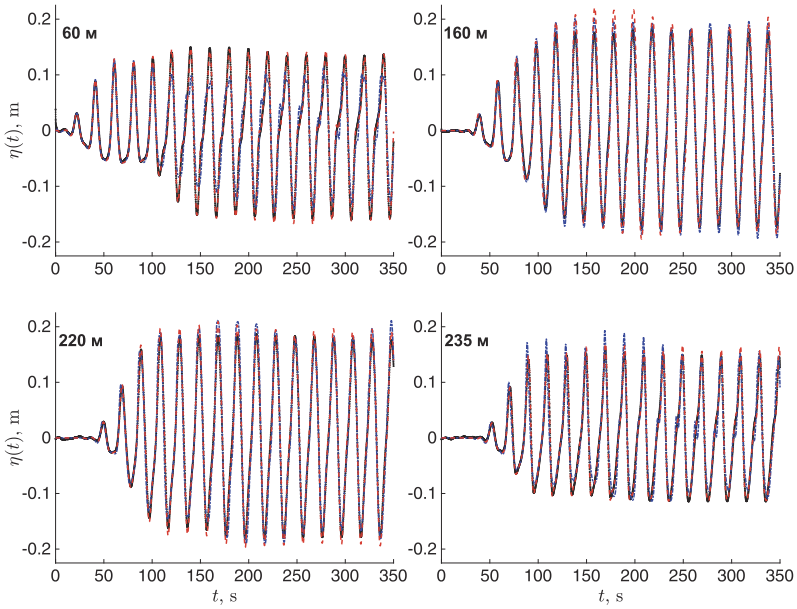

(a) Water surface elevation at different wave gauges (x = 60 m, 160 m, 220 m, and 235 m from the wave maker).

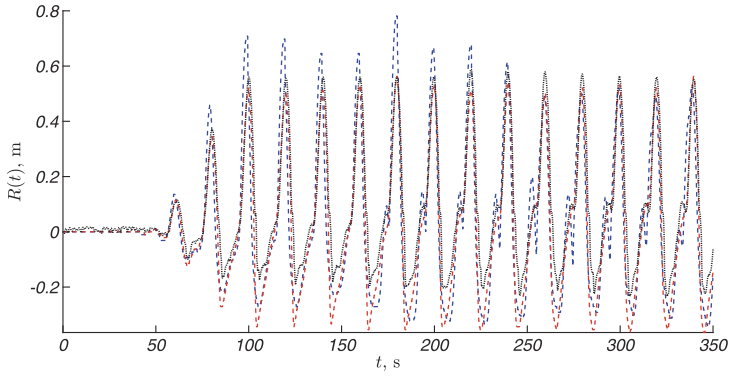

(b) Runup height.

Fig. 3.2 Wave propagation and runup for a sine wave with A = 0.2 m and T = 20 s on a beach slope $\tan\alpha$ = 1:6, mPer is shown with the red dashed line, NLSW solution is shown with blue dash dots line and the experimental record is shown with the black dotted line.

Figure 3.3 shows the biharmonic wave propagation and runup. In this case we again see a reasonably good agreement in wave structure between mPer and the measurements, but there is a clear tendency that mPer underestimates the wave amplitude both in the propagation phase and the runup phase. The NLSW solution looks fairly reasonable in the early stages, but significant discrepancies appear at $x = 180$ m and $x = 230$ m in the later stages of the wave train. The biharmonic

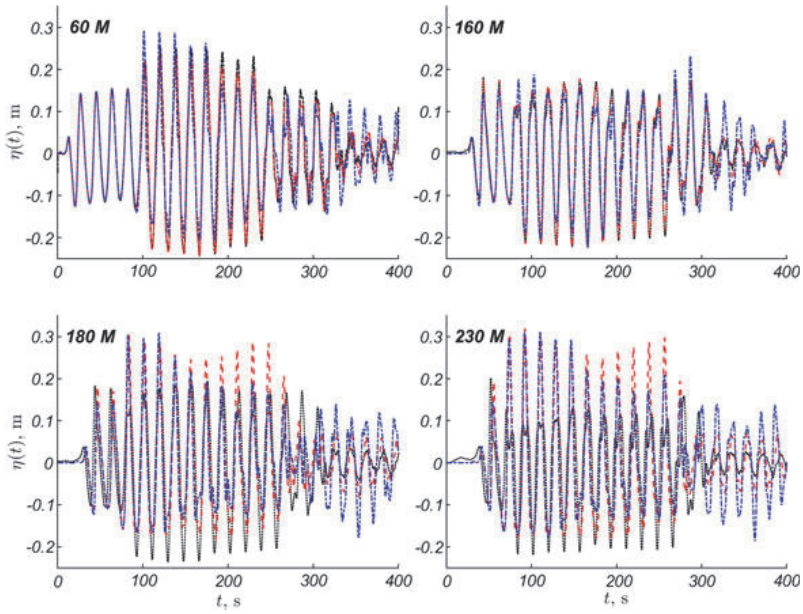

(a) Water surface elevation at different wave gauges (x = 60 m, 160 m, 180 m, and 230 m from the wave maker).

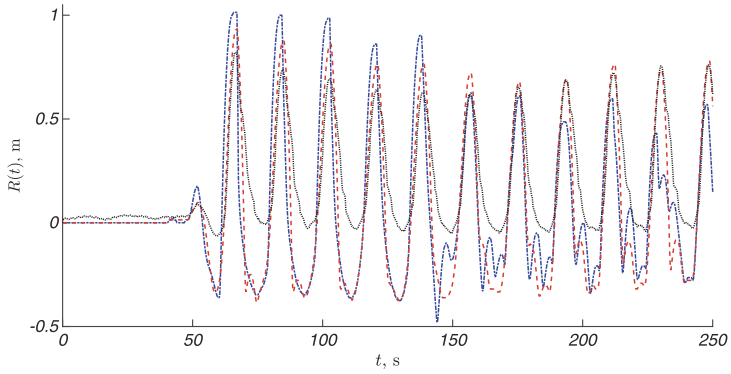

(b) Runup height.

Fig. 3.3 Wave propagation and runup for a biharmonic wave with A = 0.12 m and T = 20 s on a beach slope $\tan\alpha$ = 1:6, mPer is shown with the red dashed line, NLSW solution is shown with Blue dash dots line and the experimental record is shown with the black dots line.

signal is particularly sensitive to the phase speed as wave components may interfere both constructively and destructively at different stages, hence the inclusion of wave dispersion plays a significant role in this case.

Figure 3.4 shows a wave train with a wake-like structure, with a distinct envelope shape created by an initial long, low amplitude wave followed by shorter, higher amplitude waves. The initial phase of the wave train is captured well by both mPer

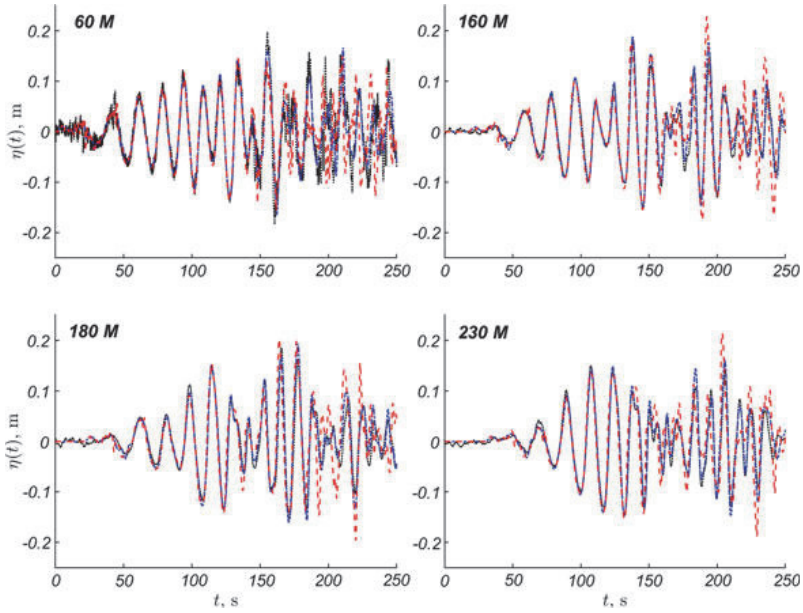

(a) Water surface elevation at different wave gauges (x = 60 m, 160 m, 180 m, and 230 m from the wave maker).

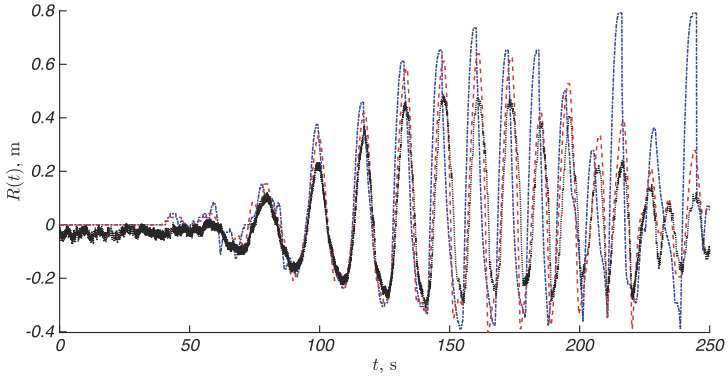

(b) Runup height.

Fig. 3.4 Wave propagation and runup for a wake-like wave train with $A = 0.1$ m and $T \in [10, 20]$ s on a beach slope $\tan\alpha$ = 1:6, mPer is shown with the red dashed line, NLSW is shown with blue dash dots line and the experimental record is shown with the black dotted line.

and NLSW, although both models struggle to reproduce the later stages of the wave train. Both models also reproduce the runup phase fairly well, although NLSW develops a slight phase shift relative to the reference solution, and both models severely overestimates the runup for the trailing waves.

Figure 3.5 shows the wave propagation and runup for single positive pulse waves. The model results for mPer and NLSW are remarkably similar for the propagation

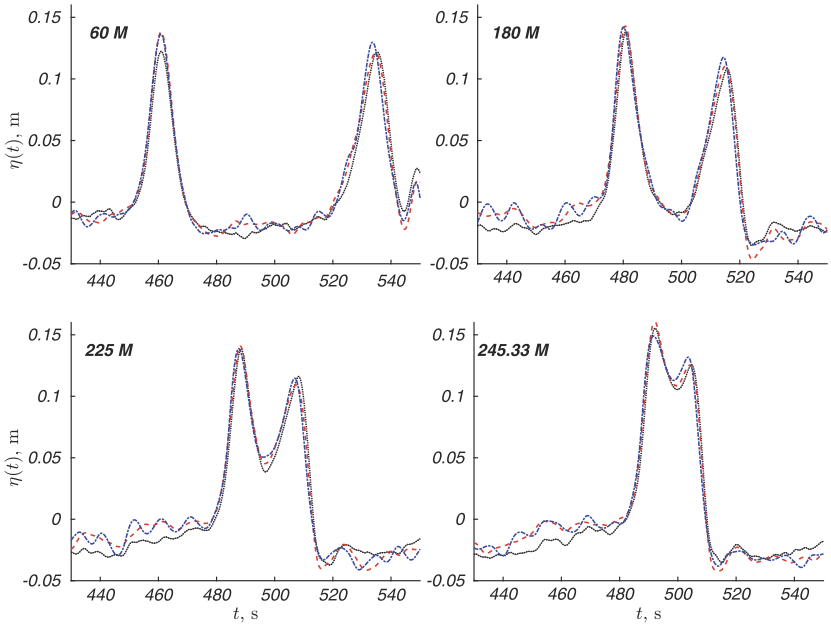

(a) Water surface elevation of a solitary wave at different wave gauges (x = 60 m, 180 m, 225 m, and 245.53 m from the wave maker).

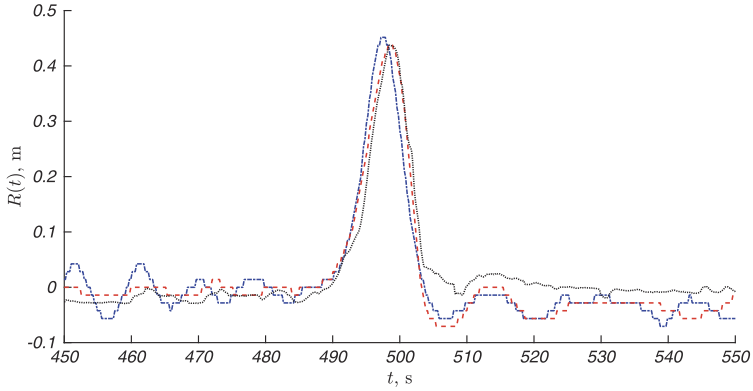

(b) Runup height.

Fig. 3.5 Wave propagation and runup for a single positive pulse (solitary wave) with A = 0.15 m and $T \in [10, 20]$ s on a beach slope $\tan\alpha$ = 1:6, mPer is shown with the red dashed line, NLSW is shown with blue dash dots line and the experimental record is shown with the black dotted line.

phase in this case, although both models tend to overestimate the wave amplitude slightly. This discrepancy can likely be explained by inaccuracies in the initial conditions for the wave, as it deviates slightly from a stable solitary wave form. The runup results are likewise very similar between mPer, NLSW and the reference solution, but again we see the tendency that mPer underestimates the runup height,

whereas NLSW overestimates the runup height and has a slight phase shift indicating that the propagation speed is slightly elevated relative to the reference solution.

3.5 Concluding Remarks

The presented results demonstrate some of the capabilities of the NLSW and modified Peregrine equation systems for representation of long wave transformations. Both models compare well with the long single wave of positive polarity. For sine waves, biharmonic signals and dispersive wake-like signals the wave dispersion clearly plays a more prominent role, in which case NLSW does not adequately represent the high frequency components.

Despite the differences in wave transformation and propagation, the differences in maximum wave runup are quite modest, suggesting that the dispersive wave properties does not influence the resulting runup to a significant extent. This suggests that NLSW could be a suitable framework for prediction of tsunami events in the future, despite the known shortcomings of the model equations for dispersive waves.

Research into surface gravity wave phenomena has a long and fascinating history. Modern day researchers benefit greatly by working within a framework where theories for, e.g., Fourier analysis, ordinary and partial differential equations, potential theory, and perturbative methods, are well established. The emergence of computational resources has created new approaches for research into complex physical phenomena by use of numerical modeling tools.

Despite these differences between modern day research and the situation faced by researchers in the eighteenth and nineteenth centuries, some properties of the research activities are remarkably similar. A constant feature of scientific research is the need to conduct accurate experiments and develop more adequate model equations to describe the natural phenomena we observe. However, there is also a debate concerning the value of accuracy and practicality in describing these phenomena. While Airy and Stokes were debating the existence and basic properties of solitary waves of permanent shape in channels on theoretical grounds, Russell was constructing boats that were capable of high speed travel in channels, helped in part by this very wave phenomenon.

To some extent, a similar debate is on-going today within the tsunami research community, where on one side there is a need to develop models that represent fundamental properties of tsunami waves as accurately as possible in order to study the wave transformation and runup processes in detail, and on the other side there is a need to develop tools for operational forecasting of tsunami wave events that are adequate and practical for warning purposes.

Acknowledgements This work was supported by Estonian Research Council (ETAg) grant PUT1378. Authors also thank the PHC PARROT project No 37456YM, which funded the authors' visits to France and Estonia and allowed this collaboration.

References

Airy, G.B.: Tides and waves. Encyclopaedia Metropolitana (1845)

Bellotti, G., Brocchini, M.: On using Boussinesq-type equations near the shoreline: a note of caution. Ocean Eng. **29**(12), 1569–1575 (2001). https://doi.org/10.1016/s0029-8018(01)00092-0

Bogacki, P., Shampine, L.F.: A 3(2) pair of Runge–Kutta formulas. Appl. Math. Lett. **2**(4), 321–325 (1989). https://doi.org/10.1016/0893-9659(89)90079-7

Boussinesq, J.: Théorie de l'intumescence liquide appelée onde solitaire on de translation, se propageant dans un canal rectangulaire. C. R. Acad. Sci. Paris **72**, 755–759 (1871)

Boussinesq, J.: Théorie des ondes et des remous qui se propagent le long d'un canal rectangulaire horizontal, en communiquant au liquide contenu dans ce canal des vitesses sensiblement pareilles de la surface au fond. Journal de Mathématiques Pures et Appliquées **17**, 55–108 (1872)

Candella, R.N., Rabinovich, A.B., Thomson, R.E.: The 2004 Sumatra tsunami as recorded on the Atlantic coast of South America. Adv. Geosci. **14**, 117–128 (2008). https://doi.org/10.5194/adgeo-14-117-2008

Chen, M.: Exact solutions of various Boussinesq systems. Appl. Math. Lett. **11**(5), 45–49 (1998). https://doi.org/10.1016/S0893-9659(98)00078-0

Clarkson, P.A.: New exact solution of the Boussinesq equation. Eur. J. Appl. Math. **1**(3), 279–300 (1990). https://doi.org/10.1017/S095679250000022X

Craik, D.D.: The origins of water wave theory. Annu. Rev. Fluid Mech. **36**, 1–28 (2004). https://doi.org/10.1146/annurev.fluid.36.050802.122118

Craik, D.D .: Georges Gabriel Stokes on water wave theory. Annu. Rev. Fluid Mech. **37**, 23–42 (2005). https://doi.org/10.1146/annurev.fluid.37.061903.175836

Darrigol, O.: The spirited horse, the engineer, and the mathematician: Water waves in nineteenth-century hydrodynamics. Arch. History Exact Sci. **58**(1), 21–95 (2003). https://doi.org/10.1007/s00407-003-0070-5

Didenkulova, I., Pelinovsky, E.: Runup of tsunami waves in U-shaped bays. Pure Appl. Geophys. **168**(6–7), 1239–1249 (2011). https://doi.org/10.1007/s00024-010-0232-8

Didenkulova, I., Pelinovsky, E., Soomere, T., Zahibo, N.: Runup of nonlinear asymmetric waves on a plane beach. In: Kundu, A. (ed.) Tsunami & Nonlinear Waves, pp. 175–190. Springer, Berlin (2007). https://doi.org/10.1007/978-3-540-71256-5_8

Didenkulova, I., Denissenko, P., Rodin, A., Pelinovsky, E.: Effect of asymmetry of incident wave on the maximum runup height. J. Coastal Res. **65**, 207–212 (2013). https://doi.org/10.2112/SI65-036.1

Durán, A., Dutykh, D., Mitsotakis, D.: Peregrine's system revisited. In: Abcha, N., Pelinovsky, E., Mutabazi, I. (eds.) Nonlinear Waves and Pattern Dynamics, pp. 3–43. Springer, Cham (2018). https://doi.org/10.1007/978-3-319-78193-8_1

Dutykh, D., Katsaounis, T., Mitsotakis, D.: Finite volume schemes for dispersive wave propagation and runup. J. Comput. Phys. **230**, 3035–3061 (2011). https://doi.org/10.1016/j.jcp.2011.01.003

Fenton, J.D.: The long wave equations. Alternative Hydraulics Paper 1, http://johndfenton.com/Papers/01-The-long-wave-equations.pdf (2010)

Glimsdal, S., Pedersen, G.K., Harbitz, C.B., Løvholt, F.: Dispersion of tsunamis: does it really matter? Nat. Hazards Earth. Syst. Sci. **13**, 1507–1526 (2013). https://doi.org/10.5194/nhess-13-1507-2013

Harten, A., Osher, S.: Uniformly high-order accurate nonscillatory schemes. SIAM J. Numer. Anal. **24**, 279–309 (1987). https://doi.org/10.1137/0724022

Horrillo, J., Kowalik, Z., Shigihara, Y.: Wave dispersion study in the Indian Ocean-tsunami of December 26, 2004. Marine Geodesy **29**(3), 149–166 (2006). https://doi.org/10.1080/01490410600939140

Korteweg, D.J., de Vries, G.: On the change of form of long waves advancing in a rectangular channel, and on a new type of long stationary waves. Phil. Mag. **39**, 422–443 (1895). https://doi.org/10.1080/14786449508620739

Kundu, P.K. Fluid Mechanics. Academic Press, San Diego (1990)
Løvholt, F., Pedersen, G., Bazin, S., Kühn, D., Bredesen, R.E., Harbitz, C.: Stochastic analysis of tsunami runup due to heterogeneous coseismic slip and dispersion. J. Geophys. Res.–Oceans **117**, C03047 (2012). https://doi.org/10.1029/2011jc007616
Madsen, P.A., Banijamali, B., Schäffer, H.A., Sørensen, O.R.: Boussinesq type equations with high accuracy in dispersion and nonlinearity. In: Edge, B. (ed.) Coastal Engineering 25th Conference 1996, vol. 1, pp. 95–108. ASCE, Hørsholm, Denmark (1997). https://doi.org/10.1061/9780784402429.008
Pelinovsky, E.N., Mazova, R.K.: Exact analytical solutions of nonlinear problems of tsunami wave run-up on slopes with different profiles. Natural Hazards **6**(3), 227–249 (1992). https://doi.org/10.1007/BF00129510
Peregrine, D.H.: Long waves on a beach. J. Fluid Mech. **27**, 815–827 (1967). https://doi.org/10.1017/s0022112067002605
[Lord] Rayleigh: On waves. Phil. Mag. **1**, 257–279 (1876)
Russell, J.S.: Report on waves. In: Report of the Fourteenth Meeting of the British Association for the Advancement of Science, pp. 311–390 (1844)
de Saint-Venant, A.J.C.B.: Théorie du mouvement non permanent des eaux, avec applications aux crues des rivières et à l'introduction des marées dans leur lit. C. R. Acad. Sci. Paris **73**, 147–154 (1871)
Stokes, G.G.: Report on recent researches in hydrodynamics. Rep. Br. Assoc. Adv. Sci. 1–20 (1846)
Yan, Z., Zhang, H.: New explicit and exact travelling wave solutions for a system of variant Boussinesq equations in mathematical physics. Phys. Lett. A **252**(6), 291–296 (1999). https://doi.org/10.1016/S0375-9601(98)00956-6

Publication III

Abdalazeez, A., Didenkulova, I., Dutykh, D., Denissenko, P. 2020. Comparison of dispersive and nondispersive models for wave runup on a beach. IZvestiya. Atmospheric and Oceanic Physics, Vol. 56, pp. 494–501.

ISSN 0001-4338, Izvestiya, Atmospheric and Oceanic Physics, 2020, Vol. 56, No. 5, pp. 494–501. © Pleiades Publishing, Ltd., 2020.
Russian Text © The Author(s), 2020, published in Izvestiya Rossiiskoi Akademii Nauk, Fizika Atmosfery i Okeana, 2020, Vol. 56, No. 5, pp. 567–574.

Comparison of Dispersive and Nondispersive Models for Wave Run-Up on a Beach

A. Abdalazeez[a], I. I. Didenkulova[a, b, c, *], D. Dutykh[d], and P. Denissenko[e]

[a] *Department of Marine Systems, Tallinn University of Technology, Tallinn, 12618 Estonia*
[b] *Nizhny Novgorod State Technical University, Nizhny Novgorod, 603950 Russia*
[c] *Institute of Applied Physics, Russian Academy of Sciences, Nizhny Novgorod, 603950 Russia*
[d] *Université Grenoble Alpes, Université Savoie Mont Blanc, CNRS, LAMA, 73000 Chamberi, France*
[e] *University of Warwick, Coventry, CV4 7AL UK*
**e-mail: dii@appl.sci-nnov.ru*

Received June 28, 2019; revised March 27, 2020; accepted April 1, 2020

Abstract—The applicability of dispersive and nondispersive wave models for describing long-wave propagation and run-up on a beach in the case of composite bottom topography is investigated: a plane beach transforms into a zone of constant depth. Numerical simulations are performed in the framework of two models: (1) nonlinear shallow-water theory and (2) the dispersive model in the Boussinesq approximation based on modified Peregrine equations. Simulations are compared with the data of a laboratory experiment for different types of waves: regular waves, biharmonic signals, and "vessel-like" wave trains strongly modulated by frequency and amplitude. Conclusions about the applicability of the corresponding theories for describing considered types of waves are drawn based on this comparison.

Keywords: waves on the surface, run-up of long waves on a coast, frequency dispersion, nonlinear shallow-water theory, dispersive theory, modified Peregrine equations

DOI: 10.1134/S0001433820050023

1. INTRODUCTION

In the modern literature, the nonlinear theory of shallow water is more often used to describe the run-up of long waves on a beach than dispersion models, in particular, equations of the Boussinesq type. There are several reasons for this. First, when approaching the coast, the dispersion term in the Boussinesq equations becomes insignificant when compared to the nonlinear term [1]. Second, the calculations of the wave run-up using dispersion codes are less stable when compared to the calculations performed using the nonlinear theory of shallow water [2]. Third, the nonlinear theory of shallow water is considered a more adequate model in the problems of tsunami risk assessment, since the time of simulations is shorter and is not related to an underestimation of the run-up height [3]. The nonlinear theory of shallow water is preferable for the operational forecast of tsunamis based on the same grounds [4].

We also note that the first (leading) tsunami wave is often described reasonably well by both models, while dispersion effects are important for describing the following waves [5]. It is noteworthy that the first tsunami wave is far from always the largest, which is often observed during transoceanic tsunamis propagating over long distances [6]. The dispersion effects can also manifest themselves in a "delay" in the propagation time of tsunami waves [7].

Most of the abovementioned studies were based only on numerical calculations without reference measurements to verify the results of the model simulations. In this paper, we compare the coastal run-up heights calculated using two models with the experimental coastal data of various types of waves: single waves, regular and biharmonic waves, and frequency modulated wave packets. The nonlinear theory of shallow water and a Boussinesq type model based on modified Peregrine equations are used as models.

2. DATA OF LABORATORY EXPERIMENTS

The laboratory experiment was carried out in the Large Wave Flume (Großer Wellenkanal) in Hanover, Germany in 2012–2013 [8, 9]. In the experiment, the standard channel geometry was used, which consists of a flat bottom section of 251 m in length, ending with a flat slope with the tangent of the coastal slope equal to 1 : 6 (Fig. 1). During the experiments, the water depth was set at 3.5 m. Water elevation was measured along the flume by 18 string wave gauges. Displacement of the moving shoreline was measured by a capacitive sensor and two high-resolution cameras. The error in

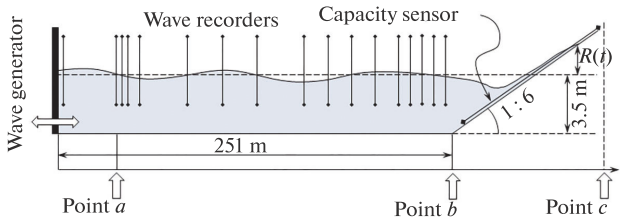

Fig. 1. Scheme of the laboratory experiment in the Large Wave Flume.

measuring the run-up by a capacitive sensor is determined by the variation of the water edge across the slope. According to visual observations, the variation is at the level of ±3% of the run-up magnitude.

The slope of the flume had a rough asphalt coating which strongly affected the measurement of the rollback of waves. When the water moved down from the edge, a layer of water remained on the slope, which touched the capacitive sensor wire and prevented the correct recording of the wave rollback.

The waves were generated using a blade wave generator, which was previously used to generate long waves of the tsunami type [10]. The wave generator was equipped with a mechanism for the active absorption of the reflected wave [11] using signals from two wave recorders as input parameters: one in the immediate vicinity and the other at a distance of 3.6 m from the blade. However, in order to exclude the influence of even a small part of the wave reflected from the wave generator, only the first four waves were used for calculations, the reflection of which has not yet been manifested.

The complete list of the studied waves included regular and biharmonic waves, as well as wave packets modulated in frequency and amplitude resembling characteristic wave records from high-speed vessels [12, 13]. In such generated wave packets, the wave period linearly decreased from 20 to 10 s.

Typical estimates of the spectral power density for the three types of waves under consideration are presented in Fig. 2. The figure shows that the main period is the same for regular and biharmonic waves. It is equal to 20 s, while for ship waves the period of 20 s corresponds to the beginning of a wide peak. The length of such waves in the channel with a depth of $h = 3.5$ m in the approximation of linear gravitational waves is 117 m (parameter $kh = 0.2$), where k is the wave number, which corresponds to shallow-water conditions.

The run-up height was used as the main parameter for comparing the calculations with the experiment.

3. NUMERICAL MODELS

Two models were used in numerical simulations: the nonlinear theory of shallow water and dispersion equations of the Boussinesq type, based on modified Peregrine equations [14]. Both models took into account bottom friction according to the Manning formula [15]. The corresponding roughness coefficient was taken equal to 0.016 s/m$^{1/3}$, which corresponds to rough asphalt coating [16]. The effect of friction when long waves run up the beach was considered in [17].

The bathymetry used in the numerical simulations repeated the geometry of the Large Wave Flume:

$$h(x) = \begin{cases} h_0, & x \in [a,b] \\ h_0 - (x-b)\tan\alpha, & x \in [b,c] \end{cases}, \qquad (1)$$

where $h_0 = 3.5$ m is the constant depth of the tank and α is the beach slope angle (tg $\alpha = 1 : 6$). We assume that $x = 0$ is the location of wave generator as the reference point for measuring all distances. Segment $[a, c]$ corresponds to the left and right boundary of the numerical tank; point $b = 251$ m corresponds to the beginning of the coastal slope (see Fig. 1).

We used the "purest" experimental record of the wave recorder at the point closest to the wave producer as the boundary condition on the left side ($x = $ a). This was a wave record at a distance of $a = 50$ m from the wave generator.

No conditions were imposed on the flow velocity. As proven in [18], the formulation of the problem with one boundary condition at each boundary in the subcritical mode is correct (the horizontal velocity of the fluid particles averaged over depth is smaller than the propagation velocity of long waves; i.e., the Froude number is less than unity). This choice of boundary conditions ensures the transparency of how they were specified.

The number of points of the spatial grid was constant and equal to 4000 in all experiments; hence, the spatial resolution was 6.3 cm. Time stepping was based on the embedded Runge-Kutta methods of orders 3 and 2 [19], implemented in MATLAB using the ode23 command [20]. Thus, in each calculation, an adjustment circuit with the specified error level equal to 10^{-4} was used to select a time step. The characteris-

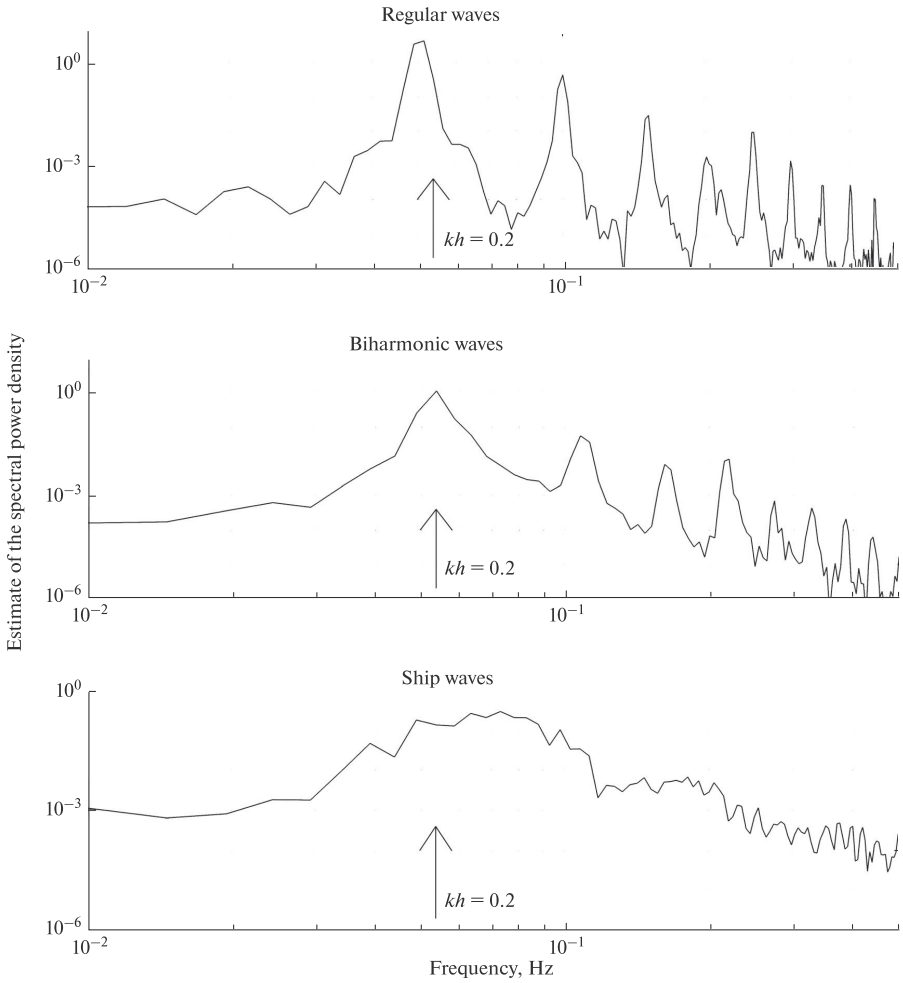

Fig. 2. Estimates of the spectral power density of the studied types of waves.

tic time step used in both models (nonlinear theory of shallow water and modified Peregrine equations) for various types of experiments is presented in Table 1.

The finite volume method was used in both models. The numerical scheme is based on the local second-order polynomial reconstruction (see [21]).

4. PROPAGATION AND RUN-UP OF WAVES

The two models described above (the nonlinear theory of shallow water and the modified Peregrine equations) were used to simulate the experiment carried out in the Large Wave Flume described in Section 2. All types of waves indicated above were simu-

Table 1. Characteristic time step of simulations; types of waves: (1) regular wave, (2) biharmonic wave, and (3) frequency modulated wave packet

Wave type	Modified Peregrine equations, Δt, s	Nonlinear shallow water theory, Δt, s
1	0.012	0.013
2	0.012	0.013
3	0.009	0.012

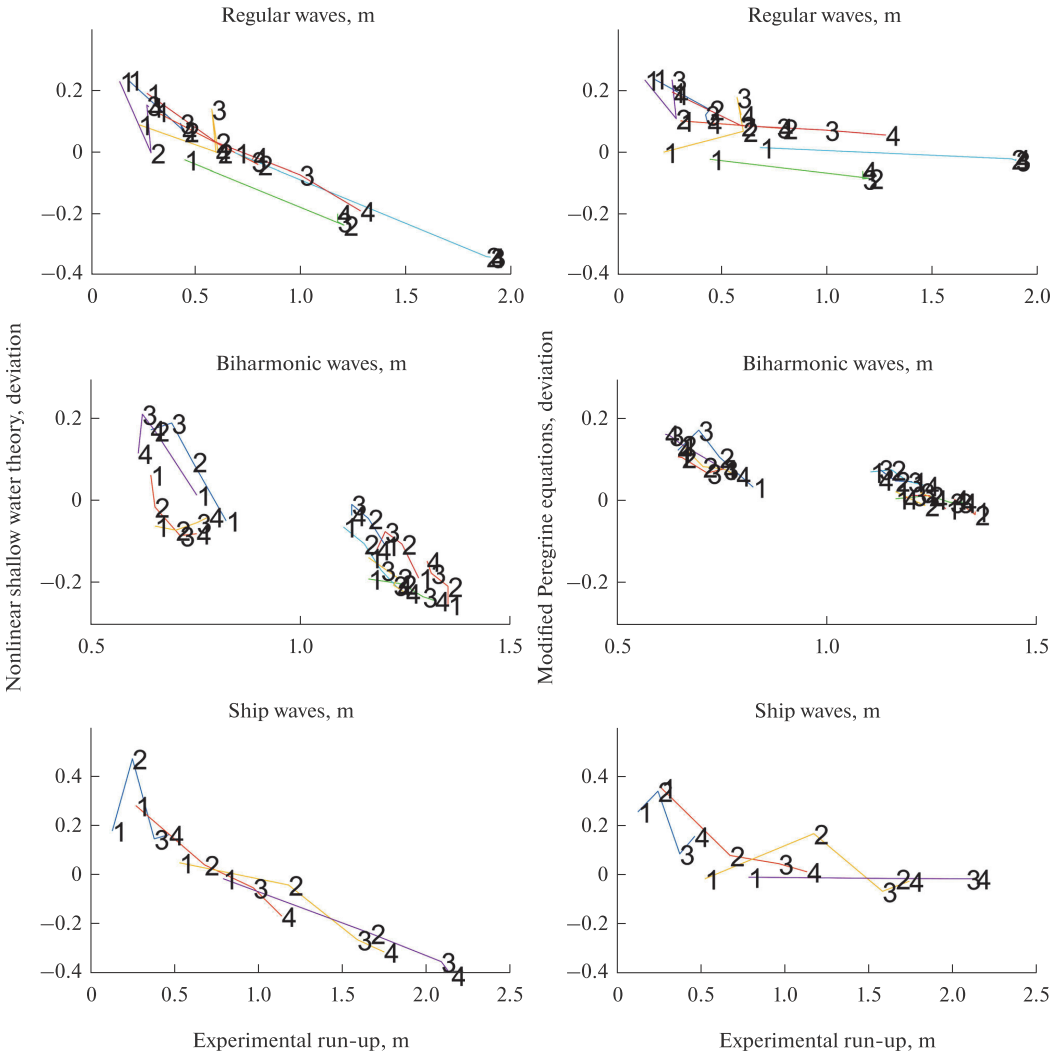

Fig. 3. Comparison of the run-up heights calculated using the nonlinear theory of shallow water (left column) and modified Peregrine equation (right column) for different types of waves. Numerals 1, 2, 3, and 4 correspond to the run-up height of the first, second, third, and fourth waves.

lated. Numerical simulations at the corresponding points were compared with the available measurements of water surface oscillations along the channel and on the shore. In particular, the simulated and measured maximum run-up heights of the first four waves for each type of wave were compared.

The deviation from the experimentally measured value was calculated for each model and for each type of wave normalized by the value of the experimental run-up (Fig. 3). The numerals on the graph represent the maximum run-up of the first, second, third, and fourth waves. It can be seen that, in the simulations using dispersion theory, the scatter between the calculation and the experiment is smaller and, in general, the dispersion theory more reliably describes the experimental data. It is also seen that, as the wave amplitude increases, the difference between the simulation and the experiment decreases and eventually leads to an underestimation of the run-up height. This effect is associated with the wave breaking.

Let us consider different types of waves separately.

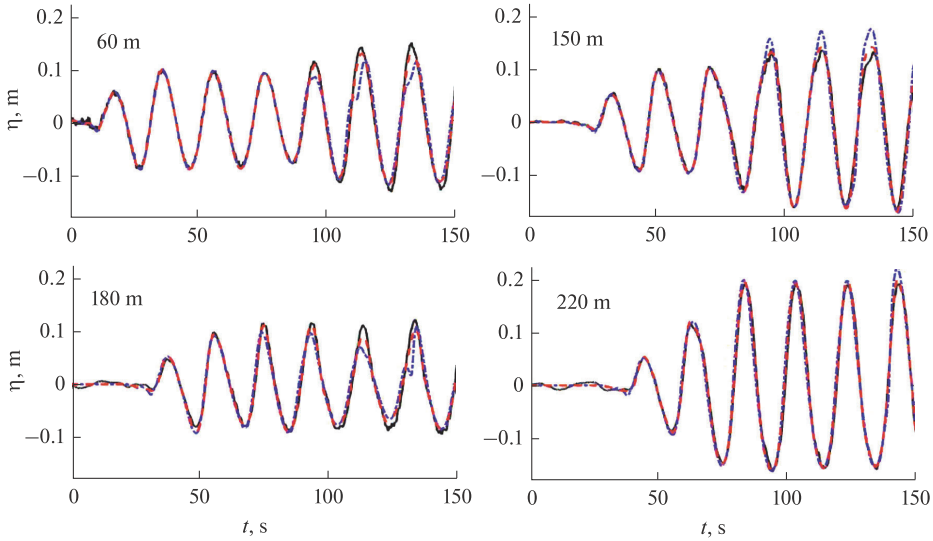

Fig. 4. Oscillations of the water surface caused by a regular wave with a height of 0.2 m. The experimental record is shown with a solid line, calculations based on the nonlinear theory of shallow water are shown with a dashed-and-dotted line, and the calculations using the modified Peregrine equations are shown with a dashed line. The horizontal segment corresponds to the arrival time of the wave reflected from the wave generator.

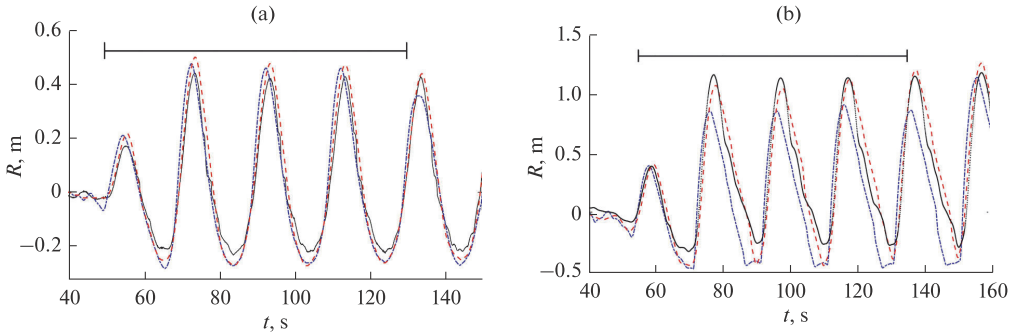

Fig. 5. Run-up of regular waves with a height of 0.2 m (a) and 0.4 m (b). The experimental record is shown with a solid line, the calculations based on the nonlinear theory of shallow water are shown with a dashed-and-dotted line, and the calculations using the modified Peregrine equations are shown with a dashed line. The horizontal segment corresponds to the arrival time of the wave reflected from the wave generator.

4.1. Regular Waves

Figure 4 shows the fluctuations of the water surface caused by a regular wave with a height of 0.2 m. It can be seen that both the nonlinear theory of shallow water and the dispersion theory describe the experimental data quite well.

Figure 5a shows a smooth run-up of a regular wave with a small height of 0.2 m, while in Fig. 5b, we see the run-up of a more nonlinear wave 0.4 m high. It can be seen that the run-up of a weakly nonlinear wave (Fig. 5a) is approximately equally described by both models, but the dispersion theory is a better model to describe the run-up of a more nonlinear wave (Fig. 5b). As noted above, when the wave rolls back in the experiment, a layer of water remains on the slope and touches the wire of the capacitive sensor, so that the sensor poorly records the signal of the rolling back

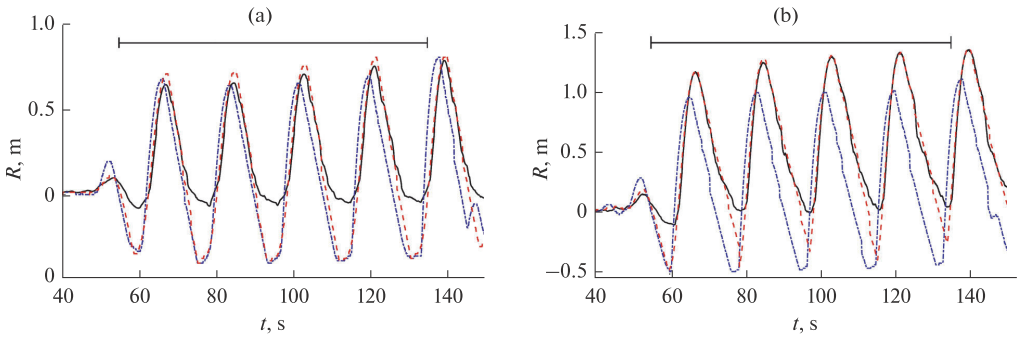

Fig. 6. Run-up of biharmonic waves with a height of 0.27 m (a) and 0.4 m (b). The experimental record is shown with a solid line, the calculations based on the nonlinear theory of shallow water are shown with a dashed-and-dotted line, and the calculations using the modified Peregrine equations are shown with a dashed line. The horizontal segment corresponds to the arrival time of the wave reflected from the wave generator.

wave. This is especially pronounced in the records of large-amplitude waves, in which nonlinear effects are most pronounced at the stage of wave rollback [22, 23].

Despite the fact that both models reproduce the experiment well at a qualitative level (see Figs. 4, 5), there is a quantitative difference, which is especially noticeable for the values of maximum run-up (Fig. 3). Figure 3 shows that the dispersion theory is characterized by a smaller deviation from the experimental data and, as a whole, more reliably describes regular waves. It is also seen that both theories tend to underestimate the run-up of large-amplitude waves, which is a consequence of the wave breaking (see Fig. 3).

4.2. Biharmonic Waves

Figure 6 shows that the descending branch (rollback) of low-amplitude biharmonic waves is described even worse by the experiment than the case of regular waves. This is probably due to the presence of a short-wave component in the spectrum.

The dispersion model proved to be more reliable for the considered model of wave heights (Fig. 6). At low wave amplitudes, it slightly overestimated the run-up height (4–17%), revealing a smaller scatter than the nonlinear theory of shallow water, which overestimated (up to 20%) and underestimated (up to 10%) the values of the run-up height. At higher amplitudes, it could slightly underestimate (no more than 3%) the height of the run-up, providing minimal scatter compared to the nonlinear theory of shallow water, which underestimates the values of the run-up to 25%.

4.3. Frequency Modulated Wave Packets

Let us now consider the most unusual type of waves in this collection: wave packets modulated by frequency and amplitude. The period of such waves decreased linearly from 20 to 10 s. The run-up of these waves in experimental tests with maximum heights of 0.12 and 0.42 m is shown in Fig. 7. It can be seen that both models give approximately the same description of waves of lower amplitude (Fig. 7a), while the shallow-water theory is clearly worse in describing waves of higher amplitude (Fig. 7b), decreasing the expected run-up height by more than 40%. This underestimation of the run-up for higher waves is due to wave breaking effects. The dispersion theory based on the modified Peregrine equations leads to a smaller error when describing the frequency modulated wave packet. Moreover, the underestimation of the run-up height for the highest waves does not exceed 7%. As in the case of regular waves, the described tendency is observed for most waves in the group (Fig. 3). If we compare the simulations of two numerical models, we see that, as in the previous case, the error of simulations based on the shallow water theory is larger than the error of simulations based on the dispersion theory (Fig. 3). However, in this case, the error in the simulations based on the shallow-water theory can be both positive (overestimation) and negative (underestimation).

5. CONCLUSIONS

In this paper, we compared the capabilities of two models: the nonlinear shallow-water theory and the dispersion theory in the Boussinesq approximation represented by modified Peregrine equations to describe the propagation and run-up of long waves on the beach slope. The basis for comparison was the experimental data from the Large Wave Flume (Hanover, Germany) in 2012–2013. During the experiment, various types of waves were tested, including single waves of positive polarity, regular waves, and biharmonic waves, as well as wave packets modulated by frequency and amplitude characteristic of the waves from high-speed vessels. All considered waves had the

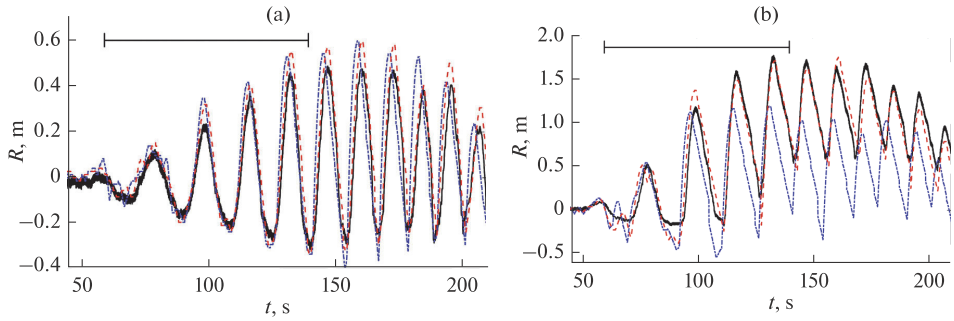

Fig. 7. Roll-up of wave packets modulated in frequency and amplitude, with a maximum height of (a) 0.12 m and (b) 0.42 m. The experimental record is represented by a solid line, the calculations in the framework of the nonlinear theory of shallow water are represented by a dashed-and-dotted line, and the calculations in the framework of modified equations Peregrina are represented by a dashed line. The horizontal segment corresponds to the arrival time of the wave reflected from the wave producer.

same period (characteristic duration) of the main signal (equal to 20 s and corresponding to shallow-water conditions).

It was shown that both models describe almost linear waves of very small amplitude well, while for more nonlinear waves of larger amplitude the dispersion theory has proven to be a more adequate model and is preferable. We emphasize that these conclusions are valid for the considered types of waves in the given range of kh.

FUNDING

Numerical simulations of frequency-modulated waves were performed with financial support from the Russian Science Foundation (grant no. 16-17-00041); other types of waves were simulated with support from the Russian Foundation for Basic Research (grant no. 18-05-80019) and grant PUT1378. Experimental data were collected as part of the Hydralab IV project, grant HyIV-FZK-03. We are also grateful to the PHC PARROT program, grant no. 37456YM, for supporting scientific visits to France and Estonia.

REFERENCES

1. P. A. Madsen, B. Banijamali, H. A. Schäffer, and O. R. Sørensen, "Boussinesq type equations with high accuracy in dispersion and nonlinearity," in *Coastal Engineering* 1996, Ed. by B. Edge (Am. Soc. Civil Eng., New York, NY), **Vol 1**, pp. 95–108.
2. G. Bellotti and M. Brocchini, "On using Boussinesq-type equations near the shoreline: a note of caution," Ocean Eng. **29** (12), 1569–1575 (2002).
3. J. Horrillo, Z. Kowalik, and Y. Shigihara, "Wave dispersion study in the Indian Ocean-tsunami of December 26, 2004," Mar. Geodesy **29** (3), 149–166 (2006).
4. S. Glimsdal, G. K. Pedersen, C. B. Harbitz, and F. Lovholt, "Dispersion of tsunamis: does it really matter?," Nat. Hazards Earth Syst. Sci. **13,** 1507–1526 (2013).
5. F. Løvholt, G. Pedersen, S. Bazin, D. Kuhn, R. E. Bredesen, and C. Harbitz, "Stochastic analysis of tsunami runup due to heterogeneous coseismic slip and dispersion," J. Geophys. Res.: Oceans **117,** C03047 (2012).
6. R. N. Candella, A. B. Rabinovich, and R. E. Thomson, "The 2004 Sumatra tsunami as recorded on the Atlantic coast of South America," Adv. Geosci. **14,** 117–128 (2008).
7. S. Watada, S. Kusumoto, and K. Satake, "Travel time delay and initial phase reversal of distant tsunamis coupled with the self-gravitating elastic Earth," J. Geophys. Res.: Solid Earth **119,** 4287–4310 (2014).
8. P. Denissenko, I. Didenkulova, A. Rodin, M. Listak, and E. Pelinovsky, "Experimental statistics of long wave runup on a plane beach," J. Coastal Res. **65,** 195–200 (2013).
9. I. Didenkulova, P. Denissenko, A. Rodin, and E. Pelinovsky, "Effect of asymmetry of incident wave on the maximum runup height," J. Coastal Res. **65,** 207–212 (2013).
10. S. Schimmels, V. Sriram, and I. Didenkulova, "Tsunami generation in a large-scale experimental facility," Coastal Eng. **110,** 32–41 (2016).
11. R. Schmidt-Koppenhagen, M. Gerdes, E. Tautenhain, and J. Grune, Online absorption control system for wave generation, in *3rd International Symposium on Ocean Wave Measurements and Analysis (WAVES'97; November 1997, Virginia Beach, Virginia, USA),* (Am. Soc. Civil. Eng., Reston, USA, 1998).
12. T. Torsvik, I. Didenkulova, T. Soomere, and K. Parnell, "Variability in spatial patterns of long nonlinear waves from fast ferries in Tallinn Bay," Nonlinear Processes Geophys. **16,** 351–363 (2009).
13. T. Torsvik, T. Soomere, I. Didenkulova, and A. Sheremet, "Identification of ship wake structures by a time-frequency method," J. Fluid Mech. **765,** 229–251 (2015).

14. A. Durán, D. Dutykh, and D. Mitsotakis, Peregrine's system revisited, in *Nonlinear Waves and Pattern Dynamics,* Ed. by N. Abcha, E. Pelinovsky, and I. Mutabazi, (Springer, Cham, 2018), pp. 3–43.
15. R. Manning, "On the flow of water in open channels and pipes," Trans. Inst. Civil Engineers Ireland **20,** 161–207 (1891).
16. Manning's Roughness Coefficients. www.engineeringtoolbox.com/mannings-roughness-d_799.html
17. A. V. Bernatskiy and M. A. Nosov, "The role of bottom friction in models of nonbreaking tsunami wave runup on the shore," Izv., Atmos. Ocean. Phys. **48** (4), 427–431 (2012).
18. M. Petcu and R. Temam, "The one-dimensional shallow water equations with transparent boundary conditions," Math. Methods Appl. Sci. **36,** 1979–1994 (2013).
19. P. Bogacki and L. F. Shampine, "A 3(2) pair of Runge-Kutta formulas," Appl. Math. Lett. **2,** 321–325 (1989).
20. L. F. Shampine and M. W. Reichelt, "The MATLAB ODE suite," SIAM J. Sci. Computing **18,** 1–22 (1997).
21. D. Dutykh, T. Katsaounis, and D. Mitsotakis, "Finite volume schemes for dispersive wave propagation and runup," J. Comput. Phys. **230** (8), 3035–3061 (2011).
22. I. I. Didenkulova, N. Zahibo, A. A. Kurkin, and E. N. Pelinovsky, "Steepness and spectrum of a nonlinearly deformed wave on shallow waters," Izv., Atmos. Ocean. Phys. **42** (6), 773–776 (2006).
23. I. I. Didenkulova, E. N. Pelinovsky, and O. I. Didenkulov, "Run-up of long solitary waves of different polarities on a plane beach," Izv., Atmos. Oceanic Phys. **50,** 532–538 (2014).

Translated by E. Morozov

Publication IV

Abdalazeez, A., Didenkulova, I., Dutykh, D., Labart, C. 2020. Extreme Inundation Statistics on a Composite Beach. Water, 12 (6), 1573−1586. 10.3390/w12061573.

water

MDPI

Article

Extreme Inundation Statistics on a Composite Beach

Ahmed Abdalazeez [1,*], Ira Didenkulova [1,2], Denys Dutykh [3] and Céline Labart [3]

[1] Department of Marine Systems, Tallinn University of Technology, Akadeemia tee 15A, 12618 Tallinn, Estonia; irina.didenkulova@taltech.ee

[2] Department of Applied Mathematics, Nizhny Novgorod State Technical University n.a. R.E. Alekseev, Minin str. 24, 603950 Nizhny Novgorod, Russia

[3] Univ. Grenoble Alpes, Univ. Savoie Mont Blanc, CNRS, LAMA, 73000 Chambéry, France; Denys.Dutykh@univ-smb.fr (D.D.); Celine.Labart@univ-smb.fr (C.L.)

* Correspondence: ahabda@taltech.ee

Received: 14 April 2020; Accepted: 28 May 2020; Published: 31 May 2020

Abstract: The runup of initial Gaussian narrow-banded and wide-banded wave fields and its statistical characteristics are investigated using direct numerical simulations, based on the nonlinear shallow water equations. The bathymetry consists of the section of a constant depth, which is matched with the beach of constant slope. To address different levels of nonlinearity, time series with five different significant wave heights are considered. The selected wave parameters allow for also seeing the effects of wave breaking on wave statistics. The total physical time of each simulated time-series is 1000 h (~360,000 wave periods). The statistics of calculated wave runup heights are discussed with respect to the wave nonlinearity, wave breaking and the bandwidth of the incoming wave field. The conditional Weibull distribution is suggested as a model for the description of extreme runup heights and the assessment of extreme inundations.

Keywords: wave statistics; wave runup; numerical modelling; nonlinear shallow water theory; wave breaking; freak runups

1. Introduction

Estimating extreme runup events in coastal zones is an important task. Flood prediction received a lot of attention in recent decades in order to reduce hazard risks in coastal zones [1–4]. The statistical distribution of wave runup characteristics is influenced by many factors, such as topography and coastline, nonlinearity and wave breaking [5–7].

Also, some individual waves at the coast may be unexpected, extreme and hazardous. This regards sneaker waves or freak wave runups [8–10]. Such extreme events at the coast often lead to human injuries and fatalities, when people are washed off to the sea from a gentle beach or from coastal rocks or sea walls, and damage to coastal structures. During the period of 2011–2018, there were cases when freak wave runups (unrelated to tsunamis) washed cars and motorcycles into the sea and damaged houses and buildings in the coastal zone [10]. These events are described by the tails of the statistical runup height distribution, and their analysis requires extremely large datasets.

Previous studies have employed different methods to study the statistics of long wave runup, including numerical models, experiments, and field measurements.

Theoretically, [11] studied the statistical characteristics of long waves on a beach of constant slope using an analytical solution of the nonlinear shallow water theory. The study revealed that the runup height was distributed according to the Rayleigh distribution, if the incident wave elevation was described as having a normal distribution and a narrow-band spectrum. In terms of the statistical moments of the moving shoreline on a beach of constant slope, this study asserts that the kurtosis is positive for weak amplitude waves and negative for strongly nonlinear waves, whereas the skewness is

always positive. Later, [12] showed that for the description of even non-breaking waves, the Gaussian distribution is inappropriate. Both theoretical studies had a number of assumptions, which were put into question the applicability of these results.

Experimentally, [13] tried to reproduce the theoretical results of [11] in the wave flume at Warwick University. However, they could not generate a "pure" Gaussian wave field. Moreover, the generated waves were affected by capillary effects. Thus, the only result that [13] could reproduce regarded an increase in the mean sea-level elevation with an increase in wave nonlinearity attributed to the known phenomenon of wave set-up. They also found that the values of the statistical moments of wave runup (skewness and kurtosis) were similar to those of the incident wave field [14] studied statistics of narrow-band and wide-band wave runups in the large wave flume of the University of Hannover, Germany. They found that wave fields with a narrow-band spectrum were associated with a higher loss in the wave energy compared to the waves with a wide-band spectrum. However, their experimental records were not long enough to discuss freak runups.

Using field measurements, [15] studied runup heights measured on a wide spectrum of sandy beaches in New South Wales; they found that runup was distributed according to the Rayleigh distribution. Meanwhile, [16,17] studied wave runup on Canadian and Australian coasts and demonstrated that wave runup deviates from the Gaussian distribution. Although some of these conclusions were similar to those of [11–13], it was not possible to put direct correspondence between these works due to a number of reasons. First, the field measurement studies lacked information about an incident wave field. Second, they had a different bathymetry and coastal topography, deviating from the ideal plane beach. Third, the data included an error associated with measurement techniques.

However, the main issue which complicates the comparison of theoretical [11,12] and experimental [13,14] results is the insufficient lengths of the experimental time-series, which do not support analysis of extreme runup statistics. Potentially, this issue can be overcome nowadays with the use of IP high-resolution cameras permanently installed on a beach and associated techniques [18–24]; however, we have not seen such works yet.

In this paper, we cover the existing gap in long-term experimental records by using digital data obtained with intensive numerical computations. This approach has clear advantages. It gives control on the initial wave field offshore and allows for checking the applicability of the approximated analytical results by [11,12] to a more realistic bathymetry: a plane beach merged with a flat bottom.

The paper is organized as follows. In Section 2, the numerical model, based on nonlinear shallow water equations, is described. The statistical moments and the distribution functions of random wave and runup fields, as well as distribution functions of wave and runup heights, are described in detail in Section 3. Then, the main results are summarized in Section 4.

2. Numerical Model

In this section, the 1D nonlinear shallow water model, which represents the mass and momentum conservation, is briefly described:

$$D_t + (Du)_x = 0 \tag{1}$$

$$\frac{\partial}{\partial t}(Du) + \frac{\partial}{\partial x}\left(Du + \frac{g}{2}D^2\right) = gD\frac{dh}{dx} \tag{2}$$

where $D = h + \eta$ is the total water depth, $\eta(x, t)$ is the water elevation, with respect to the still water level, x is the coordinate directed onshore, and t is time, $h(x)$ is the unperturbed water depth, $u(x, t)$ is the depth-averaged water flow velocity, and g is the gravitational acceleration. The dimensionless formulation can be obtained by choosing a typical water depth h_0 as the length scale (in this problem, the depth of the constant section can be taken as h_0, $\sqrt{gh_0}$ as the velocity scale and $h_0/\sqrt{gh_0}$. as the time scale. The dimensionless equations take the form of Equations (1) and (2) with $h_0 = 1$ and $g = 1$. All computations reported in this study were performed in the dimensionless formulation.

The modelling is performed in the framework of Equations (1) and (2), which are solved using a modern shock-capturing finite volume method. Although the shallow water model does not pursue the

wave breaking and undular bore formation in a general sense (including the water surface overturning), it allows shock-wave formation and propagation with the speed given by Rankine–Hugoniot jump conditions, which, to some extent, approximates wave breaking. The numerical scheme is second order accurate, thanks to the spatial reconstruction (UNO2). For details, see [25].

In this simulation, the corresponding bathymetry (Figure 1) set-up is used: the flat part of the flume matches the beach of constant slope:

$$h(x) = \begin{cases} h_0, & x \in [a, b] \\ h_0 - (x - b)\tan\alpha, & x \in [b, c] \end{cases} \tag{3}$$

where h_0 is the constant water depth, kept at 3.5 m for all simulations, [a, c] are the left and right boundaries of the numerical flume, [b] is the point where the slope starts, and tan α = 1:6 is the tangent of the bottom slope. For simplicity, the left boundary is taken as (a = 0). The length of the section of constant depth is b = 251.5 m, and the right limit of the numerical flume is taken as c = 291.5 m. The number of spatial grid points along the distance between [a] and [c] is fixed and equal to 1000 for all experiments. The time step is chosen to satisfy the Courant–Friedrichs–Lewy condition for all considered significant wave heights. The spatial grid step is, therefore, 25 cm, which corresponds to 4 cm vertical resolution for runup height. This was done in order to limit simulation time, when running 10,000 h of physical time of wave propagation. However, this also implies that we have a low resolution and not so reliable statistics, especially for small amplitude waves H_s = 0.1 m. In a similar manner to the significant wave height, H_s, the significant runup height, R_s, is introduced as an average of one third of the largest runup heights in the time-series. The significant runup height for this small amplitude case is R_s = 0.23 m, so even in this case, the resolution is low, but considerable.

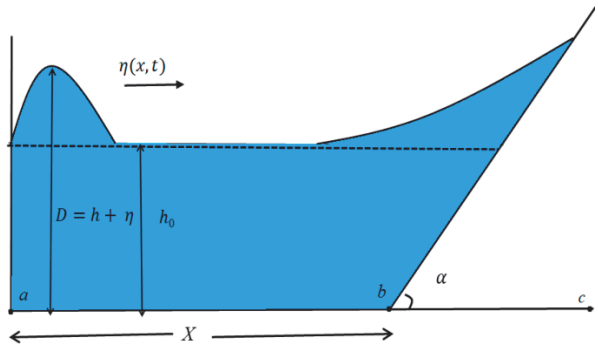

Figure 1. Bathymetry sketch of numerical experiment.

Of course, the number of extreme runups in this resolution is also somehow underrepresented; however, all qualitative and comparative conclusions of this study still hold on.

Boundary Condition

On the left extremity $x = a$ of the computational domain, the Dirichlet boundary condition on the total water depth component $D(a, t) = h_0 + \eta_0(t)$ of the solution (D, Du) is imposed. Namely, the free surface elevation function, η_0, is drawn from a narrow- or wide-band Gaussian signal depending on the experiment. These data turn out to be enough to obtain a well-posed initial boundary-value problem provided that the flow is subcritical at the point $x = a$, i.e., $|u(a, t)| < \sqrt{gD(a, t)}$, which is always the case for Riemann waves (see [26] for the rigorous mathematical justification of this fact in case of transparent boundary conditions). The boundary conditions are implemented in the finite volume scheme according to the method described in [27] (see also [28] for more details on the application to the nonlinear shallow water equations).

The considered boundary condition (wave field offshore) is distributed by the Gaussian distribution:

$$f(\xi) = \frac{1}{\sigma\sqrt{2\pi}} e^{-\frac{1}{2}\left(\frac{\xi-\mu}{\sigma}\right)^2} \quad (4)$$

where σ is a standard deviation, and μ is a mean value of the distribution. To ensure this, all individual time-series have been verified by the Kolmogorov-Smirnov test [29].

The spectrum of the generated waves is:

$$S(f) = \frac{S_0}{\sqrt{2\pi\Delta f / f_0}} e^{-\frac{(f/f_0-1)^2}{2\Delta f/f_0}} \quad (5)$$

where f is the wave frequency, Δf is the frequency band, $f_0 = 0.1$ Hz is the central frequency, and S_0 is the constant, which is calculated in order to achieve the desired H_s.

In this work, the case with $\Delta f/f_0 = 0.1$ is referred to as the narrow-band spectrum, while the case with $\Delta f/f_0 = 0.4$ is referred to as the wide-band spectrum. In order to study the influence of wave nonlinearity during wave propagation to the coast, waves of different significant wave heights, which are calculated as the average of one third of the largest wave heights in the time-series (H_s = 0.1, 0.2, 0.3, 0.4, and 0.5 m), are considered. The calculated time-series for each H_s is 1000 h (360,000 wave periods). Parallel computations facilitated the calculation of the statistics of wave runup characteristics for 5000 h, for each bandwidth, and 10,000 h in total. The numerical computations were carried out in MATLAB and run on a cluster containing 28 cores.

The parameter of the nonlinearity for generated waves was estimated as H_s/h_0 and changed from 0.03 to 0.14. The characteristic parameter $kh_0 = 0.38$ is at the border of validity of the shallow water theory, taking into account the horizontal extent of the wave tank. The phase velocity relative error committed by non-dispersive theory for $kh_0 = 0.38$ is only 2.3%. Thus, at the end of the numerical wave tank, the difference between wave crest positions (between dispersive and non-dispersive models) is less than 10%. Since the focus of this paper is on wave runup, the choice of this theory is justifiable. The choice of wave parameters allows us to see the effects of wave breaking on the statistics of their runups. The type of wave breaking is defined by the Iribarren number [5]:

$$Ir = \frac{\alpha}{\sqrt{H/L}} \quad (6)$$

where H is the wave height and L is the characteristic wavelength offshore. It is surging or collapsing for $Ir \geq 3.3$, plunging for $0.5 \leq Ir \leq 3.3$, and spilling for $Ir \leq 0.5$. In our dataset, only the first two types of wave breaking, surging or collapsing and plunging, are observed. For $H_s/h_0 = 0.03$, less than 1% of waves experience plunging breaking, while most of the waves are surging. With an increase in H_s/h_0, the percentage of plunging waves increases. For $H_s/h_0 = 0.06$, 32–35% of the waves are plunging, for $H_s/h_0 = 0.09$, 61–65% of the waves are plunging, for $H_s/h_0 = 0.11$, 71–76% of the waves are plunging, and for the most nonlinear case, $H_s/h_0 = 0.14$, 85–88% of the waves are plunging.

3. Data Analysis and Results

Figure 2 shows probability density functions (PDF) of narrow-band and wide-band wave fields for different nonlinearities, H_s/h_0. The data of the narrow-band spectra, $\Delta f/f_0 = 0.1$ are shown by triangles (different colors correspond to different nonlinearities), while the corresponding Gaussian distribution ($\mu = 0$, $\sigma = 0.25$) is shown by the black solid line. The data of the wide-band spectra, $\Delta f/f_0 = 0.4$ are shown by pluses, and the corresponding Gaussian distribution ($\mu = 0$, $\sigma = 0.27$) is shown by the red solid line. It can be seen that the generated waves are well described by the Gaussian distribution, which has zero mean, skewness and kurtosis for all nonlinearities, H_s/h_0.

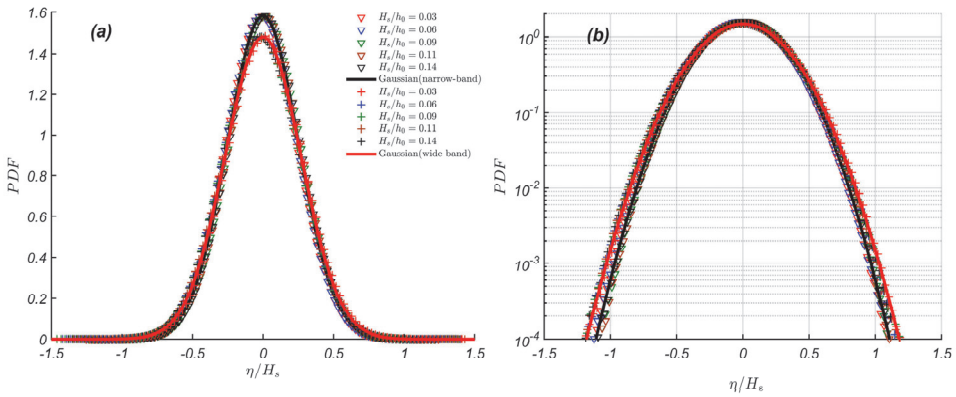

Figure 2. Probability density functions of normalized narrow-band and wide-band wave fields offshore for different nonlinearities, H_s/h_0 in linear (**a**) and logarithmic (**b**) scales. Solid lines correspond to Gaussian distributions fitted to the corresponding datasets, shown with a red color for wide-band data and with black color for narrow band data.

To describe the wave statistics in Figure 2, the Rayleigh distribution, which is well used for this type of problem [5], is applied:

$$f(\xi) = \begin{cases} \frac{\xi}{\lambda^2} e^{-\xi^2/(2\lambda^2)}, & \xi \geq 0 \\ 0, & \xi < 0 \end{cases} \tag{7}$$

where ξ is a data vector and λ is the scale parameter. For a better fit, a two-parameter Weibull distribution is also considered:

$$f(\xi) = \begin{cases} \frac{k}{\lambda}\left(\frac{\xi}{\lambda}\right)^{k-1} e^{-(\xi/\lambda)^k}, & \xi \geq 0 \\ 0, & \xi < 0 \end{cases} \tag{8}$$

where λ is the scale parameter and k is the shape parameter.

The wave height distributions of both narrow-band and wide-band wave fields are shown in Figure 3. As expected, the narrow-band data are well described by a Rayleigh distribution ($\lambda = 0.5$), although a Weibull distribution gives a slightly better fit ($\lambda = 0.74$, $k = 2.27$). The data of wide-band spectra tend to be distributed according to a Weibull distribution ($\lambda = 0.71$, $k = 2.06$).

The waves which are two times higher than the significant wave height ($H/H_s \geq 2$) are the so-called freak waves. It can be seen from Figure 3 that the probability of the freak wave occurrence in the initial wave field is higher for narrow-band signals than for wide-band ones.

The calculated significant runup heights R_s for narrow-band and wide-band signals are shown in Figure 4. It is interesting to see that R_s for wide-banded waves is always higher than for narrow-banded waves, which can be explained by the higher variability in wave periods for wide-banded waves. Also, Figure 4 indirectly shows us how many of our waves are breaking. The wave runup height, at which the first wave breaking occurs in the wave trough, can be estimated as $R_{cr}/h_0 = g(\alpha T/(2\pi))^2/h_0 = 0.2$ (see [30] for details). This means that our case of "small" nonlinearity $H_s/h_0 = 0.03$ is affected very little by wave breaking (<1% according to Iribarren criterion). The case of $H_s/h_0 = 0.06$ is affected by wave breaking only for extreme runups (32–35% according to Iribarren criterion). In the case of $H_s/h_0 = 0.09$, more than a half of waves are breaking (61–65% according to Iribarren criterion). However, in the cases of $H_s/h_0 = 0.11$ and $H_s/h_0 = 0.14$, the majority of waves are breaking.

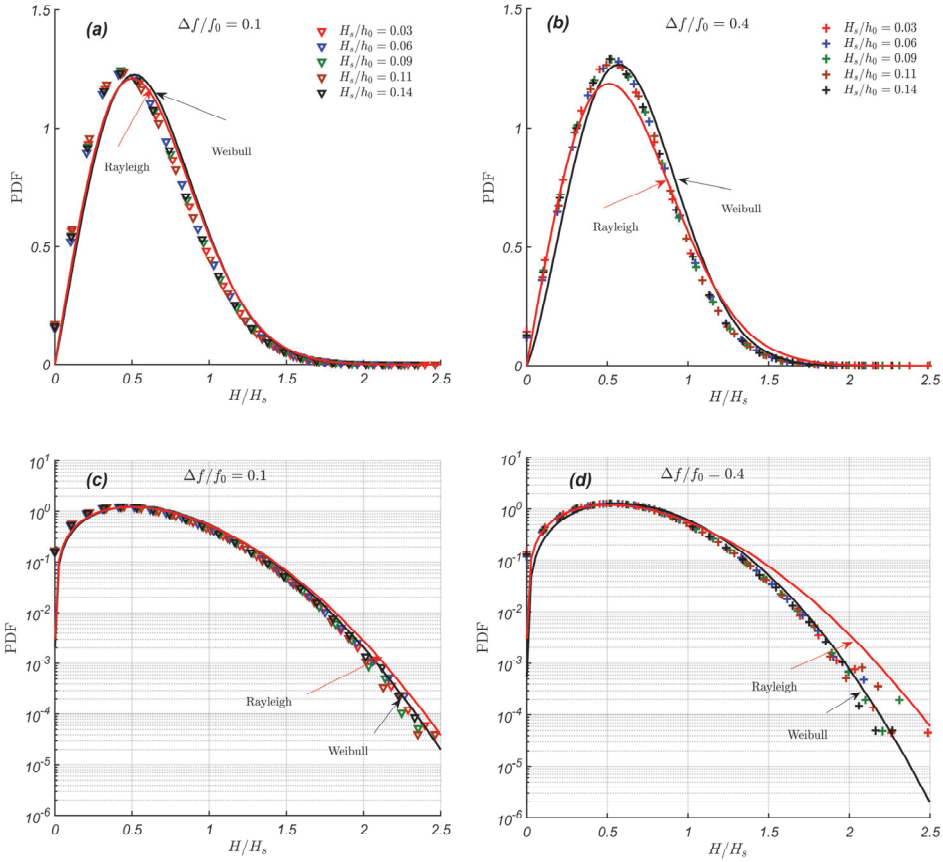

Figure 3. Probability density functions of normalized trough-to-crest wave heights of the initial narrow-band (**a**) and (**c**), and wide-band (**b**) and (**d**) wave fields for different nonlinearities, H_s/h_0 in linear (top) and logarithmic (bottom) scales. The red solid line corresponds to the Rayleigh distribution; the black solid line corresponds to the Weibull distribution fitted to the corresponding dataset.

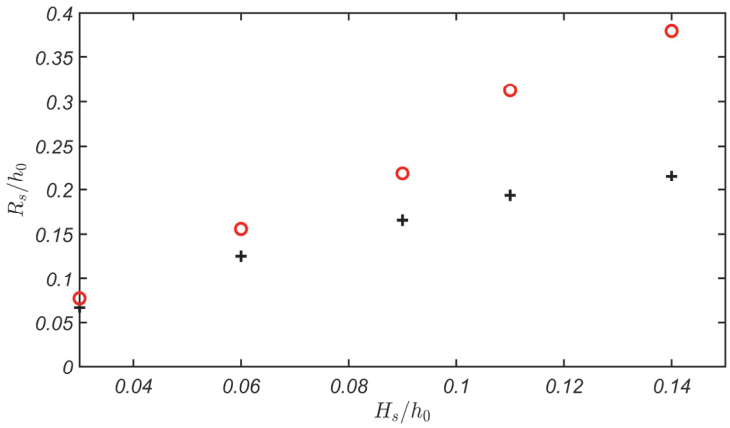

Figure 4. Significant runup height, R_s for wide-band (red circles) and narrow-band (black crosses) signals for different nonlinearities.

Figure 5 shows the probability distribution functions of runup oscillations, r/R_s for initial Gaussian narrow-banded and wide-banded wave signals. It can be seen from Figure 5a that runup oscillations of narrow-banded waves are no longer distributed by a normal distribution and are slightly shifted to the right towards larger positive values with an increase in nonlinearity. This effect was partially observed both theoretically for an infinite plane beach [11,12] and experimentally [13,14]. What is interesting and peculiar is a strong deformation of the distribution itself. In addition, the tails of these distributions are much thinner than of Gauss, and reflect a relatively weak probability of extreme floods for narrow-banded waves.

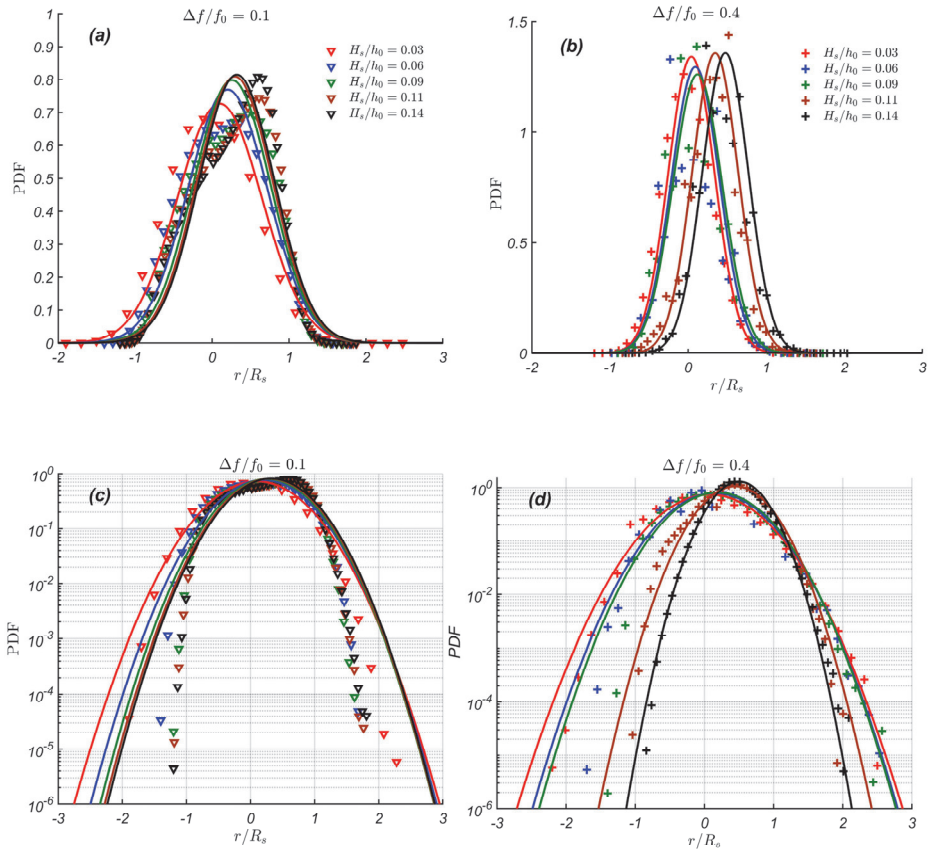

Figure 5. Probability density functions of runup oscillations, normalized by a significant runup height, R_s, for different nonlinearities for narrow-banded (**a**) and (**c**), and wide-banded (**b**) and (**d**) waves in linear (top) and logarithmic (bottom) scales. Solid lines correspond to Gaussian distributions, fitted to the corresponding datasets, using the matching colors.

The distributions of runup oscillations of the initial wide-band signal are also shifted to the right towards higher runups with an increase in nonlinearity, but this shift is much larger compared to that of the narrow-band signal. Moreover, the tails of these distributions are much thicker than those for narrow-band data, and are rather close to the normal distribution, which corresponds to a relatively large probability of extreme floods for wide-banded waves.

It can also be seen that for both narrow-banded and wide-banded waves, the probability of large waves decreases with an increase in wave nonlinearity, which can be explained by wave breaking.

These effects can also be seen in Figure 6, which shows the statistical moments of narrow-banded and wide-banded waves offshore, normalized by H_s, and the corresponding runup oscillations on a beach, normalized by R_s. The statistical moments, mean, variance, skewness, and (normalized) kurtosis are calculated as:

$$< \xi >= \frac{1}{n}\sum_{i=1}^{n} \xi_i, \sigma^2(\xi) = \frac{1}{n}\sum_{i=1}^{n} (\xi_i - < \xi >)^2 \quad (9)$$

$$Sk(\xi) = \sum_{i=1}^{n} \frac{1}{n\sigma^3(\xi)} (\xi_i - < \xi >)^3, Kurt(\xi) = \sum_{i=1}^{n} \frac{1}{n\sigma^4(\xi)} (\xi_i - < \xi >)^4 - 3 \quad (10)$$

where ξ is a data vector, and n is its length.

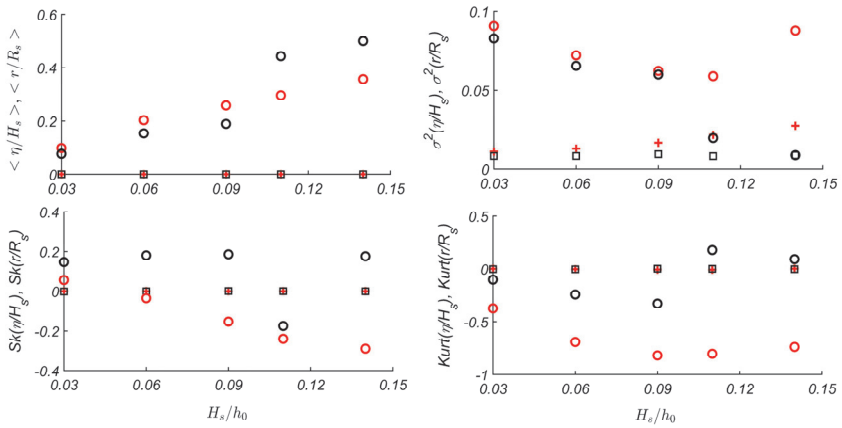

Figure 6. Statistical moments of runup oscillations (normalized by R_s) of narrow-banded (red circles) and wide-banded (black circles) waves on a beach, r, versus nonlinearity, H_s/h_0. Statistical moments of narrow-band and wide-band wave fields offshore (normalized by H_s) are shown by red crosses and black squares, respectively.

Notably, the mean, skewness and kurtosis of both narrow-banded and wide-banded wave fields are zero, providing the desired Gaussian statistics. Regarding runup oscillations, one can see that for both narrow- and wide-banded waves, the mean of runup oscillations rises with the nonlinearity, which reflects the known effect of wave set-up on a beach. For small-amplitude waves, the set-up for narrow-banded waves is larger than for wide-banded ones, while for large amplitude waves, affected by wave breaking, it is the opposite. For wide-banded waves, the variance decreases with an increase in nonlinearity, while for narrow-banded waves it changes non-monotonically. The higher moments, skewness and kurtosis of runup oscillations for waves with a narrow-band spectrum are negative, while for waves with wide-band spectrum they are sign-variable. Also for the narrow-banded waves, the skewness decreases with an increase in wave nonlinearity, while kurtosis changes non-monotonically with an increase in wave nonlinearity. Moreover, for wide-banded waves, both skewness and kurtosis change non-monotonically with an increase in nonlinearity. This somehow only partially corresponds to the theoretical findings in [11], where the kurtosis was positive for weak amplitude waves and negative for strongly nonlinear waves, while the skewness was always positive. However, in the experimental study of [13], the skewness was both positive and negative. It is also important to say that for all four moments, one can see different dynamics for small-amplitude non-breaking or almost non-breaking waves and large-amplitude waves, strongly affected by wave breaking.

Runup oscillations deviate from the Gaussian distribution even for weak-amplitude waves (see Figure 6). With an increase in nonlinearity, all statistical moments of runup oscillations change. It can

be seen that statistical moments of narrow-banded irregular waves (except kurtosis) change with H_s monotonically, while for the wide-banded waves, they vary non-monotonically (except mean values).

The large (extreme) wave runup heights, $R_{extrm} = R/R_s \geq s$, where s is some threshold value, somehow behave similarly to a conditional Weibull law whose density is given by Equation (11):

$$f(R_{extrm}) = \begin{cases} \frac{k}{\lambda}\left(\frac{R_{extrm}}{\lambda}\right)^{k-1} e^{-(R_{extrm}/\lambda)^k + (s/\lambda)^k}, & R_{extrm} \geq s \\ 0, & R_{extrm} < s \end{cases} \tag{11}$$

A conditional Weibull law is characterized by three parameters: the shape k, the scale λ and the threshold s. Given the data, $(R_{i\ extrm}) = 1 \ldots n$, s is fixed and k and λ are computed by maximum likelihood estimator. The scale parameter, λ can be obtained from Equation (12):

$$\lambda = \left(\frac{1}{n}\sum_{i=1}^{n}\left(R_{i\ extrm}^k - s^k\right)\right)^{\frac{1}{k}} \tag{12}$$

where n is the number of extreme wave runups. In order to obtain the shape parameter, k, one should solve Equation (13):

$$\frac{1}{k}(I_n - s^k) + (\ln s)s^k + M_n(I_n - s^k) - V_n = 0 \tag{13}$$

$$M_n = \frac{1}{n}\sum_{i=1}^{n} \ln R_{i\ extrm} \tag{14}$$

$$I_n = \frac{1}{n}\sum_{i=1}^{n} R_{i\ extrm}^k \tag{15}$$

$$V_n = \frac{1}{n}\sum_{i=1}^{n} (\ln R_{i\ extrm}) R_{i\ extrm}^k \tag{16}$$

Similarly to freak waves, the waves on a beach whose runup height is two times larger than the significant runup height ($R/R_s \geq 2$) are called freak runups. On gentle beaches, such freak runups are manifested as sudden floods and may result in human injuries and fatalities [8–10].

Figure 7 shows probability distribution functions of large runup heights ($R \geq 0.7R_s$), for narrow-band and wide-band spectra, for different nonlinearities. It can be seen in Figure 7 that the tails of distributions for runup heights corresponding to freak events for narrow-banded waves decay much faster than those for wave heights offshore (except waves of weak amplitude with $H_s/h_0 = 0.03$), which means that for narrow-banded waves, the probability of freak runup occurrence on a beach is less than the probability of freak wave occurrence in the sea coastal zone, and a gentle beach works as some kind of "filter" for narrow-banded freak events. This is also manifested in the numbers of actual freak events, given in Table 1. It can be seen that for non-breaking waves of the smallest amplitude $H_s/h_0 = 0.03$, the number of freak events on a beach was reduced twice compared to the original number of freak waves offshore, while for waves of larger amplitude, which were affected by the wave breaking, there were no freak runups at all.

In contrast, for wide-banded waves, the probability of freak events on a beach is more or less the same as in the sea coastal zone and may even be higher (Figure 7). The number of freak runups for small non-breaking wide-banded waves increased twice compared to the original number of freak waves offshore (see Table 1). With an increase in wave amplitude (and consequently, wave breaking), the number of freak runups on a beach decreases; however, for waves of moderate amplitude, the number of freak runups is still larger than the number of freak waves offshore, while for waves strongly affected by the wave breaking ($H_s/h_0 = 0.11$ and 0.14), the number of freak runups on a beach suddenly drops down (see Table 1).

Probability of extreme wave runups on a beach is noticeably higher for waves with wide-band spectra than for waves with narrow-band spectra (see Figure 7), although the probability of extreme wave heights in the wave field offshore is significantly higher for narrow-banded waves than for wide-banded ones (see Figure 3, Table 1).

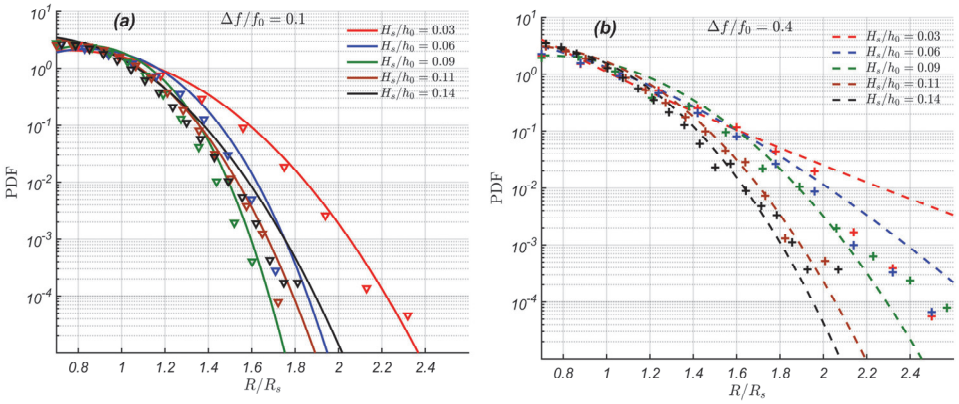

Figure 7. Probability density functions of large runup heights ($R \geq 0.7R_s$) for (**a**) narrow-banded (triangles) and (**b**) wide-banded (pluses) waves. Lines correspond to conditional Weibull distributions (Equation (11)), fitted to the narrow-band (solid lines) and wide-band (dashed lines) datasets, using the matching colors.

Table 1. The number of freak events in the sea coastal zone and on a beach for different wave regimes.

	$\Delta f/f_0 = 0.1$			$\Delta f/f_0 = 0.4$		
H_s/h_0	Number of Waves	Freak Waves Offshore	Freak Runups	Number of Waves	Freak Waves Offshore	Freak Runups
0.03	362255	125	61	389232	51	118
0.06	362380	117	0	389385	45	76
0.09	362096	89	0	389444	49	62
0.11	362319	88	0	389263	53	2
0.14	362302	102	0	389728	34	1

The probability of extreme runup formation changes with the wave nonlinearity. It decreases with an increase in wave nonlinearity for wide-banded waves and changes non-monotonically with nonlinearity for narrow-banded waves. It is also interesting to see that the tails of distributions in Figure 7 are somehow gathered into clusters and can be separated in two groups for "relatively large H_s" and "relatively small H_s", where the "small H_s" group is always higher than the "large H_s" group. The latter holds for both narrow-banded and wide-banded waves and can be explained by the wave breaking.

The corresponding data of wave runup heights are also approximated by a conditional Weibull distribution (Equation (11)), which gives reasonable results and can be used to evaluate the probability of freak runups. Here, the threshold s is selected as 0.7 and the calculated parameters k and λ are given in Table 2.

Table 2. Parameters of conditional Weibull distribution fitted to the corresponding datasets in Figure 7.

	$\Delta f/f_0 = 0.1$		$\Delta f/f_0 = 0.4$	
H_s/h_0	k	λ	k	λ
0.03	2.747	0.886	0.76	0.116
0.06	3.6	0.92	1.43	0.48
0.09	4.06	0.89	2.58	0.86
0.11	3.08	0.777	2.6	0.772
0.14	3.08	0.72	2.718	0.762

4. Conclusions

In this paper, irregular wave runups on a plane beach are studied by means of direct numerical simulations. The numerical model is based on the nonlinear shallow water equations and is of the second order of accuracy. The corresponding bathymetry consists of a section of constant depth, which is matched with the beach of a constant slope. The irregular waves are represented by the Gaussian wave field with spectra of two different bandwidths, which are referred to as narrow-banded and wide-banded waves. To address different levels of wave nonlinearity, time-series with five different significant wave heights are considered. The selected wave regimes represent (i) non-breaking waves, (ii) waves slightly affected by wave breaking, (iii) moderate wave breaking and (iv) significant wave breaking, when the majority of waves are breaking. Each of these time-series has a duration of 1000 h (360,000 wave periods).

The heights of narrow-banded waves are well described by Rayleigh distribution, while heights of wide-banded waves are described by Weibull distribution, irrespective of the wave nonlinearity. However, for wide-banded waves, the tails of these distributions show larger variability than for narrow-banded ones.

As expected, the runup oscillations are not Gaussian, which confirms that results of many previous studies, both theoretical [11,12] and experimental [13,16,17]. For both narrow-band and wide-band cases, one can observe the effect of wave set-up (increase in the mean value of runup oscillations), which increases with an increase in wave nonlinearity. However, for wide-banded waves, this increase is significantly stronger than for narrow-banded ones.

Regarding extreme, so-called "freak events", their statistics in the initial narrow-banded wave signal offshore are more representative than on the beach ("freak runups"), even for non-breaking waves. Therefore, for narrow-banded waves, gentle beaches reduce the number of freak events as compared to the sea coastal zone, and work as a 'low-pass filter' for extreme wave heights. This may explain why freak events on a beach are so unexpected [8–10]. However, for wide-banded waves, such an effect has not been observed and the probability of freak events on a beach was similar to or even larger than the one in the sea coastal zone.

The number of freak events in wide-band and narrow-band cases varies, such that increase in the bandwidth leads to a substantial increase in the number of freak events. This can be explained by higher variability in wave periods for wide-banded waves, and wave runup height is rather sensitive to these variations. In addition, the number of freak waves decreases with an increase in wave amplitude and consequently, wave breaking. The largest number of freak waves was observed for non-breaking wide-banded waves, which almost doubled the number of freak waves in the boundary condition wave record.

Finally, to describe statistics of extreme wave runup heights on a gentle beach, a conditional Weibull distribution is suggested. It gives reasonable results and may be used for the assessment of extreme inundations on a beach (freak runups). In addition, in future applications, the statistical analysis hereby provided might also be useful in the study of the wave run-up phenomenon in other applications, e.g., in structures placed in shallow water conditions [31,32].

The limitation imposed by the resolution of the numerical simulations should also be taken into account. Although the number of freak waves on the beach may be somehow reduced by a coarse

model resolution, the qualitative and comparative conclusion of this study should not be affected. This point will be improved in our future studies.

Author Contributions: Conceptualization, I.D.; methodology, I.D., D.D., C.L.; software, D.D.; resources, I.D., D.D.; data curation, A.A.; writing—original draft preparation, A.A.; writing—review and editing, A.A., I.D., D.D. and C.L.; numerical simulations and data analysis, A.A.; Conditional Weibull distribution conceptualization and fitting C.L. All authors have read and agreed to the published version of the manuscript.

Funding: The study of distribution functions and the statistical moments of irregular wave runup was performed with the support of an RSF grant (16-17-00041). The numerical simulations of wave runup were supported by an ETAG grant (PUT1378). The authors also thank the PHC PARROT project (No. 37456YM), which funded the visits to France and Estonia, thus facilitating this collaboration.

Acknowledgments: The computations were performed using the computer cluster of the Department of Marine Systems of Tallinn University of Technology.

Conflicts of Interest: The authors declare no conflicts of interest.

References

1. Didier, D.; Baudry, J.; Bernatchez, P.; Dumont, D.; Sadegh, M.; Bismuth, E.; Bandet, M.; Dugas, S.; Sévigny, C. Multihazard simulation for coastal flood mapping: Bathtub versus numerical modelling in an open estuary, Eastern Canada. *Flood Risk Manag.* **2019**, *12*, 12505. [CrossRef]
2. Gallien, T.W.; Sanders, B.F.; Flick, R.E. Urban coastal flood prediction: Integrating wave overtopping, flood defenses and drainage. *Coast. Eng.* **2014**, *91*, 18–28. [CrossRef]
3. Beck, M.W.; Losada, I.J.; Menéndez, P.; Reguero, B.G.; Díaz-Simal, P.; Fernández, F. The global flood protection savings provided by coral reefs. *Nat. Commun.* **2018**, *9*, 1–9. [CrossRef] [PubMed]
4. Lyddon, C.E.; Brown, J.M.; Leonardi, N.; Saulter, A.; Plater, A.J. Quantification of the uncertainty in coastal storm hazard predictions due to wave-current interaction and wind forcing. *Geophys. Res. Lett.* **2019**, *46*, 14576–14585. [CrossRef]
5. Massel, R.S. *Ocean Surface Waves: Their Physics and Prediction*, 2nd ed.; World scientific: Hackensack, NJ, USA, 1996.
6. Stocker, J.J. *Water Waves: The Mathematical Theory with Applications*; Interscience: New York, NY, USA, 1957.
7. Mei, C.C. *The Applied Dynamics of Ocean Surface Waves*; World Scientific: Singapore, 1983.
8. Nikolkina, I.; Didenkulova, I. Catalogue of rogue waves reported in media in 2006–2010. *Nat. Hazards* **2012**, *61*, 989–1006. [CrossRef]
9. García, M.G.; Özkan, H.T.; Ruggiero, P.; Holman, R.A.; Nicolini, T. Analysis and catalogue of sneaker waves in the US Pacific Northwest between 2005 and 2017. *Nat. Hazards* **2018**, *94*, 583–603. [CrossRef]
10. Didenkulova, E. Catalogue of rogue waves occurred in the World Ocean from 2011 to 2018 reported by mass media sources. *Ocean Coast. Manag.* **2020**, *188*, 105076. [CrossRef]
11. Didenkulova, I.; Pelinovsky, E.; Sergeeva, A. Statistical characteristics of long waves nearshore. *Coast. Eng.* **2011**, *58*, 94–102. [CrossRef]
12. Gurbatov, S.; Pelinovsky, E. Probabilistic characteristics of narrow-band long-wave run-up onshore. *Nat. Hazards Earth Syst. Sci.* **2019**, *19*, 1925–1935. [CrossRef]
13. Denissenko, P.; Didenkulova, I.; Pelinovsky, E.; Pearson, J. Influence of the nonlinearity on statistical characteristics of long wave runup. *Nonlinear Process. Geophys.* **2011**, *18*, 967–975. [CrossRef]
14. Denissenko, P.; Didenkulova, I.; Rodin, A.; Listak, M.; Pelinovsky, E. Experimental statistics of long wave runup on a plane beach. *J. Coast. Res.* **2013**, *65*, 195–200. [CrossRef]
15. Nielsen, P.; Hanslow, D.J. Wave runup distributions on natural beaches. *Coast. Res.* **1991**, *7*, 1139–1152.
16. Huntley, D.A.; Guza, R.T.; Bowen, A.J. A universal form for shoreline run-up spectra. *Geophys. Res.* **1977**, *82*, 2577–2581. [CrossRef]
17. Hughes, M.G.; Moseley, A.S.; Baldock, T.E. Probability distributions for wave runup on beaches. *Coast. Eng.* **2010**, *57*, 575–584. [CrossRef]
18. Simarro, G.; Bryan, K.R.; Guedes, R.M.; Sancho, A.; Guillen, J.; Coco, G. On the use of variance images for runup and shoreline detection. *Coast. Eng.* **2015**, *99*, 136–147. [CrossRef]
19. Salmon, S.A.; Bryan, K.R.; Coco, G. The use of video systems to measure run-up on beaches. *J. Coast. Res.* **2007**, *50*, 211–215.

20. Aagaard, T.; Holm, J. Digitization of wave run-up using video records. *J. Coast. Res.* **1989**, *5*, 547–551.
21. Khoury, A.; Jarno, A.; Marin, F. Experimental study of runup for sandy beaches under waves and tide. *Coast. Eng.* **2019**, *144*, 33–46. [CrossRef]
22. Park, H.; Cox, D.T. Empirical wave run-up formula for wave, storm surge and berm width. *Coast. Eng.* **2016**, *115*, 67–78. [CrossRef]
23. García-Medina, G.; Özkan-Haller, H.T.; Holman, R.A.; Ruggiero, P. Large runup controls on a gently sloping dissipative beach. *J. Geophys. Res. Ocean.* **2017**, *122*, 5998–6010. [CrossRef]
24. Di Luccio, D.; Benassai, G.; Budillon, G.; Mucerino, L.; Montella, R.; Carratelli, E.P. Wave run-up prediction and observation in a micro-tidal beach. *Nat. Hazards Earth Sys. Sci.* **2018**, *18*, 2841–2857. [CrossRef]
25. Dutykh, D.; Katsaounis, T.; Mitsotakis, D. Finite volume schemes for dispersive wave propagation and runup. *Comput. Phys.* **2011**, *230*, 3035–3061. [CrossRef]
26. Petcu, M.; Temam, R. The one-dimensional shallow water equations with transparent boundary conditions. *Math. Methods Appl. Sci.* **2013**, *36*, 1979–1994. [CrossRef]
27. Ghidaglia, J.M.; Pascal, F. The normal flux method at the boundary for multidimensional finite volume approximations in CFD. *Eur. J. Mech. B/Fluids* **2005**, *24*, 1–17. [CrossRef]
28. Dutykh, D.; Poncet, R.; Dias, F. The VOLNA code for the numerical modeling of tsunami waves: Generation, propagation and inundation. *Eur. J. Mech. B/Fluids* **2011**, *30*, 598–615. [CrossRef]
29. Dodge, Y. *Kolmogorov–Smirnov Test*; The Concise Encyclopedia of Statistics; Springer: New York, NY, USA, 2008.
30. Didenkulova, I. New trends in the analytical theory of long sea wave runup. In *Applied Wave Mathematics: Selected Topics in Solids, Fluids, and Mathematical Methods*; Quak, E., Soomere, T., Eds.; Springer: Berlin/Heidelberg, Germany, 2009; pp. 265–296.
31. Vanem, E.; Fazeres-Ferradosa, T.; Rosa-Santos, P.; Taveira-Pinto, F. Statistical description and modelling of extreme ocean wave conditions. In *Proceedings of the Institution of Civil Engineers-Maritime Engineering*; Thomas Telford Ltd.: London, UK, December 2019; Volume 172, pp. 124–132.
32. Fazeres-Ferradosa, T.; Taveira-Pinto, F.; Vanem, E.; Reis, M.T.; Neves, L.D. Asymmetric copula–based distribution models for met-ocean data in offshore wind engineering applications. *Wind Eng.* **2018**, *42*, 304–334. [CrossRef]

Curriculum Vitae

Personal data

Name:	Ahmed Alkarory Ahmed Abdalazeez
Date of birth:	01/01/1984
Place of birth:	Sudan
Citizenship:	Sudanese

Contact data

E-mail:	ahabda@taltech.ee; karory48@hotmail.com

Education

2016– 2020	Ph.D., Tallinn University of Technology / Marine System Institute, Tallinn, Estonia
2016–2017	Scholar of the Nippon Foundation-POGO Centre of Excellence (NF-POGO CofE), intense training on the operational oceanography at the Alfred Wegener Institute for Polar and Marine Research, Helgoland - Sylt - Bremerhaven, Germany
2010–2012	M.Sc., Faculty of Mathematics and Natural Science, Geophysical Institute, University of Bergen, Bergen, Norway.
2004–2008	B.Sc., Physics (with honour), Sudan University of Science & Technology (SUST), Khartoum, Sudan
2004–2008	High school

Language competence

Arabic	Native speaker
English	Fluent
German	Basic skills

Professional employment

2017–2020	Tallinn University of Technology, School of Science, Department of Marine Systems, Early Stage Researcher (1,00)
2014–2016	Red Sea University, Institute of Marine Research, Sudan, Junior Researcher (1,00)

Scientific work

1.1. *(Articles indexed by the ISI WEB of science)*

Abdalazeez, A. A.; Didenkulova, I.; Dutykh, D. (2019). Nonlinear deformation and runup of single tsunami waves of positive polarity: numerical simulations and analytical predictions. Natural Hazards and Earth System Sciences, 19, 2905−2913.10.5194/nhess- 19-2905-2019.

Abdalazeez, A.; Didenkulova, I.; Dutykh, D.; Labart, C. (2020). Extreme Inundation Statistics on a Composite Beach. Water, 12 (6), 1573−1586.10.3390/w12061573.

Abdalazeez, A.; Didenkulova, I.; Dutykh, D.; Denissenko, P. (2020). Comparison of dispersive and nondispersive models for wave run-up on a beach. Izvestiya, Atmospheric and Oceanic Physics, Vol. 56, pp. 494–501.

3.1. *(Articles in proceeding indexed by the ISI WEB of science)*

Abdalazeez, A.; Didenkulova, I.; Dutykh, D. (2020). Dispersive effects during long wave run-up on a plane beach. Proceedings of the 2nd International Workshop on Natural Hazards: NatHaz19 - Hydrological Risks, Pico Island (Azores), May 9–10, 2019. Ed. Francisco FernandesAna MalheiroHelder I. Chaminé. Springer, 143−146. (Advances in Science, Technology & Innovation).10.1007/978-3-030-34397-2_28.

Torsvik, T.; Abdalazeez, A.; Dutykh, D.; Denissenko, P.; Didenkulova, I. (2019). Dispersive and non-dispersive nonlinear long wave transformations: Numerical and experimental results. In: A. Berezovski, T. Soomere (Ed.). Applied Wave Mathematics II. Selected Topics in Solids, Fluids, and Mathematical Methods and Complexity (41−60). Swizerland : Springer.10.1007/978-3-030-29951-4_3.

3.4. *(Articles published in conference proceedings)*

Abdalazeez Ahmed and Knut Barthel (2014). Estimation of Wave Run-up in the Northern Indian Ocean using WAM model. Proceedings of the 11th International Conference on Hydroscience & Engineering. Ed. Lehfeldt & Kopmann. Karlsruhe: Bundesanstalt für Wasserbau, 385−390.

Abdalazeez, A. (2014). Wave runup estimates at gentle beaches in the Northern Indian Ocean. Proceedings of 11th International Conference on Coasts, Ports and Marine Structures: 11th International Conference on Coasts, Ports and Marine Structures, Tehran, Iran, 24–26 November 2014, CIVILICA.

5.2*. (Conference abstracts)*

Didenkulova, I.; Kurkin, A.; Rodin, A.; Abdalazeez, A.; Dutykh, D. (2020). Runup of long waves on composite coastal slopes: numerical simulations and experiment. EGU General Assembly 2020, EGU.

Abdalazeez, A.; Dutykh, D.; Didenkulova, I.; Labart, C. (2020). Run-up of narrow and wide-banded irregular waves on a beach. EGU General Assembly 2020*,* EGU.

Didenkulova, I.; Abdalazeez, A.; Dutykh, D.; Torsvik, T.; Denissenko, P. (2019). Dispersive effects during long wave runup on a beach. Geophysical Research Abstracts, 21: EGU General Assembly 2019, Vienna, Austria, 7–12 April 2019, EGU.

Abdalazeez, A.; Didenkulova, I.; Dutykh, D. (2019). Nonlinear deformation and run-up of elongated solitary waves: numerical simulations and analytical predictions. Geophysical Research Abstracts, 21: EGU General Assembly 2019, Vienna, Austria, 7–12 April 2019, EGU.

Abdalazeez, A.; Didenkulova, I.; Dutykh, D. (2019). Nonlinear deformation and run-up of tsunami waves of positive polarity: numerical simulations and analytical predictions. Eurasian RISK2019 Conference, Baku, Azerbaijan, 22–24 May 2019. Azerbaijan: Republican Seismic Survey Center of Azerbaijan National Academy of Sciences, 101.

Abdalazeez, A. (2016). Seasonal variations of runup, wave height and wind speed in the northern Indian Ocean. International Conference on Coastal Zones, Osaka, Japan, May 16–18, 2016. OMICS.

Elulookirjeldus

Isikuandmed

Nimi:	Ahmed Alkarory Ahmed Abdalazeez
Sünniaeg:	01/01/1984
Sünnikoht:	Sudaan
Kodakondsus:	Sudaani

Kontaktandmed

E-post:	ahabda@taltech.ee; karory48@hotmail.com

Hariduskäik

2016–2020	Ph.D., Tallinna Tehnikaülikool
2010–2012	M.Sc., matemaatika- ja loodusteaduste teaduskond, Bergeni ülikooli geofüüsikaline instituut, Bergen, Norra
2004–2008	B.Sc., Füüsika (*cum laude*), Sudaani teaduse ja tehnoloogia ülikool (SUST), Khartoum, Sudaan
2000–2003	keskharidus

Keelteoskus

Inglise keel	kõrgtase
Araabia	emakeel
Saksa	põhioskused

Teenistuskäik

2017–2020	Tallinna Tehnikaülikool, Loodusteaduskond, Meresüsteemide instituut, doktorant-nooremteadur (1,00)
2014–2016	Punase mere ülikool, Sudaani mereuuringute instituut, nooremteadur (1,00)